Physics Reports 1067 (2024) 1–62

Contents lists available at ScienceDirect

Physics Reports

journal homepage: www.elsevier.com/locate/physrep

Vibrational resonance: A review

Jianhua Yang [a], S. Rajasekar [b], Miguel A.F. Sanjuán [c,*]

[a] Jiangsu Key Laboratory of Mine Mechanical and Electrical Equipment, School of Mechatronic Engineering, China University of Mining and Technology, Xuzhou, 221116, Jiangsu, People's Republic of China
[b] School of Physics, Bharathidasan University, Tiruchirapalli, 620024, Tamilnadu, India
[c] Nonlinear Dynamics, Chaos and Complex Systems Group, Departamento de Fisica, Universidad Rey Juan Carlos, Tulipan s/n, Mostoles, 28933, Madrid, Spain

ARTICLE INFO

Article history:
Received 20 November 2023
Received in revised form 5 March 2024
Accepted 5 March 2024
Available online 18 March 2024
Editor: Campbell

Keywords:
Vibrational resonance
Nonlinear systems
Nonlinear response
Aperiodic signal
Logical computation
Noise

ABSTRACT

Over the past two decades, vibrational resonance has garnered significant interest and evolved into a prominent research field. Classical vibrational resonance examines the response of a nonlinear system excited by two signals: a weak, slowly varying characteristic signal, and a fast-varying auxiliary signal. The characteristic signal operates on a much longer time scale than the auxiliary signal. Through the cooperation of the nonlinear system and these two excitations, the faint input can be substantially amplified, showcasing the constructive role of the fast-varying signal. Since its inception, vibrational resonance has been extensively studied across various disciplines, including physics, mathematics, biology, neuroscience, laser science, chemistry, and engineering. Here, we delve into a detailed discussion of vibrational resonance and the most recent advances, beginning with an introduction to characteristic signals commonly used in its study. Furthermore, we compile numerous nonlinear models where vibrational resonance has been observed to enhance readers' understanding and provide a basis for comparison. Subsequently, we present the metrics used to quantify vibrational resonance, as well as offer a theoretical formulation. This encompasses the method of direct separation of motions, linear and nonlinear vibrational resonance, re-scaled vibrational resonance, ultrasensitive vibrational resonance, and the role of noise in vibrational resonance. Later, we showcase two practical applications of vibrational resonance: one in image processing and the other in fault diagnosis. This presentation offers a comprehensive and versatile overview of vibrational resonance, exploring various facets and highlighting promising avenues for future research in both theory and engineering applications.

Contents

* Corresponding author.
E-mail address: miguel.sanjuan@urjc.es (M.A.F. Sanjuán).

https://doi.org/10.1016/j.physrep.2024.03.001

1. Introduction

Multiple excitations with different time scales are frequently utilized across various disciplines. These excitations may manifest as forces, electric currents, or other signal types. When a nonlinear system is subjected to simultaneous multiple excitations, the response to the slow varying excitation closely depends on the fast varying excitation. This phenomenon is known as *vibrational resonance* discovered by Landa and McClintock in their seminal paper [1]. Inspired by another well known nonlinear phenomenon, stochastic resonance [2,3], Landa and McClintock termed this new phenomenon as vibrational resonance. In their work, the role of noise in stochastic resonance is replaced by a high-frequency harmonic signal in vibrational resonance. Although vibrational resonance shares some similarities with stochastic resonance, particularly regarding dynamical behaviors, they possess distinct essential properties, thus constituting a new subfield of nonlinear dynamics [4]. Initially, vibrational resonance primarily focused on the response amplitude of a nonlinear system to a weak low-frequency harmonic excitation. Landa and McClintock conducted their initial studies of vibrational resonance in a typical bistable Duffing oscillator, examining both overdamped and underdamped versions. They found that

the response amplitude of the nonlinear system at low frequencies depends nontrivially on the amplitude of the high-frequency signal. Specifically, the curve depicting the response amplitude at low frequencies versus the amplitude of the high-frequency signal exhibits a resonance-like shape. This shape resembles the well-known frequency–response curve. At the resonance peak, the amplitude of the weak, low-frequency excitation component in the response is significantly amplified by the high-frequency signal. The classical vibrational resonance comprises three basic elements: (i) nonlinear systems, (ii) slowly varying excitation (characteristic signal), and (iii) fast varying excitation (auxiliary signal). It is important to note that the terms "fast" and "slow" are primarily used for comparing the two excitation signals, with the slowly varying excitation typically being weak. Through the interaction of these three basic elements, vibrational resonance emerges. In many cases, valuable information is conveyed through a weak, low-frequency, or slowly varying signal. Therefore, the development of vibrational resonance theory is crucial for detecting and amplifying weak signals.

In their pioneering work, Landa and McClintock introduced vibrational resonance based on numerical simulations. Subsequently, Gitterman analyzed a second-order bistable system and provided an analytical explanation for the occurrence of vibrational resonance [5]. Later, Blekhman and Landa conducted a more specific analytical study on vibrational resonance in overdamped and underdamped Duffing oscillators [6], deriving conditions for single and double resonance patterns. Furthermore, they highlighted errors between analytical and numerical simulations. The analytical technique commonly used to analyze vibrational resonance is known as the method of direct separation of motions [7–9]. This method is typically employed to obtain responses at the excitation frequency of the slowly varying harmonic signal. For more accurate results or results at nonlinear frequency components, such as the response amplitude at subharmonic, superharmonic, or combination frequencies, other analytical methods like the average method, perturbation method, multiscale method, and harmonic balance method can be used [7,10]. Compared to other methods, the derivation process of the method of direct separation of motions is simpler and more straightforward, making it the preferred choice when responses primarily involve fast and slow motions. Blekhman and Landa extensively explored vibrational resonance using the method of direct separation of motions. They analyzed vibrational resonance with single or multiple resonance patterns in various systems, including quintic oscillators with potential function in different configurations [11–14], coupled anharmonic oscillators [15,16], one-way coupled bistable systems [17], rough potential systems [18], Toda potential systems [19], periodic potential systems [20–23], quantum systems [24–26], nano-electromechanical systems [27], and chemical reaction models [28], among others.

Effects of time delay have been incorporated into the study of vibrational resonance. The delay parameter has been observed to induce periodic vibrational resonance in a simple delayed bistable system, with the period of the resonance peak relative to the time delay parameter being equal to the period of the high-frequency excitation signal [29]. In coupled systems [30–32], delay-induced vibrational resonance exhibits two periods when the delay time is sufficiently long, coinciding with the periods of the two excitations [30,32,33]. Analysis of vibrational resonance considering time delay has been conducted in various systems, including two coupled overdamped anharmonic oscillators [15], the Duffing oscillator [34,35], an asymmetric bistable system [36], the FitzHugh–Nagumo system [37–39], the discrete Rulkov neuronal model [40], a genetic toggle switch [41], a gene transcriptional regulatory system [42], and a harmonically trapped potential system [43], among others. In time-delayed systems, it has been observed that high-frequency excitation alone is not always sufficient to induce resonance in some cases [44,45]. The high-frequency excitation does influence the waveform of the response. When considering time delay in vibrational resonance, it is necessary to account for the Hopf bifurcation induced by the time delay [46]. Additionally, due to the coexistence of time delay and multiple excitations, it is essential to consider the combined effect of high-frequency excitation and the delay term on the response simultaneously.

In recent years, fractional nonlinear systems have become an important type of system for addressing various science and engineering problems. Fractional systems incorporate fractional-order derivatives, originating from the long-standing issue of fractional calculus. Specifically, while the traditional derivative order is an integer, in some special cases, it can be non-integer. Fractional nonlinear systems find widespread use in fields such as dynamic modeling, automatic control, electromagnetism, among others, and are even referred to as the 21st century system [47]. There are many interesting findings regarding vibrational resonance in fractional systems. A double resonance pattern caused by a fractional-order derivative term has been observed in an overdamped fractional Duffing oscillator [48]. Vibrational resonance has also been observed in the Duffing system with fractional-order external and intrinsic damping [49,50], fractional multistable systems [51], fractional anharmonic coupled systems [52], fractional quintic systems [53–55], fractional birhythmic biological systems [56], and fractional Toda oscillators [57], among others. Furthermore, the effects of fractional-order damping terms on vibrational resonance are directly related to the static bifurcation of fixed points of the equivalent system [58]. Specifically, at critical points of the pitchfork bifurcation [48,59–63], the saddle–node bifurcation [64], and the transcritical bifurcation [65], the response amplitude curve exhibits an inflection point, thus influencing the resonance pattern of the curve.

Vibrational resonance in neuronal models and complex networks is currently a topic of significant interest. Ullner et al. [66] investigated vibrational resonance in the FitzHugh–Nagumo neuron model. Additionally, vibrational resonance in the FitzHugh–Nagumo model has been studied from different perspectives [67–76], along with analysis in a neuron–astrocyte coupled model [77]. Vibrational resonance is also observed in single or coupled Hindmarsh–Rose neuronal systems [78]. These networks may consist of various clusters of neuronal oscillators or other types of oscillators. The influences of different network factors on vibrational resonance have been analyzed, leading to many interesting findings [79–93].

In a nonlinear system subjected to a harmonic characteristic excitation, vibrational resonance is not limited to linear response but also extends to nonlinear response frameworks. Specifically, vibrational resonance manifests at nonlinear frequencies, including the second harmonic frequency [94] and even higher-order frequencies [95–97] of the low-frequency signal. It occurs at subharmonic [98–100], superharmonic, and combination frequencies [98], as well as at the sum and difference frequencies of the low-frequency and the natural frequency of a system [101]. This phenomenon has been investigated in a two-level quantum system for both linear and nonlinear vibrational resonance responses [26].

One type of vibrational resonance is ghost vibrational resonance, which occurs as a high-frequency excitation-induced resonance at a fundamental frequency absent in the input low-frequency excitation [102–105]. Similar to stochastic resonance, ghost vibrational resonance exhibits features akin to ghost stochastic resonance [106]. Another variant, entropic vibrational resonance [107,108], shares similarities with entropic stochastic resonance [109].

Vibrational resonance induced by various characteristic signals has garnered significant attention. Apart from harmonic signals, characteristic signals can take the form of anharmonic periodic signals, aperiodic binary signals, frequency modulated signals, and other complex forms in engineering applications. Notably, binary aperiodic signals can induce aperiodic vibrational resonance. Chizhevsky and Giacomelli [110] analyzed aperiodic vibrational resonance induced by aperiodic binary excitation, introducing the cross-correlation coefficient index for analysis.

Furthermore, traditional vibrational resonance typically involves dealing with slowly varying characteristic signals. However, in many scenarios, the characteristic signal manifests as fast-varying. Vibrational resonance has been investigated in the presence of a fast characteristic signal [111–113], amplitude-modulated signals [114], aperiodic binary signals [115–117], and frequency-modulated signals [118,119]. Exploring resonance with a complex frequency-modulated signal amidst strong noise background is intriguing [120]. To quantify frequency-modulated signal-induced vibrational resonance, spectral amplification factors [119] and fusion indices [121] have been introduced. The fusion index serves to measure the necessary and sufficient conditions for vibrational resonance and describe amplification and the "similarity" of the output waveform compared to the input waveform simultaneously. Additionally, a modified cross-correlation coefficient has been utilized to eliminate errors between the input signal and system output induced by phase delay [122], thereby enhancing performance measures for aperiodic vibrational resonance.

Noise is nearly ubiquitous across various scientific and engineering fields. Understanding how nonlinear systems respond to simultaneous noise, fast, and slow excitations is a crucial concern [123]. Particularly, much work has been done to explore the beneficial effects of different types of noise on vibrational resonance. Zaikin et al. [124] have investigated vibrational resonance in coupled oscillators excited by parametric noise. They utilized a piecewise linear system for each oscillator, approximating the classical bistable system. Their findings revealed that multiplicative noise applied to each oscillator induces a phase transition, resulting in bistability. Consequently, vibrational resonance occurs, enhancing the weak signal. Essentially, a certain amount of noise fosters vibrational resonance. Subsequent analyses have delved into the interplay between stochastic resonance and vibrational resonance in various nonlinear models [125–147]. Some of these studies have identified instances where vibrational resonance enhances and controls stochastic resonance.

Very recently, there has been a growing interest in exploring vibrational resonance across various engineering applications. One notable area of exploration is vibrational resonance within energy harvesting systems [148–151]. Additionally, research has been done to investigate its potential utility in equipment fault diagnosis [152–157]. Moreover, vibrational resonance in image processing has also been investigated [158,159]. Recognizing the significance of vision research, there is a growing interest in further exploring vibrational resonance in the realm of image perception. We believe that vibrational resonance will continue to play a vital role in various engineering applications, prompting increased attention and research in this domain.

In 2020, to commemorate the 20th anniversary since the inception of the concept of vibrational resonance, as well as McClintock P V E's 80th birthday, Vincent et al. organized a thematic/special issue on nonlinear resonances in driven systems, encompassing vibrational and stochastic resonance [160,161]. This issue was published by *Philos. T. R. Soc. A*. The first part of the issue was released online in January 2021, followed by the second part in April 2021. Within this compilation, there are 11 papers dedicated to vibrational resonance [26,77,93,159,162–168]. These papers delve into vibrational resonance within quantum systems, laser systems, signal processors, logic gates, position-dependent mass systems, and energy harvesters.

Although there are monographs on vibrational resonance [58,169], a comprehensive review article is still lacking to aid researchers in gaining a better understanding of vibrational resonance and its related topics. This serves as the primary motivation behind this work. The slow-varying excitation may manifest in periodic or aperiodic forms. On one hand, different forms of excitations can induce various resonance patterns. On the other hand, vibrational resonance occurs across a spectrum of nonlinear systems. Therefore, it is essential to provide summaries of these excitations and nonlinear models. In Section 2, we introduce some typical characteristic signals in periodic or aperiodic forms. Next, we summarize the nonlinear models for vibrational resonance in Section 3. Standard performance measures of different kinds of vibrational resonance are presented in Section 4. In Section 5, we delve into the theoretical formulation of the method of direct separation of motions, linear and nonlinear vibrational resonance, and ultrasensitive vibrational resonance. Additionally, the re-scaled vibrational resonance is introduced to address the fast-varying characteristic signal, with a brief analysis of the role of noise in vibrational resonance. In Section 6, two applications of vibrational resonance are presented. Finally, in Section 7, we offer the main conclusions of the review paper and provide some future outlooks.

2. The excitations

Typically, vibrational resonance excitation consists of two signals: the characteristic signal and the auxiliary signal, which can take various forms. The characteristic signal in the following common signal types is often considered.

2.1. Periodic signal

A periodic signal is the most frequently used in various fields. Among them, the commonly used characteristic or auxiliary signal is a harmonic function. The harmonic signal with amplitude A can be in a sine waveform $s(t) = A\sin(\omega t+\phi)$ or $s(t) = A\sin(2\pi ft+\phi)$, and in a cosine waveform $s(t) = A\cos(\omega t+\phi)$ or $s(t) = A\cos(2\pi ft+\phi)$. For ω and f, their units are rad/s and Hz, respectively. The initial phase is ϕ. Additionally, there are anharmonic periodic signals, each with different effects on vibrational resonance and related phenomena. Below, we provide examples of typical anharmonic periodic signals, including:

(i) Square signal

$$s(t) = \begin{cases} A, & (2n-2)\pi/\omega < t < (2n-1)\pi/\omega, \\ -A, & (2n-1)\pi/\omega < t < 2n\pi/\omega, \end{cases} \qquad n = 1, 2, \ldots. \tag{1}$$

(ii) Asymmetric sawtooth signal

$$s(t) = \begin{cases} \frac{2At}{T}, & (2n-2)\pi/\omega < t < (2n-1)\pi/\omega, \\ \frac{2At}{T} - 2A, & (2n-1)\pi/\omega < t < 2n\pi/\omega, \end{cases} \qquad n = 1, 2, \ldots. \tag{2}$$

(iii) Symmetric sawtooth signal

$$s(t) = \begin{cases} \frac{4At}{T}, & (2n-2)\pi/\omega < t < (\frac{4n-3}{2})\pi/\omega, \\ -\frac{4At}{T} + 2A, & (\frac{4n-3}{2})\pi/\omega < t < (\frac{4n-1}{2})\pi/\omega, \\ \frac{4At}{T} - 4A, & (\frac{4n-1}{2})\pi/\omega < t < 2n\pi/\omega, \end{cases} \qquad n = 1, 2, \ldots. \tag{3}$$

(iv) Modulus of sine signal

$$s(t) = A\left|\sin\left(\frac{\omega}{2}t\right)\right|. \tag{4}$$

(v) Rectified sine signal

$$s(t) = \begin{cases} A\sin\omega t, & (2n-2)\pi/\omega < t < (2n-1)\pi/\omega, \\ 0, & (2n-1)\pi/\omega < t < 2n\pi/\omega, \end{cases} \qquad n = 1, 2, \ldots. \tag{5}$$

In the above formulas, T is the period of the excitation that is equal to $2\pi/\omega$. The slow excitation in anharmonic periodic form has been used in some works of stochastic resonance in nonlinear systems [170,171], however not much work on vibrational resonance has been done. The form of the periodic signal is found to influence directly the static bifurcation and the appearance of the vibrational resonance [172]. By Fourier series expansion, an anharmonic excitation can be viewed as the superposition of constant and infinite harmonic terms. Moreover, an anharmonic periodic excitation may induce much more complex dynamical behaviors [142,173–176]. This suggests that it is crucial to conduct more in-depth analysis of vibrational resonance induced by various anharmonic periodic excitations, encompassing both the characteristic and auxiliary signals in an anharmonic periodic form. The waveforms of a harmonic and anharmonic periodic signals mentioned above and certain other signals are given in Fig. 1. Among them, in Fig. 1(a)–(e), the periodic signals corresponding to **(i)**-**(v)** are sequentially presented. The parameters of these signals, such as the period, the duty ratio, etc., have important effects on vibrational resonance and related dynamic phenomena.

2.2. Aperiodic binary signal

The aperiodic vibrational resonance is reported in [110,115,116]. The aperiodic binary signal is governed by

$$s(t) = A\sum_{j=-\infty}^{+\infty} R_j\Gamma(t-jT), \quad \Gamma(\tau) = \begin{cases} 1, & \tau \in [0,\ T] \\ 0, & \tau \notin [0,\ T] \end{cases}. \tag{6}$$

and R_j is a random number sequence of $+1$ or -1 with an independent stochastic distribution. A is the amplitude of the aperiodic signal. $\Gamma(t)$ is a random pulse sequence with minimal pulse width T. The time series of an aperiodic binary signal is shown in Fig. 1(f).

The aperiodic vibrational resonance has been used in noisy image enhancement [158,159]. For monochrome image processing, the image is usually transformed to an aperiodic binary signal. Hence, a further study on aperiodic vibrational resonance is important. As an extension, stochastic resonance induced by an M-ary signal has been investigated in certain systems [177–179]. As an example of an application, if we deal with a gray image, we must first transform the image into an M-ary signal. Therefore, the vibrational resonance induced by an M-ary signal is worth exploring.

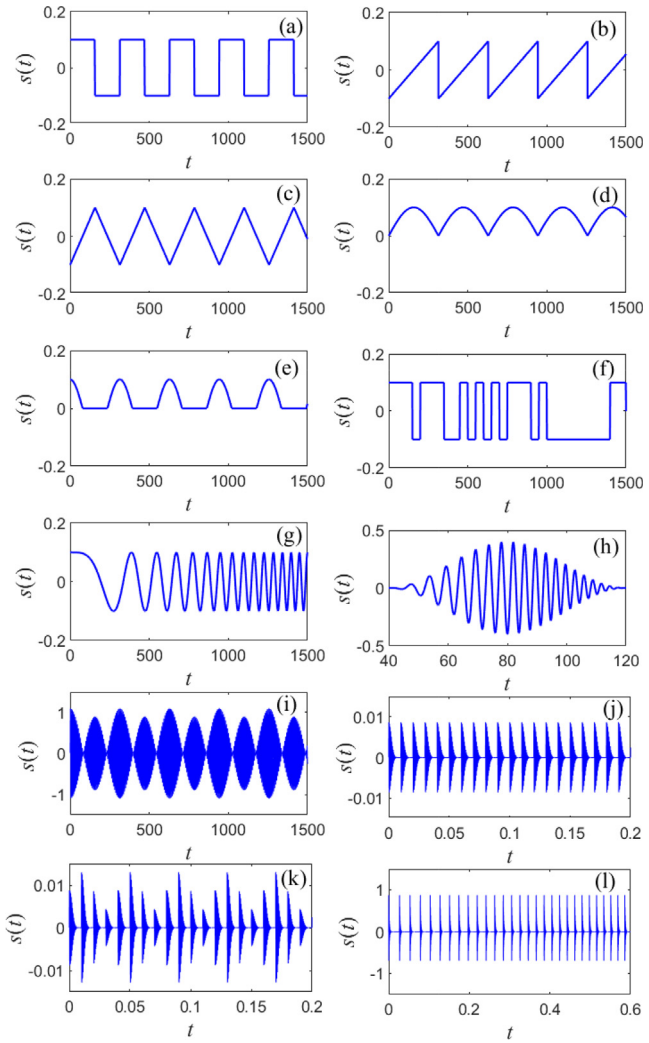

Fig. 1. Waveforms of different types of characteristic signals. (a) square signal, (b) asymmetric sawtooth signal, (c) symmetric sawtooth signal, (d) modulus of sine signal, (e) rectified cosine signal, (f) aperiodic binary signal, (g) frequency modulated signal, (h) echo chirp signal, (i) amplitude modulated harmonic signal, (j) vibration signal of a bearing with fault in out race (constant speed condition), (k) vibration signal of a bearing with fault in inner race (constant speed condition), (l) vibration signal of a bearing with fault in out race (time-varying speed condition).

2.3. Frequency-modulated signal

The linear frequency modulated signal is a simple and typical signal in science and engineering, whose form is

$$s(t) = A\cos(\pi\gamma t^2 + 2\pi f t + \phi), \tag{7}$$

where A and ϕ are the amplitude and the initial phase, respectively. γ (the chirp rate) and f (the starting frequency) characterize the modulation characteristics of the frequency. The instantaneous frequency $f_{\text{in}}(t)$ is the derivative of the phase, i.e., $f_{\text{in}}(t) = 2\pi\gamma t + 2\pi f$. The vibrational resonance caused by the linear frequency modulated signal has been studied in [118,119].

Another typical frequency modulated signal is the echo chirp signal, which is widely applied in compressed sensing, range measurement, velocity estimation, and so on [121]. The expression of each echo chirp component is

$$e(t) = \begin{cases} e^{j2\pi\left[(B/(2T))t^2 + (f_c - B/2)t\right]}, & 0 \le t \le T \\ 0, & \text{otherwise} \end{cases}. \tag{8}$$

Herein, B, T and $f_c > 0$ are the bandwidth, the duration and the central frequency, respectively. The instantaneous frequency of the echo chirp component is $f_{\text{in}} = (B/T)t + f_c - B/2$. The echo chirp signal which is composed by n chirp

components is defined as [180]

$$s(t) = \sum_{i=1}^{n} \alpha^{i-1} w(t - id - c)\Re(e(t - id - c)), \tag{9}$$

where α is the attenuation rate, d is the delay between adjacent chirp components, and c is the initial delayed time. In addition, the symbol $\Re(\bullet)$ represents the real part of the chirp signal, and $w(t)$ is given by

$$w(t) = \left\{ \begin{array}{ll} 0.5[1 - \cos(2\pi t/T)], & 0 \le t \le T \\ 0, & \text{otherwise} \end{array} \right\}. \tag{10}$$

The plots of the linear frequency modulated signal and the echo chirp signal are shown in Figs. 1(g) and 1(h), respectively. Usually, the frequency modulated signals have a very clear physical or engineering background. For example, the characteristic frequency of a vibration signal of a faulty rolling bearing is in the frequency-modulated form when the equipment operating in a variable speed condition [120]. Further, it is interesting to analyze the features of vibrational resonance induced by different forms of the nonlinear frequency modulated signal [181–185] in different engineering fields.

2.4. Amplitude modulated signal

The amplitude modulated harmonic signal induced vibrational resonance have been studied in [31,114,186–190]. The corresponding signal model is

$$s(t) = [A + B\cos \Omega t]\cos \omega t. \tag{11}$$

Its plot is given in Fig. 1(i). In addition, the amplitude modulated aperiodic binary signal is [114]

$$s(t) = [A + B\cos \Omega t] \sum_{j=-\infty}^{+\infty} R_j \Gamma(t - jT). \tag{12}$$

In fact, the vibration signal of a faulty bearing can be considered as an amplitude modulated signal. For the vibration signal of a bearing with outer race fault, its simulated signal form is [191–193]

$$\left\{ \begin{array}{c} s(t) = A\sin(2\pi f_n t)\exp\left\{-B[t - i(t)/f_0]^2\right\} \\ i(t) = \text{floor}[f_0 t] \end{array} \right., \tag{13}$$

where A is the amplitude of the pulse signal, B is the attenuation coefficient, f_n and f_0 are the natural frequency and the characteristic fault frequency, respectively. The function $i(t)$ represents the repetitions, and the function $floor[\bullet]$ is the floor function.

With an inner race or a ball element fault, the bearing vibration simulated signal is [194,195]

$$\left\{ \begin{array}{c} s(t) = \sum_i H(t)h(t - iT) \\ H(t) = A_0\cos(2\pi f_r t) + C \\ h(t) = A\cos(2\pi f_n t)\exp\left(-Bt^2\right) \end{array} \right., \tag{14}$$

where the characteristic frequency is $1/T$, and T is the period of the pulse. The function $H(t)$ is the modulated signal with amplitude A_0, C is the modulation bias, and f_r is the rotating frequency.

As shown in Figs. 1(j) and 1(k), for the signals in Eqs. (13) and (14), the periodic property and the amplitude modulation are apparently manifested. Vibrational resonance is investigated with the signals of Eqs. (13) and (14) on bearing fault diagnosis [152–157]. Different from other signal amplifier, not only the characteristic frequency is enhanced but other disturbed frequencies are suppressed.

Sometimes, the frequency and the amplitude of the characteristic signal are modulated simultaneously. We still use the bearing fault diagnosis as the engineering background. While the rotating machinery is operating in variable work conditions, the vibration signal of the bearing has both the frequency and the amplitude modulated property. For example, under the variable speed condition, the vibration signal of a bearing with outer race fault is simulated by the following signal [196]

$$\left\{ \begin{array}{l} s(t) = \sum_{m=1}^{M} A\exp\{-B[t - v(t)]\}\sin\{2\pi f_n[t - v(t)] + \phi\} \\ v(t) = \sum_{i=1}^{m-1} T_i \end{array} \right., \tag{15}$$

where m is the impulse index, T_i is the repeating period of the ith impulse. The function $v(t)$ is the total occurrence time of $(m-1)$ impulses and is a function of time t. The plot of this signal is presented in Fig. 1(l). The effect of the above signal

has been investigated by the stochastic resonance method [196]. We still need to analyze the vibrational resonance caused by this signal in the bearing fault diagnosis under different variable working conditions. With the rapid development of mechanical industry, we need to pay enough attention to the research of vibrational resonance in the field of mechanics.

2.5. Logical signal

Logical vibrational resonance has been investigated and interesting results have been reported [143,197–201]. As a result, the logical inputs can be as the characteristic signals, which are random permutations consisting of four logic states (0, 0), (0, 1), (1, 0), (1, 1). Since logical operations are widely used in the field of electronics and computer technology, the theoretical analysis, as well as the analysis oriented towards applications of logical vibrational resonance are of great importance for the future.

3. Nonlinear models of vibrational resonance

Depending on whether the system incorporates fractional damping, time delay, or noise, nonlinear models for vibrational resonance are typically classified into five main categories: ordinary differential systems, mapping systems, fractional differential systems, delayed differential systems, and stochastic differential systems. In the literature, authors may adopt different expressions or symbols to label the excitations and the equations. To simplify the system model without the need for a specific notation, we employ $s_{\mathrm{L}}(t)$, $s_{\mathrm{H}}(t)$, and $\xi(t)$ to denote the slowly-varying characteristic signal, the fast-varying auxiliary signal, and the noise, respectively.

3.1. Models with ordinary differential systems

We present several common nonlinear systems characterized by ordinary differential equation models in the investigation of vibrational resonance. These models are categorized based on the shape of the potential function, the type of damping (linear or nonlinear), the number of subsystems, and the application context of the systems.

3.1.1. Symmetric bistable oscillators

The overdamped and underdamped symmetric bistable Duffing oscillator systems are governed by

$$\dot{x} + \omega_0^2 x + \beta x^3 = s_{\mathrm{L}}(t) + s_{\mathrm{H}}(t) \tag{16}$$

and

$$\ddot{x} + \delta\dot{x} + \omega_0^2 x + \beta x^3 = s_{\mathrm{L}}(t) + s_{\mathrm{H}}(t), \tag{17}$$

respectively.

In Eqs. (16) and (17), $\omega_0^2 < 0$, $\beta > 0$ and $\delta > 0$. The potential function is

$$V(x) = \frac{1}{2}\omega_0^2 x^2 + \frac{1}{4}\beta x^4 . \tag{18}$$

In absence of $s_{\mathrm{L}}(t)$ and $s_{\mathrm{H}}(t)$, these two systems have three equilibria $x = 0$ and $x_{\pm} = \pm\sqrt{\omega_0^2/\beta}$. Many vibrational resonance works have considered this kind of system [1,5,6,94,96,98,101,102,111,119,121,127,132,141,152–155,202–205]. Vibrational resonance in a bistable system is shown in an experimental setup of Eq. (17) [206]. The symmetric bistable system is a typical model for many physical and engineering systems. In addition, if $\omega_0^2 > 0$ and $\beta > 0$, the potential function is in a monostable form with only a stable equilibrium $x = 0$; if $\omega_0^2 > 0$ and $\beta < 0$, then the system is a softening Duffing system and the potential function has a stable equilibrium $x = 0$ and two unstable equilibria $x_{\pm} = \pm\sqrt{\omega_0^2/\beta}$ [207]. In current researches on vibrational resonance, the bistable systems of Eqs. (16) and (17) are the most typical and studied models. There is a need for further research on the connection between vibrational resonance and more complex dynamical phenomena, including various bifurcation patterns, safe basin erosion [208], and others, within the framework of this typical bistable system model.

Another overdamped symmetric bistable system wherein vibrational resonance is investigated [114,115,118,209] is

$$\dot{x} + \omega_0^2 x + \beta x\,|x|^{\alpha-1} = s_{\mathrm{L}}(t) + s_{\mathrm{H}}(t). \tag{19}$$

The potential function is

$$V(x) = \frac{1}{2}\omega_0^2 x^2 + \frac{\beta}{\alpha+1}\,|x|^{\alpha+1}, \quad \omega_0^2 < 0,\ \beta > 0,\ \alpha > 0. \tag{20}$$

When $\alpha > 1$, the potential function has two stable equilibria $x_{\pm} = \pm\left(-\frac{\omega_0^2}{\beta}\right)^{\frac{1}{\alpha-1}}$ and an unstable equilibrium $x = 0$. The parameter α is a real irrational or rational number. In engineering applications, the value of α is usually related to the

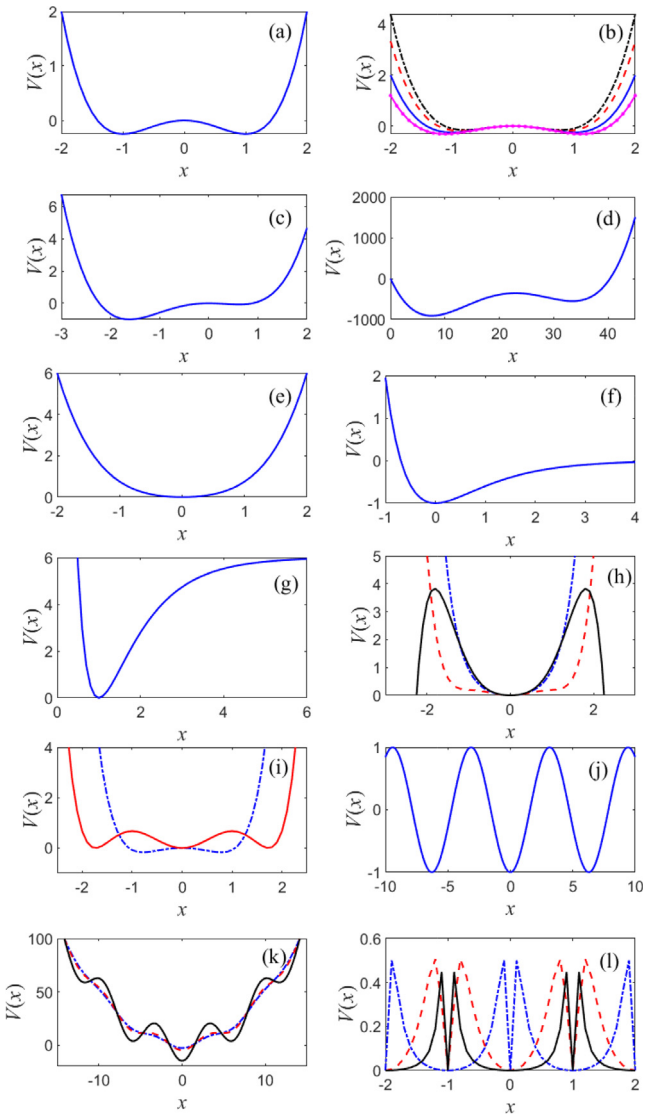

Fig. 2. Plots of the potential function of some nonlinear oscillators, (a) symmetric bistable potential in Eq. (18), (b) symmetric bistable potential in Eq. (20), (c) asymmetric bistable potential in Eq. (22), (d) asymmetric bistable potential in Eq. (24), (e) monostable potential in Eq. (18), (f) Morse potential function in Eq. (29), (g) Tietz–Hua potential in Eq. (31), (h) function in Eq. (33) with monostable potential, (i) function in Eq. (33) with bistable and tristable potentials, (j) periodic potential function, (k) harmonically trapped potential function, (l) asymmetric deformable potential function.

material property. The detailed physical background has been explained in previous works [210–212]. For the potential function, the value of α mainly influences its deepness. In the study of vibrational resonance, this kind of system can be viewed as a signal processor. For the case $\alpha = 3$, the shape of the potential function presents the typical bistable configuration which is described by Eq. (18). In addition, a suitable value of α can cause the system response to be in a stronger resonance state. It is important to investigate this kind of potential further by using analytical, experimental and numerical ways. The plots of the symmetric bistable potential function corresponding to Eqs. (18) and (20) are given in Figs. 2(a) and 2(b), respectively. Herein, we choose four different values of α to obtain the curves in Fig. 2(b).

3.1.2. Asymmetric bistable oscillators

There are many interesting asymmetric bistable systems, such as

$$\ddot{x} + \delta\dot{x} + \frac{\mathrm{d}V}{\mathrm{d}x} = s_{\mathrm{L}}(t) + s_{\mathrm{H}}(t), \tag{21}$$

where the potential function is

$$V(x) = \frac{1}{2}\omega_0^2 x^2 + \frac{1}{3}\alpha x^3 + \frac{1}{4}\beta x^4. \tag{22}$$

The potential function is in asymmetric double-well form for $\omega_0^2 < 0$, $\beta > 0$ and $\alpha \neq 0$ (see Fig. 2(c)). Vibrational resonance also takes place in the asymmetric bistable system of Eq. (21) for a wide range of input signal frequencies for which the resonance is impossible in the symmetric bistable system [213].

Another asymmetric bistable potential is

$$V(x) = \frac{1}{2}\omega_0^2 x^2 + \frac{1}{4}\beta x^4 + \gamma x, \quad \omega_0^2 < 0, \ \beta > 0, \tag{23}$$

where γ is a parameter indicating the asymmetry. Vibrational resonance is investigated also in overdamped systems with the above asymmetric potential function theoretically, numerically and experimentally [95,110,129,214]. Interestingly, the asymmetric property is necessary for the occurrence of certain types of resonances. As an illustration, logical vibrational or stochastic resonance typically manifests only in the presence of a bias parameter, and the distinct logical resonances achieved through *AND*, *NAND*, *OR*, and *NOR* calculations are contingent upon the tilting direction of the potential function. In addition, the asymmetry of the potential also influences the response amplitude curve of vibrational resonance, especially when the initial conditions are located in different potential wells in numerical calculations [64].

Another asymmetric bistable potential exists in the three-level atomic optical bistable system, e.g.,

$$\dot{x} = -\frac{\mathrm{d}V}{\mathrm{d}x} + s_\mathrm{L}(t) + s_\mathrm{H}(t), \tag{24a}$$

$$V(x) = -yx + x^2\left(\frac{c_1}{2} + \frac{c_2}{3}x + \frac{c_3}{4}x^2\right) \tag{24b}$$

where y, c_1, c_2, c_3 are all constants [215]. Here, the potential $V(x)$ is an asymmetric bistable form. The curve of the potential function is given in Fig. 2(d).

The groundwater-dependent plant ecosystem also has an asymmetric potential with three equilibria (two stable and one unstable) [216]

$$\dot{x} = x(x_\mathrm{cc} - x), \tag{25a}$$

where

$$x_\mathrm{cc} = \begin{cases} a\left[d(t) - d_\mathrm{inf}\right]\left[d_\mathrm{sup} - d(t)\right], & \text{if } d_\mathrm{inf} < d < d_\mathrm{sup} \\ 0, & \text{otherwise} \end{cases} \tag{25b}$$

$$d(t) = d_0 + \beta x + s_\mathrm{L}(t) + s_\mathrm{H}(t), \tag{25c}$$

where x is the phreatophyte biomass of the considered species, x_cc is the carrying capacity of the studied ecosystem, and $d(t)$ is the depth of groundwater level. The two excitations describe the variation of the groundwater table that caused by some factors. The potential function of the system presents an asymmetric bistable form with $x > 0$.

3.1.3. Monostable oscillators

The nano-electromechanical resonator is a monostable system [27]

$$\ddot{x} + \delta\dot{x} + \omega_0^2 x + \beta x^3 = F[1 + s_\mathrm{L}(t) + s_\mathrm{H}(t)]\cos\omega_\mathrm{f} t, \tag{26}$$

where $\omega_0^2 > 0$, $\beta > 0$, and ω_f is in the vicinity of the fundamental mode frequency. Its potential function is given by Eq. (18) with $\omega_0^2 > 0$ and $\beta > 0$. The plot of the monostable potential function is shown in Fig. 2(e).

The monostable system excited by biharmonic signals is [217]

$$\ddot{x} + \delta\dot{x} + \omega_0^2 x + \alpha x^2 + \beta x^3 = s_\mathrm{L}(t) + s_\mathrm{H}(t). \tag{27}$$

The potential function is given by Eq. (22). When $\alpha = 0$, ω_0^2, $\beta > 0$, the potential function is monostable and symmetric about $x = 0$. When $0 < \alpha^2 < 4\omega_0^2\beta$, the potential function is still in monostable form but asymmetric. When $\alpha^2 > 4\omega_0^2\beta$, the potential turns to a bistable form. An experimental setup for the system Eq. (27) was built and the underlying vibrational resonance was also investigated in this work.

The Morse oscillator can describe the photodissociation and the interatomic potential of molecules. It is a monostable system and the dynamical equation of motion is [218]

$$\ddot{x} + \delta\dot{x} + \beta\mathrm{e}^{-x}\left(1 - \mathrm{e}^{-x}\right) = s_\mathrm{L}(t) + s_\mathrm{H}(t). \tag{28}$$

The corresponding potential function is expressed as

$$V(x) = \frac{1}{2}\beta\mathrm{e}^{-x}\left(1 - \mathrm{e}^{-x}\right). \tag{29}$$

The plot of the potential function of the Morse oscillator is given in Fig. 2(f), and $V(x)$ has only one local minimum.

The system with a two-frequency-excited Tietz–Hua quantum well is also a monostable system exhibiting quantum resonance [25]. The Hamiltonian of the system is

$$H = \frac{1}{2m}p_x^2 + V_{\mathrm{TH}} + \lambda x\left(s_{\mathrm{L}}(t) + s_{\mathrm{H}}(t)\right). \tag{30}$$

The Tietz–Hua potential function is

$$V_{\mathrm{TH}}(x) = V_0\left[\frac{1-\mathrm{e}^{-b_h(x-x_{\mathrm{e}})}}{1-c_{\mathrm{h}}\mathrm{e}^{-b_{\mathrm{h}}(x-x_{\mathrm{e}})}}\right]^2. \tag{31}$$

Its graph of $V_{\mathrm{TH}}(x)$ is presented in Fig. 2(g). The Tietz–Hua potential reduces to the classical Morse potential when its potential constant c_{h} is zero.

In the above four kinds of monostable systems, all the excitations are in harmonic form, and yet the monostable system especially has advantages in processing aperiodic pulse signal under noisy background, which has been verified in extracting steel wire rope flaw detection signal based on stochastic resonance [219,220]. At present, there is very little work on vibrational resonance of monostable system under the action of different aperiodic pulse signals. The related theoretical and applied researches are worthwhile to do in the near future.

3.1.4. Quintic oscillators

Single or multiple vibrational resonance can occur in a quintic oscillator [11–14,221]

$$\ddot{x} + \delta\dot{x} + \omega_0^2 x + \beta x^3 + \gamma x^5 = s_{\mathrm{L}}(t) + s_{\mathrm{H}}(t). \tag{32}$$

The potential function is

$$V(x) = \frac{1}{2}\omega_0^2 x^2 + \frac{1}{4}\beta x^4 + \frac{1}{6}\gamma x^6. \tag{33}$$

By choosing different system parameters, the potential may be in a monostable, bistable, or tristable configuration. When $\omega_0^2, \beta, \gamma > 0$, the potential has a single-well. When $\omega_0^2, \gamma > 0$, $\beta < 0$, and $\beta^2 < 4\omega_0^2\gamma$, the potential also has a single well. When $\omega_0^2, \beta > 0$, and $\gamma < 0$, the potential has a double-hump single-well. The potential curves with different single-well shapes are presented in Fig. 2(h). When $\omega_0^2 < 0, \beta, \gamma > 0$, the potential is bistable. When $\omega_0^2, \gamma > 0$, $\beta < 0$, and $\beta^2 > 16\omega_0^2\gamma/3$, the potential has a triple-well shape. The plots of the potential with bistable and tristable cases are plotted in Fig. 2(i). The potential $V(x)$ can be used in different occasions, e.g., modeling dynamics of optical bistability, magnetoelastic beam, folded intermediates of proteins, among some other problems [11].

3.1.5. Periodic potential oscillators

There is a series of vibrational resonances appearing in the pendulum system [20,140], with overdamped version

$$\dot{x} + \sin x = s_{\mathrm{L}}(t) + s_{\mathrm{H}}(t) \tag{34}$$

or with underdamped version

$$\ddot{x} + \delta\dot{x} + \sin x = s_{\mathrm{L}}(t) + s_{\mathrm{H}}(t). \tag{35}$$

The potential function is $V(x) = -\cos x$ and its form is shown in Fig. 2(j). There are also some other modified periodic potential functions, such as $V(x) = -(1/k)[\sin kx + (1/4)\sin 2kx]$ which represents a rocking ratchet [21]. Vibrational resonance has been explored in a system featuring periodic potential, and it has been investigated in the context of cold atoms confined in an optical lattice [222].

Furthermore, vibrational resonance has been studied in a nonlinear dissipative system which has a symmetric periodic potential and a space-dependent nonlinear damping coefficient [22,223]. The system is

$$\ddot{x} + \gamma_0\left[1 - \lambda\sin(kx+\phi)\right]\dot{x} + V_0\sin kx = s_{\mathrm{L}}(t) + s_{\mathrm{H}}(t), \tag{36}$$

which is a more general case of Eq. (35).

3.1.6. Harmonically trapped and deformable potential systems

The harmonically trapped potential system is [224]

$$\ddot{x} + \delta\dot{x} + \omega_0^2 x + \beta\sin x = s_{\mathrm{L}}(t) + s_{\mathrm{H}}(t), \quad \omega_0^2 > 0, \ \beta > 0. \tag{37}$$

Its potential is $V(x) = (1/2)\omega_0^2 x^2 - \beta\cos x$. For different values of β, the potential may have one well, three wells and even more odd wells, as shown in Fig. 2(k).

Another interesting system exhibiting vibrational resonance is [225]

$$\ddot{x} + \delta\dot{x} + \frac{V_0\left(1-r^2\right)^2}{\pi}\frac{\sin(\pi x)\left[2r + \left(1+r^2\right)\cos(\pi x)\right]}{\left[1+r^2+2r\cos(\pi x)\right]^3} = s_{\mathrm{L}}(t) + s_{\mathrm{H}}(t), \tag{38}$$

with an asymmetrical deformable (Remoissenet–Peyrard) potential

$$V(x) = \frac{V_0\left(1-r^2\right)^2\left[1-\cos(2\pi x)\right]}{(2\pi)^2\left[1+r^2+2r\cos(\pi x)\right]^2}. \tag{39}$$

With different values of r, the potential presents different asymmetric deformable potentials, as shown in Fig. 2(l). When $r = 0$, the system turns to a periodic potential system. The potential described in Eq. (39) is commonly employed when examining one-dimensional atomic chains.

3.1.7. Parametric oscillators

An oscillator with one or more parameters varying with time is a parametric oscillator, also called a parametrically excited oscillator. The parametric oscillator constitutes a very important class of nonlinear systems. The parametric factor may appear in the inertia, the damping, or the stiffness term.

A bistable system with linear stiffness modulated by a low-frequency signal and excited by an external high-frequency signal is [99]

$$\ddot{x} + \delta\dot{x} + \left(\omega_0^2 x + s_{\mathrm{L}}(t)\right)x + \beta x^3 = s_{\mathrm{H}}(t). \tag{40}$$

In Eq. (40), the frequency $s_{\mathrm{H}}(t)$ is far greater than both the frequency of $s_{\mathrm{L}}(t)$ and the natural frequency ω_0.

The model of a controllable parametrically excited buckled beam is [226]

$$\ddot{x} + \delta\dot{x} + \left(\omega_0^2 + s_{\mathrm{H1}}(t)\right)x + \beta x^3 = s_{\mathrm{L}}(t) + s_{\mathrm{H2}}(t). \tag{41}$$

The oscillator is of Mathieu–Duffing type. The natural frequency of the oscillator is adjusted by a high-frequency signal and the oscillator is subjected to a low-frequency signal and another high-frequency signal simultaneously.

Besides, a cantilever beam parametrically excited is described by [227]

$$\left(1+\alpha_1 x^2\right)\ddot{x} + 2\mu_1\dot{x} + \mu_2\left|\dot{x}\right|\dot{x} + \alpha_2 x\dot{x}^2 + \left(\omega_0^2 + s_{\mathrm{L}}(t) + s_{\mathrm{H}}(t)\right)x + \alpha_3 x^3 = 0\,. \tag{42}$$

A van der Pol–Mathieu–Duffing oscillator with nonlinear damping and two external harmonic excitations with two widely different frequencies is given by [228]

$$\ddot{x} + \gamma\left(x^2-1\right)\dot{x} - \omega_0^2\left(1+h\cos\omega_{\mathrm{p}}t\right)x + \beta x^3 = s_{\mathrm{L}}(t) + s_{\mathrm{H}}(t). \tag{43}$$

The model in Eq. (43) can describe the dynamics of a micro-electro-mechanical system.

Not only the linear stiffness but also the damping can be parametrically varied with time, such as the nonlinear vibrational resonance in the van der Pol–Duffing oscillator with a parametric damping [100]

$$\ddot{x} + \gamma(1+s_{\mathrm{L}}(t))(x^2-1)\dot{x} - \omega_0^2 x + \alpha x^3 = s_{\mathrm{H}}(t). \tag{44}$$

The role of periodically parametric damping on vibrational resonance was studied also in a modulated signal excited asymmetric mixed Rayleigh–Liénard oscillator as follows [190]

$$\ddot{x} + (a_0 + s_{\mathrm{L}}(t))\dot{x} + b_1 x\dot{x} + b_2\dot{x}^2 + b_3\dot{x}^3 - E_0 - x + cx^3 = (d_1 + s_{\mathrm{H}}(t))s_{\mathrm{L}}(t). \tag{45}$$

3.1.8. Position-dependent mass oscillators

Another important kind of nonlinear system related to vibrational resonance is the position-dependent mass oscillator. The model with varying mass is usually encountered in many fields such as aeronautical and astronautical engineering, astronomy, aerology, offshore engineering, civil engineering, condensed matter physics, semiconductor heterogeneous structures, etc.

A Duffing oscillator with position-dependent mass is described by [164]

$$m(x)\ddot{x} - m^2(x)\gamma\lambda x\dot{x}^2 + \alpha\dot{x} + m^2(x)\gamma\omega_0^2 x + \beta x^3 = s_{\mathrm{L}}(t) + s_{\mathrm{H}}(t). \tag{46}$$

Herein, $m(x)$ is a position-dependent function. Roy–Layinde et al. used Eq. (46) to study the dynamics of a gas bubble.

Another position-dependent mass oscillator is [229]

$$m(x)\ddot{x} + \frac{1}{2}m'(x)\dot{x}^2 + \alpha\dot{x} + m(x)\omega_0^2 x + \beta x^3 = s_{\mathrm{L}}(t) + s_{\mathrm{H}}(t). \tag{47}$$

that describes vibrational resonance in the model of a NH3 molecule. In Eqs. (46) and (47), not only the mass but also the damping and stiffness are position-dependent.

The following nonlinear oscillator with position-dependent mass and phase-dependent damping is used to model the current through a Josephson junction [23]

$$m(x)\ddot{x} + \frac{1}{2}m'(x)\dot{x}^2 + \gamma(x)\dot{x} + V_0\sin(kx) = s_{\mathrm{L}}(t) + s_{\mathrm{H}}(t). \tag{48}$$

There is another interesting position-dependent mass oscillator which is given by [230]

$$(1+\mu x^2)\ddot{x} + \mu x\dot{x}^2 + \alpha\dot{x} + \omega_0^2 x = s_{\mathrm{L}}(t) + s_{\mathrm{H}}(t). \tag{49}$$

that describes a particle that moves on a rotating-parabola system. By some calculations and simplifications, Eq. (49) can be transformed into a quintic oscillator which is also a parametrically excited system. Vibrational resonance in a Mathews–Lakshmanan oscillator similar to Eq. (49) was also investigated in [231].

3.1.9. Nonlinearly damped oscillators

As the name implies, a nonlinearly damped oscillator has a nonlinear damping. Apparently, the systems in Eqs. (36), (42)–(49) are all nonlinearly damped oscillators. In addition to these, there are other nonlinearly damped systems that exhibit vibrational resonance. We summarize them here.

The nonlinearly damped oscillator with a rough potential is given by [18]

$$\ddot{x} - \mu\left(1 - x^2 + \nu x^4\right)\dot{x} + \frac{\mathrm{d}V}{\mathrm{d}x} = s_{\mathrm{L}}(t) + s_{\mathrm{H}}(t) \tag{50}$$

with a potential

$$V(x) = \frac{1}{2}\omega_0^2 x^2 + \frac{1}{4}\beta x^4 + \frac{1}{6}\gamma x^6 + \epsilon(\cos\omega_1 x + \sin\omega_2 x). \tag{51}$$

The model comes from a set of quasihydrodynamic equations and describes a two-fluid magnetized plasma oscillator of motion. When $\epsilon = 0$, the potential is smooth and has been given in Eq. (33). When $\epsilon \neq 0$, the potential is perturbed and increases roughly with the increase of ϵ.

The Toda oscillator in the presence of a dual-frequency forcing is [19]

$$\ddot{x} + k_0(1 + \varepsilon\cos x)\dot{x} + \mathrm{e}^x - 1 = s_{\mathrm{L}}(t) + s_{\mathrm{H}}(t). \tag{52}$$

The Toda potential is given by $V(x) = \mathrm{e}^x - x + 1$. The Toda oscillator has abundant dynamic behaviors such as bifurcations, chaos, nonlinear resonance, etc. This model comes from the study of different types of lasers. It has been also applied to DNA, and molecular dynamics of muscle contraction [232].

Anharmonic plasma oscillation induced by bi-harmonic forces is expressed as [233]

$$\ddot{x} + \varepsilon\left(1 + x^2\right)\dot{x} + \frac{\mathrm{d}V(x)}{\mathrm{d}x} = s_{\mathrm{L}}(t) + s_{\mathrm{H}}(t). \tag{53}$$

The potential function here is

$$V(x) = \frac{1}{2}\omega_0^2 x^2 + \frac{1}{3}\alpha x^3 + \frac{1}{4}\beta x^4. \tag{54}$$

This physical model refers to high density plasma interactions caused by high frequency electromagnetic waves. The model in Eq. (53) is also used to study the ghost-vibrational resonance when a multi-frequency signal with the form $\sum_{i=1}^{nf} f_i\cos(\omega_i + \Delta\omega_0)t$ instead of the slow-varying signal $s_{\mathrm{L}}(t)$ [105].

A beam with boundary conditions of two ends fixed and prestressed is modeled by [234]

$$\ddot{x} + \left(\beta_0 + \beta_2\dot{x}^2\right)\dot{x} + x + \gamma_2 x^2 + \gamma_3 x^3 = s_{\mathrm{L}}(t) + s_{\mathrm{H}}(t). \tag{55}$$

The nonlinear damping is the nonlinear dissipation of the Rayleigh type. The background of the biharmonic excitation comes from wind (slow-varying excitation) and earthquake (fast-varying excitation), or flow of people crossing the same bridge (slow-varying excitation) and vehicles crossing the bridge (fast-varying excitation).

A base-excited, tilted cantilever beam is given as [235]

$$\ddot{x} + 2\mu_1\dot{x} + \mu_2\dot{x}^3 + x + \alpha_1 x^3 + \alpha_2(x^2\ddot{x} + x\dot{x}^2) = (\eta\cos\beta - \lambda x\sin\beta)(\ddot{z}_p), \tag{56a}$$

$$z_p = s_{\mathrm{L1}}(t) + s_{\mathrm{L2}}(t) + s_{\mathrm{H}}(t), \tag{56b}$$

where z_p is the base excitation. The terms $z_p\sin\beta$ and $z_p\cos\beta$ are two displacements in two mutually perpendicular directions.

Vibrational resonance occurs in the nonlinear Rayleigh–Plesset oscillator [236]

$$\begin{aligned}\ddot{x} + \dot{x}[\alpha_0 - \alpha_1 x + \alpha_2 x^2 - \alpha_3 x^3 + \alpha_4 x^4] + \eta\dot{x}^2[1 - x + x^2] \\ -x\{\beta - [s_{\mathrm{H}}(t) + \varepsilon]s_{\mathrm{L}}(t)\} + x^2\{\gamma - [s_{\mathrm{H}}(t) + \varepsilon]s_{\mathrm{L}}(t)\} \\ -\gamma x^3 + \lambda x^4 = [s_{\mathrm{H}}(t) + \varepsilon]s_{\mathrm{L}}(t).\end{aligned} \tag{57}$$

The model is used for the study of the dynamics of a gas bubble under the excitations of complex parametric and external forces.

There is also a dynamical equation of a charged bubble excited by a modulated acoustic field and vibrating in a liquid given by [189]

$$\ddot{x} = \psi_1\psi_2 \tag{58a}$$

$$\psi_1 = \left[\frac{z_1}{x^{3\Gamma}}(1 + z_2\dot{x}) - \frac{\dot{x}^2}{2}\left(3 - \frac{\dot{x}}{c}\right) + \frac{z_3}{x^4}\left(1 - \frac{3\dot{x}}{c}\right) - \frac{z_4 + z_5\dot{x}}{x} - \Delta_1(t) - \Delta_2(t)\right] \tag{58b}$$

$$\psi_2 = \left[(1-\frac{\dot{x}}{c})x + z_{10}\right]^{-1} \tag{58c}$$

where $\Delta_1 t$ and $\Delta_2 t$ are the functions contained in the parametric modulated excitations

$$\Delta_1(t) = (1+\frac{\dot{x}}{c})\left[z_6 + z_7(1+G\sin(\Omega t))\sin(\omega t)\right], \tag{59a}$$

$$\Delta_2(t) = x\left[z_8(1+G\sin(\Omega t))\cos(\omega t) + z_9 G\sin(\omega t)\cos(\Omega t)\right]. \tag{59b}$$

Under a dual-frequency excitation, the gyroscope system mounted on a vibrating base is given by [237]

$$\ddot{x} + c_1\dot{x} + c_2\dot{x}^3 + \alpha^2\frac{(1-\cos x)^2}{\sin^3 x} - [\beta + s_{\mathrm{H}}(t)]\sin x = s_{\mathrm{L}}(t). \tag{60}$$

The system has a nonlinear damping and a parametric excitation, and the potential function may be present in a double-well or a single-well form.

Another typical damping is the resistance force expressed by the signum function. The vibrational resonance is studied in a nonlinear system with a signum nonlinearity [238]

$$\ddot{x} + \delta\dot{x} + \omega_0^2 x + \beta\,\mathrm{sgn}(x) = s_{\mathrm{L}}(t) + s_{\mathrm{H}}(t). \tag{61}$$

The sign sgn(•) is the signum function. Here, the nonlinear damping depends on the displacement of the coordinate. In fact, the nonlinear damping that depends on the velocity of the coordinate is much more widely used especially in mechanical devices. The nonlinear damping sgn($\dot{x}$) is usually viewed as a simple model of the dry friction [239]. It is significant to study vibrational resonance in friction systems due to the fact that a fast-varying excitation can quench the vibration and can be viewed as an antiresonance. There are many mathematical models belonging to different friction damping [240]. Further, the high-frequency excitation has a very important role on the friction induced mechanical vibration. It can change the properties of the stiffness, bias, and smoothness of the system [7,241–243]. Vibrational resonance in much more complex friction systems is almost blank. Investigating works in this area will contribute to nonlinear vibration and control significantly.

3.1.10. Coupled oscillators

Vibrational resonance and antiresonance in unidirectionally coupled overdamped oscillators have been studied under low-frequency and high-frequency excitations in different oscillators, as described in [244]

$$\dot{x} = x - x^3 + s_{\mathrm{H}}(t), \tag{62a}$$

$$\dot{y} = y - y^3 + \gamma x + s_{\mathrm{L}}(t), \tag{62b}$$

and mutually coupled overdamped oscillators

$$\dot{x} = x - x^3 + \gamma(x-y) + s_{\mathrm{L}}(t), \tag{63a}$$

$$\dot{y} = y - y^3 + \gamma(y-x) + s_{\mathrm{H}}(t). \tag{63b}$$

An anharmonic coupled overdamped oscillator subjected to both low-frequency and high-frequency excitations is [245]

$$\dot{x} = a_1 x - b_1 x^3 + \gamma x y^2 + s_{\mathrm{L}}(t) + s_{\mathrm{H}}(t), \tag{64a}$$

$$\dot{y} = a_2 y - b_2 y^3 + \gamma x^2 y. \tag{64b}$$

The system is viewed as a dynamical system modeling the competition between two different species. Here, $a_1 \neq a_2$ and the potential function is

$$V(x,y) = -\frac{1}{2}a_1 x^2 + \frac{1}{4}b_1 x^4 - \frac{1}{2}a_2 y^2 + \frac{1}{4}b_2 y^4 - \frac{1}{2}\gamma x^2 y^2. \tag{65}$$

If a_1, a_2, b_1, b_2, $\gamma > 0$, the potential presents a four-well shape. The system has nine or five fixed points corresponding to $\gamma^2 < b_1 b_2$ and $\gamma^2 > b_1 b_2$, respectively. In the study of this kind of oscillators, one usually chooses $a_1 \neq a_2$, and the potential has an asymmetric potential structure. Vibrational resonance of the coupled system in Eq. (65) was also studied when the excitation is in the amplitude modulated form [186].

The chemical reaction model between four molecules is described by [28]

$$\dot{x} = -2k_1 x^2 y^2 + k_2 x(1-x-y) + (F + s_{\mathrm{H}}(t))s_{\mathrm{L}}(t), \tag{66a}$$

$$\dot{y} = k_1 x^2 y^2 - k_3 y(1-x-y). \tag{66b}$$

This oscillator has abundant nonlinear dynamics such as hysteresis, vibrational resonance, multistability and chaos.

Vibrational antiresonance is investigated in the following coupled nonlinear oscillators [16]

$$\ddot{x}_1 + 2\gamma_1\dot{x}_1 - 2g_1 x_2 + \beta_1 x_1^3 - \omega_1^2 x_1 = s_{\mathrm{L}}(t) + s_{\mathrm{H}}(t), \tag{67a}$$

$$\ddot{x}_2 + 2\gamma_2\dot{x}_2 - 2g_2 x_1 + \beta_2 x_2^3 - \omega_2^2 x_2 = s_{\mathrm{H}}(t). \tag{67b}$$

Vibrational resonance and its extend application in signal transmission are investigated in a one-way coupled bistable system [17]

$$\dot{x}_1 = a_1 x_1 - b_1 x_1^2 + s_L(t) + s_H(t), \tag{68a}$$

$$\dot{x}_i = a_1 x_i - b_1 x_i^2 + \epsilon x_{i-1}, \quad i = 2, 3, \ldots, n. \tag{68b}$$

In Eq. (68), when the signal $s_L(t)$ is added on all elements x_i, there is a vibrational resonance phenomenon. When the signal $s_L(t)$ is added only on x_1, it is a signal transmission phenomenon.

Ferroelectric liquid crystal is also modeled as a coupled system [246]

$$\dot{x}_i = x_i - x_i^3 + \sum_{j=1}^{n} J_{ij}(x_j - x_i) + s_L(t) + s_H(t) + x_i w_i, \quad i = 1, 2, \ldots, n, \tag{69}$$

where J_{ij} means the coupling strength and w_i is the local liquid crystal polymer interaction. Vibrational resonance appears in this physical system as well.

3.1.11. Neural models and complex networks

Vibrational resonance has garnered increasing attention within various neural models and complex networks. Below, we provide a list of some of these models.

The single FitzHugh–Nagumo model

$$\varepsilon\dot{x} = x - \frac{1}{3}x^3 - y, \tag{70a}$$

$$\dot{y} = x + a + s_L(t) + s_H(t), \tag{70b}$$

is a typical system exhibiting vibrational resonance [66–73]. In Eq. (70b), without the excitations, a is usually considered as the bifurcation parameter. Specifically, when $a > 1$, the FitzHugh–Nagumo model has a stable equilibrium; whereas when $a < 1$, the system undergoes a supercritical Hopf bifurcation, producing a stable limit cycle, and then the equilibrium point becomes the focus of instability. The variable ε means the time scale separation parameter which is considered to be small. Under different response patterns, the subthreshold vibrational resonance or suprathreshold vibrational resonance will be present in the FitzHugh–Nagumo system [69]. In addition, vibrational resonance in a modified FitzHugh–Nagumo dynamical system has also been studied and the resonance patterns are discussed in [76]. When the excitation in Eq. (70b) is replaced by $[S_1(t) + S_2(t)][S_L(t) + S_H(t)]$, where S_1 and S_2 represent two logical signals, a comprehensive analysis of logical vibrational resonance has been carried out in detail in [201].

Vibrational resonance also occurs in small-word neuronal networks with different types of synapses [74,80,86,90,97]

$$\varepsilon\dot{x}_i = x_i - \frac{1}{3}x_i^3 - y_i - I_i^{\mathrm{syn}}, \tag{71a}$$

$$\dot{y}_i = x_i + a + s_L(t) + s_H(t), \tag{71b}$$

where I_i^{syn} is the synapse coupling expressing the synaptic current. For the case of an electrical synapse coupling, I_i^{syn} is

$$I_i^{\mathrm{syn}} = g_{\mathrm{syn}} \sum_j C_e(i,j)(x_i - x_j), \tag{71c}$$

and for case of the chemical synapse coupling, I_i^{syn} is

$$I_i^{\mathrm{syn}} = g_{\mathrm{syn}} \sum_j C_c(i,j) s_j (x_i - x_{\mathrm{syn}}), \tag{71d}$$

$$\dot{s}_j = \frac{1}{\varepsilon}\alpha(x_j)(1 - s_j) - \frac{s_j}{\tau_{\mathrm{syn}}}, \quad \alpha(x_j) = \frac{\alpha_0}{1 + \exp(-x_j/x_{\mathrm{shp}})}, \tag{71e}$$

where $\tau_{\mathrm{syn}} = 1/\delta$ represents the decay rate of the synapse. Usually, the chemical synaptic coupling is much more efficient on the low-frequency signal transmission than that of the electrical coupling due to its selective coupling.

Vibrational resonance is analyzed in small-world neuronal networks that have spike-timing-dependent plasticity [81]. This kind of networks are described as

$$\varepsilon\dot{x}_i = x_i - \frac{1}{3}x_i^3 - y_i + I_i^{\mathrm{syn}} + s_L(t) + s_H(t), \tag{72a}$$

$$\dot{y}_i = x_i + a - b_i y_i, \tag{72b}$$

with

$$I_i^{\mathrm{syn}} = -\sum_{j=1,\, j\neq i}^{N} g_{ij} C_{ij} s_j(t)(x_i - x_{\mathrm{syn}}), \quad \dot{s}_j = \alpha(x_j)(1 - s_j) - \beta s_j, \tag{72c}$$

and

$$\alpha(x_j) = \alpha_0 / \left(1 + \mathrm{e}^{-x_j/x_{\mathrm{shp}}}\right), \tag{72d}$$

$$g_{ij}^{\mathrm{ex}} = g_{ij}^{\mathrm{ex}} + \Delta g_{ij}^{\mathrm{ex}}, \quad \Delta g_{ij}^{\mathrm{ex}} = g_{ij}^{\mathrm{ex}} F(\Delta t), \tag{72e}$$

$$F(\Delta t) = \begin{cases} A_+ \exp(-|\Delta t|/\tau_+), & \text{if } \Delta t > 0, \\ -A_- \exp(-|\Delta t|/\tau_-), & \text{if } \Delta t > 0, \\ 0, & \text{if } \Delta t = 0. \end{cases} \tag{72f}$$

It was found that the inhibitory synapses may weaken vibrational resonance in this model.

Vibrational resonance was also studied in a feedforward neuron network in [87]

$$\varepsilon \dot{x}_{i,j} = x_{i,j} - \frac{1}{3}x_{i,j}^3 - y_{i,j} + I_{i,j}^{\mathrm{syn}}(t), \tag{73a}$$

$$\dot{y}_{i,j} = x_{i,j} + a_{i,j} - y_{i,j} + S_{i,j}(t), \tag{73b}$$

$$I_{i,j}^{\mathrm{syn}} = \sum_{k=1}^{N_{\mathrm{syn}}} g_{\mathrm{syn}} \alpha(t - t_{i-1,k})(V_{i,j} - V_{\mathrm{syn}}), \tag{73c}$$

where, $\alpha(t) = (t/\tau)\mathrm{e}^{-t/\tau}$. While in a feedforward neuron network with unreliable synapses [82]

$$\varepsilon \dot{x}_{i,j} = x_{i,j} - \frac{1}{3}x_{i,j}^3 - y_{i,j} + I_{i,j}^{\mathrm{syn}}, \tag{74a}$$

$$\dot{y}_{i,j} = x_{i,j} + a + I_{i,j}, \quad I_{i,j} = s_{\mathrm{L}}(t) + s_{\mathrm{H}}(t) + \varphi_{i,j}, \tag{74b}$$

$$I_{i,j}^{\mathrm{syn}} = \frac{1}{N}\sum_{k=1}^{N} G(i,j;k,j-1)[E_{\mathrm{syn}} - x_{i,j}], \tag{74c}$$

$$G(i,j;k,j\text{–}1) \leftarrow G(i,j;k,j\text{–}1) + J(i,j;k,j\text{–}1)h(i,j;k,j\text{–}1), \tag{74d}$$

and in a heterogeneous scale free neuron network [83]

$$\varepsilon \dot{x}_i = x_i - \frac{1}{3}x_i^3 - y_i + \sum_j g_{ij}(x_j - x_i), \tag{75a}$$

$$\dot{y}_i = x_i + a_i + I_{\mathrm{ex}}, \quad \langle a_i \rangle = a_0, \quad \langle (a_i - a_0)(a_j - a_0) \rangle = \delta_{ij}\sigma^2. \tag{75b}$$

Different network connections are important for weak signal propagation based on the vibrational resonance mechanism.

Vibrational resonance can also be caused by a special heterogeneous aperiodic fast-varying signal in a FitzHugh–Nagumo neuronal parallel array without connections between the neurons [89]

$$\varepsilon \dot{x}_i = x_i - \frac{1}{3}x_i^3 - y_i + s(t), \tag{76a}$$

$$\dot{y}_i = x_i + a + S_i(t), \tag{76b}$$

or with locally coupled neurons

$$\varepsilon \dot{x}_i = x_i - \frac{1}{3}x_i^3 - y_i + g[x_{i+1} + x_{i-1} - 2x_i] + s(t), \tag{77a}$$

$$\dot{y}_i = x_i + a + S_i(t), \tag{77b}$$

where g is the strength of the coupling. Herein, $s(t)$ represents the slow-varying harmonic signal, and $S_i(t)$ denotes the heterogeneous aperiodic fast-varying signal. $S_i(t)$ is generated by randomly modulating the amplitude and frequency of a sinusoidal signal. The general expression of the aperiodic stimuli is defined as $S_i(\tau_{i,j-1} + t) = A_{i,j}\sin(2\pi t/T_{i,j})$ with amplitude $A_{i,j}$ and period $T_{i,j}$. Both $A_{i,j}$ and $T_{i,j}$ obey a certain stochastic distribution.

Besides the standard FitzHugh–Nagumo neuron models, vibrational resonance was also studied in a modified FitzHugh–Nagumo neuron model [247], where the model equation is described by

$$\varepsilon \dot{x} = x - \frac{x^3}{3} - y - k_1\rho(\varphi)x + s_{\mathrm{L}}(t) + s_{\mathrm{H}}(t), \tag{78a}$$

$$\dot{y} = x + a - by, \tag{78b}$$

$$\dot{\varphi} = k_2 x - 0.5\varphi + \varphi_{ext}, \tag{78c}$$

$-k_1\rho(\varphi)x$ is the modified term, and φ_{ext} is a high-low-frequency electromagnetic radiation. They also considered vibrational resonance in the coupled modified FitzHugh–Nagumo models, i.e.,

$$\varepsilon \dot{x}_1 = x_1 - \frac{x_1^3}{3} - y_1 + s_{\mathrm{L}}(t) + s_{\mathrm{H}}(t) - k_1\rho(\varphi_1)x_1 + g(x_1 - x_2), \tag{79a}$$

$$\dot{y}_1 = x_1 + a - by_1, \tag{79b}$$
$$\dot{\varphi}_1 = k_2 x_1 - 0.5\varphi_1 + \varphi_{ext}, \tag{79c}$$
$$\varepsilon\dot{x}_2 = x_2 - \frac{x_2^3}{3} - y_2 + s_{\mathrm{L}}(t) + s_{\mathrm{H}}(t) - k_1\rho(\varphi_2)x_2 + g(x_2 - x_1), \tag{79d}$$
$$\dot{y}_2 = x_2 + a - by_2, \tag{79e}$$
$$\dot{\varphi}_2 = k_2 x_2 - 0.5\varphi_2 + \varphi_{ext}. \tag{79f}$$

Vibrational resonance is analyzed in a synthetic gene network [91]

$$\dot{x} = \frac{1 + x^2 + \alpha\sigma x^4}{[1 + x^2 + \sigma x^4][1 + y^4]} - \gamma_x x, \tag{80a}$$
$$\tau_y\dot{y} = \frac{1 + x^2 + \alpha\sigma x^4}{[1 + x^2 + \sigma x^4][1 + y^4]} - \gamma_y y + s_{\mathrm{L}}(t) + s_{\mathrm{H}}(t). \tag{80b}$$

It is interesting that the ratio of the amplitude to the frequency of the fast-varying excitation is always a definite constant when the optimal vibrational resonance occurs in this system.

The Hodgkin–Huxley neuron model excited by a biharmonic signal is studied in the equation [248]

$$\begin{aligned} C_m\dot{V} = &-\left[g_k n^4(V - V_K) + g_{\mathrm{Na}} m^3 h(V - V_{\mathrm{Na}}) + g_1(V - V_1)\right] \\ &+ I_{\mathrm{aut}} + I_0 + s_{\mathrm{L}}(t) + s_{\mathrm{H}}(t), \end{aligned} \tag{81a}$$
$$\dot{m} = \alpha_m(1 - m) - \beta_m m, \tag{81b}$$
$$\dot{n} = \alpha_n(1 - n) - \beta_n n, \tag{81c}$$
$$\dot{h} = \alpha_h(1 - h) - \beta_h h. \tag{81d}$$

In Eqs. (81), C_m is the cell capacitance, and V is the membrane potential. The parameters g_k, g_{Na} and g_l represent the maximum conductances of the potassium, the sodium and leak currents, respectively. In addition, V_K, V_{Na} and V_{l} stand for the potassium, the sodium, and the leakage reversal potentials in turn. I_0 represents the stimulus current. Based on the vibrational resonance mechanism, the inhibitory autapse significantly enhances the low-frequency subthreshold signal, despite its typically suppressive role in neuronal dynamics.

A neuron model related to the dynamics of Na^+ and K^+ is described in detail in [249]

$$C\dot{V} = -\left(I_{\mathrm{Na}} + I_{\mathrm{K}} + I_{\mathrm{sLeak}} + I_{\mathrm{pump}} + I_{\mathrm{sd}}\right) + s_{\mathrm{L}}(t) + s_{\mathrm{H}}(t), \tag{82}$$

where C is the soma capacitance and V is the membrane potential. I_{Na} and I_{K} represent the sum of Na^+ currents and the sum of K^+ currents, respectively. I_{sLeak}, I_{pump} and I_{sd} represent the leakage current, the current induced by the Na^+ and K^+ pump, and the axial current in turn. The continuous changes of the K^+ and Na^+ concentrations will cause and enhance vibrational multi-resonances.

Multiple instances of vibrational resonance were explored in various neuron systems, including a single Hindmarsh–Rose neuron, a modified Hindmarsh–Rose neuron, and coupled Hindmarsh–Rose neuron systems with or without an electric field, as reported in [78,250]. The different models are listed below.

The single Hindmarsh–Rose model is

$$\dot{x} = y - ax^3 + bx^2 - z + I_0 + s_{\mathrm{L}}(t) + s_{\mathrm{H}}(t), \tag{83a}$$
$$\dot{y} = c - dx^2 - y, \tag{83b}$$
$$\dot{z} = r[s(x + 1.56) - z], \tag{83c}$$

where x is the membrane potential, y is the recovery variable, z is the adaptation current, and I_0 represents a direct current stimulation. Multiple vibrational resonances have been observed in this single Hindmarsh–Rose neuron model.

For coupled Hindmarsh–Rose neurons without electric field, the dynamical model is

$$\dot{x}_1 = y_1 - ax_1^3 + bx_1^2 - z_1 + g_1(x_1 - x_2) + s_{\mathrm{L}}(t), \tag{84a}$$
$$\dot{y}_1 = c - dx_1^2 - y_1, \tag{84b}$$
$$\dot{z}_1 = r[s(x_1 + 1.56) - z_1], \tag{84c}$$
$$\dot{x}_2 = y_2 - ax_2^3 + bx_2^2 - z_2 + g_2(x_2 - x_1) + s_{\mathrm{H}}(t), \tag{84d}$$
$$\dot{y}_2 = c - dx_2^2 - y_2, \tag{84e}$$
$$\dot{z}_2 = r[s(x_2 + 1.56) - z_2]. \tag{84f}$$

Herein, the coupling between the two neurons are $g_1(x_1 - x_2)$ and $g_2(x_2 - x_1)$ with coupling strength g_1 and g_2. The improved Hindmarsh–Rose neuron model with external electric field is

$$\dot{x} = y - ax^3 + bx^2 - z + I_0 + s_{\mathrm{L}}(t) + s_{\mathrm{H}}(t), \tag{85a}$$

$$\dot{y} = c - dx^2 - y + RE, \tag{85b}$$
$$\dot{z} = r[s(x + 1.56) - z], \tag{85c}$$
$$\dot{E} = my + E_{\text{ext}}, \tag{85d}$$

where R is the radius size of the cell, E is the intensity of the uniform electric field, m is a parameter corresponding to the polarization property, and E_{ext} is the external electric field.

For coupled Hindmarsh–Rose neurons with electric field, the model is

$$\dot{x}_1 = y_1 - ax_1^3 + bx_1^2 - z_1 + s_{\text{L}}(t) + g_1(x_1 - x_2), \tag{86a}$$
$$\dot{y}_1 = c - dx_1^2 - y_1 + RE_1, \tag{86b}$$
$$\dot{z}_1 = r[s(x_1 + 1.56) - z_1], \tag{86c}$$
$$\dot{E}_1 = my_1 + E_{\text{ext1}}, \tag{86d}$$
$$\dot{x}_2 = y_2 - ax_2^3 + bx_2^2 - z_2 + s_{\text{H}}(t) + g_2(x_2 - x_1), \tag{86e}$$
$$\dot{y}_2 = c - dx_2^2 - y_2 + RE_2, \tag{86f}$$
$$\dot{z}_2 = r[s(x_2 + 1.56) - z_2], \tag{86g}$$
$$\dot{E}_2 = my_2 + E_{\text{ext2}}. \tag{86h}$$

Multiple vibrational resonances are prominent regardless of the presence of an electric field. Moreover, the electric field appears to attenuate the impact of multiple vibrational resonances in the single Hindmarsh–Rose neuron. Conversely, it enhances the effect of multiple vibrational resonances in the case of bidirectional coupling between two Hindmarsh–Rose neurons.

3.1.12. Circuit systems

Chua's circuit is a renowned nonlinear model known for its complex dynamical behaviors. Vibrational resonance has been observed through simulation or experimentation in numerous studies involving Chua's circuit. Below, we outline the Chua's circuit models that have been extensively discussed in the context of vibrational resonance.

The model of a single Chua's circuit is [251]

$$C_1\dot{v}_1 = (1/R)(v_2 - v_1) - f(v_1), \tag{87a}$$
$$C_2\dot{v}_2 = (1/R)(v_1 - v_2 + i_L), \tag{87b}$$
$$L\dot{i}_L = -v_2 + s_{\text{L}}(t) + s_{\text{H}}(t), \tag{87c}$$

where

$$f(v_1) = G_b v_1 + 0.5(G_a - G_b)\left[|v_1 + BP_1| - |v_1 - BP_1|\right], \tag{87d}$$

and its n-coupled form

$$C_1\dot{v}_1^{(i)} = (1/R)(v_2^{(i)} - v_1^{(i)}) - f(v_1^{(i)}), \tag{88a}$$
$$C_2\dot{v}_2^{(i)} = (1/R)(v_1^{(i)} - v_2^{(i)} + i_L^{(i)}), \tag{88b}$$
$$L\dot{i}_L^{(i)} = -v_2 + \delta_i[s_{\text{L}}(t) + s_{\text{H}}(t)] + \varepsilon_i\left(v_1^{(i-1)} - i_L^{(i)}R_C\right). \tag{88c}$$

There are two stable equilibria for the single Chua's circuit. Vibrational resonance appears when the response switches between the two stable equilibrium state. In the coupled Chua's circuits, the low-frequency signal propagation is discussed for a wide range of coupling parameter by carrying out a vibrational resonance analysis. The response amplitude at the low frequency of the ith circuit increases with its size i, eventually reaching saturation.

The modified Chua's circuit model is [103,252]

$$\dot{x} = \alpha y - \alpha F(x) + s_{\text{L}}(t) + s_{\text{H}}(t), \tag{89a}$$
$$\dot{y} = x - y + z, \tag{89b}$$
$$\dot{z} = -\beta y, \tag{89c}$$

where

$$F(x) = \epsilon x + \epsilon A\text{sgn}(x) - \epsilon A\sum_{j=0}^{n-1}[\text{sgn}(x + 2jA) + \text{sgn}(x - 2jA)] \tag{89d}$$

or

$$F(x) = \epsilon x - \epsilon A\sum_{j=0}^{n-1}[\text{sgn}(x + (2j+1)A) + \text{sgn}(x - (2j+1)A)] \tag{89e}$$

with

$$\mathrm{sgn}(x) = \begin{cases} 1, & \text{if } x > 0 \\ 0, & \text{if } x = 0 \\ -1, & \text{if } x < 0 \end{cases} \tag{89f}$$

and α, β, ϵ, $A > 0$ and $n \geq 1$. Both expressions of $F(x)$ represent sawtooth functions, yet they have distinct equilibrium points and breakpoints. Typically, the number of resonance peaks corresponds to the number of breakpoints.

The piecewise linear nonautonomous Murali–Lakshmanan–Chua circuit is [200]

$$\dot{x} = y - h(x), \tag{90a}$$
$$\dot{y} = -\beta(1+v)y - \beta x + s_{\mathrm{L}}(t) + s_{\mathrm{H}}(t), \tag{90b}$$

where

$$h(x) = \begin{cases} bx + (a-b), & \text{if } x > 1 \\ ax, & \text{if } |x| < 1 \\ bx - (a-b), & \text{if } x < -1 \end{cases} \tag{90c}$$

Both vibrational resonance and logical vibrational resonance occurs in this kind of Chua's circuit.

In addition to the Chua's circuit mentioned above, there are various models within the Chua's circuit family [253]. The dynamics induced by fast-varying and slow-varying excitations in these variants of Chua's circuits may reveal novel vibrational resonance phenomena with practical implications.

3.1.13. Energy harvesting system

Vibrational resonance occurs in an energy harvesting system which is governed by [148,149]

$$\ddot{x} + 2\delta\dot{x} - kx\left(1 - x^2\right) - \chi y = s_{\mathrm{L}}(t) + s_{\mathrm{H}}(t), \tag{91a}$$
$$\dot{y} + \lambda y + \kappa\dot{x} = 0, \tag{91b}$$

where x is the transverse displacement of the beam, while δ and k describe the damping ratio the stiffness, respectively. Regarding the other parameters, y, χ, κ denote the voltage across the load resistor, the piezoelectric coupling strength of the mechanical equation, and the piezoelectric coupling strength of the electrical equation, respectively. Additionally, $\lambda \propto 1/RC$ represents the reciprocal of the electrical circuit, where R denotes the load resistance and C represents the capacitance.

Another study on vibrational resonance involves a tri-stable energy harvester connected to a standard rectifier circuit, as discussed in [150]

$$\ddot{x} + \delta\dot{x} + \frac{dV}{dx} + \chi y = s_L(t) + s_H(t), \tag{92a}$$
$$\dot{y} + I = \dot{x}, \tag{92b}$$

where x, δ, χ and y have the same meaning as in Eq. (89), while I represents the current supplied to the standard rectifier circuit. The expression for $V(x)$ remains identical to the one presented in Eq. (33)".

Besides the external form, both slow-varying and fast-varying excitations may also manifest in parametric form within an energy harvesting system, as illustrated in the model proposed by [151]

$$\ddot{x} + 2\delta\dot{x} - kx\left(1 - x^2\right) - \chi y + [s_{\mathrm{L}}(t) + s_{\mathrm{H}}(t)]x = 0, \tag{93a}$$
$$\dot{y} + \lambda y + \kappa\dot{x} = 0, \tag{93b}$$

Here, the parametric excitation is the axial load onto the piezoelectric buckled beam harvester.

Investigation of vibrational resonance in an energy harvesting system holds promise for enhancing the efficiency of converting vibrational energy into electrical energy, offering significant engineering applications.

3.1.14. Laser system

The optimal Bloch vibrational resonance model is [24,26,254]

$$\dot{x} = -\omega_0 y, \tag{94a}$$
$$\dot{y} = \omega_0 x + \chi z f(t), \tag{94b}$$
$$\dot{z} = -\chi y f(t), \tag{94c}$$
$$f(t) = f_0 + s_{\mathrm{L}}(t) + s_{\mathrm{H}}(t), \tag{94d}$$

where $x^2 + y^2 + z^2 = 1$, ω_0 is the transition frequency of the atom, χ and f_0 are constants. Vibrational resonance in vertical-cavity surface-emitting lasers are also studied mainly experimentally [162,255–258]. In laser systems, vibrational resonance has the capability to amplify not just the weak low-frequency signal at the fundamental frequency, but also to enhance the response at subharmonic or superharmonic frequencies by appropriately selecting a high-frequency signal.

3.2. Models with maps

Depending on the complexity of the map, the response exhibits not only the conventional vibrational resonance phenomenon but also a broader range of additional dynamical phenomena.

Vibrational resonance was analyzed in the one-dimensional Bellows map [259]

$$x_{n+1} = \frac{rx_n}{1+x_n^b} + s_{\mathrm{L}}(n) + s_{\mathrm{H}}(n), \tag{95}$$

which describes the dynamical evolution of the population density of an organism, and it was analyzed also in the two-dimensional Rulkov map

$$x_{n+1} = \frac{\alpha}{1+x_n^2} + y_n + s_{\mathrm{L}}(n) + s_{\mathrm{H}}(n), \tag{96a}$$

$$y_{n+1} = y_n - \beta x_n - \sigma, \tag{96b}$$

that mimics the behavior of complex continuous time neuronal models.

The sine square map, which characterizes the hybrid optical bistable interferometer, and the sine circle map under biharmonic signals are respectively defined as follows [260]

$$x_{n+1} = A\sin^2(x_n - b) + s_{\mathrm{L}}(n) + s_{\mathrm{H}}(n) \tag{97}$$

and

$$y_{n+1} = y_n + \mu\sin(y_n) + s_{\mathrm{L}}(n) + s_{\mathrm{H}}(n). \tag{98}$$

These two kinds of maps exhibit vibrational resonance induced by high-frequency excitation.

Vibrational resonance was analyzed in detail in coupled neuronal maps in [79]

$$x_{n+1} = a_i/\left(1+x_n^2\right) + y_n + s_{\mathrm{L}}(n) + s_{\mathrm{H}}(n), \tag{99a}$$

$$y_{n+1} = y_n - \beta x_n - \gamma, \tag{99b}$$

and in small-word networks

$$x_{i,n+1} = a_i/\left(1+x_{i,n}^2\right) + y_{i,n} + \varepsilon\sum_j C(i,j)\left(x_{j,n} - x_{i,n}\right) + s_{\mathrm{L}}(n) + s_{\mathrm{H}}(n), \tag{100a}$$

$$y_{i,n+1} = y_{i,n} - \sigma_i x_{i,n} - \beta_i x_n \tag{100b}$$

and in modular networks

$$x_{I,i,n+1} = \alpha/\left(1+x_{I,i,n}^2\right) + y_{I,i,n} + I_{I,i,n}^{\mathrm{syn}} + s_{\mathrm{L}}(n) + s_{\mathrm{H}}(n), \tag{101a}$$

$$y_{I,i,n+1} = y_{I,i,n} - \beta x_{I,i,n} - \gamma, \tag{101b}$$

where

$$I_{I,i,n}^{\mathrm{syn}} = \varepsilon_{\mathrm{intra}}\sum_j A_I(i,j)\left(x_{I,j,n} - x_{I,i,n}\right) + \varepsilon_{\mathrm{inter}}\sum_j B_{I,J}(i,j)\left(x_{J,j,n} - x_{I,i,n}\right). \tag{101c}$$

The delayed discrete Rulkov neuron model is [40]

$$x_{n+1} = \frac{\alpha}{1+x_n^2} + y_n + s_{\mathrm{L}}(n) + s_{\mathrm{H}}(n), \tag{102a}$$

$$y_{n+1} = y_n - \beta x_{n-\tau} - \gamma. \tag{102b}$$

Vibrational resonance in the above Rulkov neuron model has also been explored.

3.3. Models with fractional differential systems

Three commonly used definitions for the fractional-order derivative are the Riemann–Liouville, Caputo, and Grünwald–Letnikov definitions [261] (see Appendix for details). Vibrational resonance has been investigated in certain systems involving fractional-order derivatives. The presence of fractional-order damping may lead to new vibrational resonance patterns. We outline these systems below.

There are different fractional Duffing oscillators, such as it in the overdamped version [48,112]

$$\frac{\mathrm{d}^\alpha x}{\mathrm{d}t^\alpha} + \omega_0^2 x + \beta x^3 = s_{\mathrm{L}}(t) + s_{\mathrm{H}}(t), \tag{103}$$

or in the underdamped version

$$\frac{\mathrm{d}^2x}{\mathrm{d}t^2}+\delta\frac{\mathrm{d}^\alpha x}{\mathrm{d}t^\alpha}+\omega_0^2x+\beta x^3=s_{\mathrm{L}}(t)+s_{\mathrm{H}}(t), \tag{104}$$

or with both external and intrinsic fractional-order damping terms [49]

$$\frac{\mathrm{d}^\beta x}{\mathrm{d}t^\beta}+\delta\frac{\mathrm{d}^\alpha x}{\mathrm{d}t^\alpha}+\omega_0^2x+bx^3=s_{\mathrm{L}}(t)+s_{\mathrm{H}}(t). \tag{105}$$

The fractional Duffing oscillator with asymmetric bistable potential is [64]

$$\frac{\mathrm{d}^\alpha x}{\mathrm{d}t^\alpha}-\omega_0^2x+ax^2+bx^3=s_{\mathrm{L}}(t)+s_{\mathrm{H}}(t). \tag{106}$$

Vibrational resonance is analyzed also in a quadratic oscillator [65]

$$\frac{\mathrm{d}^\alpha x}{\mathrm{d}t^\alpha}-\mu x+x^2=s_{\mathrm{L}}(t)+s_{\mathrm{H}}(t). \tag{107}$$

The fractional Mathieu–Duffing oscillator is [61]

$$\frac{\mathrm{d}^2x}{\mathrm{d}t^2}+\delta\frac{\mathrm{d}^\alpha x}{\mathrm{d}t^\alpha}+\left(\omega_0^2+s_{\mathrm{H}}(t)\right)x+\beta x^3=s_{\mathrm{L}}(t). \tag{108}$$

There are two kinds of quintic oscillators with fractional-order damping, as shown in [53,62]

$$\frac{\mathrm{d}^2x}{\mathrm{d}t^2}+\delta\frac{\mathrm{d}^\alpha x}{\mathrm{d}t^\alpha}+\omega_0^2x+\beta x^3+\gamma x^5=s_{\mathrm{L}}(t)+s_{\mathrm{H}}(t), \tag{109}$$

or in the other form [54]

$$\frac{\mathrm{d}^\beta x}{\mathrm{d}t^\beta}+\delta\frac{\mathrm{d}^\alpha x}{\mathrm{d}t^\alpha}+\omega_0^2x+\beta x^3+\gamma x^5=s_{\mathrm{L}}(t)+s_{\mathrm{H}}(t). \tag{110}$$

Under the excitations of a fast-varying parametric signal and a slow-varying external signal, the model of an oscillator with two fractional-order damping terms is given by [50]

$$\frac{\mathrm{d}^q x}{\mathrm{d}t^q}+\delta\frac{\mathrm{d}^p x}{\mathrm{d}t^p}+\left(\omega_0^2+s_{\mathrm{H}}(t)\right)x+\beta x\left|x\right|^{r-1}=s_{\mathrm{L}}(t). \tag{111}$$

The fractional-order system with the periodic potential is [51]

$$\frac{\mathrm{d}^\alpha x}{\mathrm{d}t^\alpha}+\cos ax+\frac{1}{2}\Delta\cos 2ax=s_{\mathrm{L}}(t)+s_{\mathrm{H}}(t). \tag{112}$$

Coupled fractional anharmonic oscillators are given as [52]

$$\frac{\mathrm{d}^\alpha x}{\mathrm{d}t^\alpha}=a_1x-b_1x^3+\gamma xy^2+s_{\mathrm{L}}(t)+s_{\mathrm{H}}(t), \tag{113a}$$

$$\frac{\mathrm{d}^\alpha y}{\mathrm{d}t^\alpha}=a_2y-b_2y^3+\gamma x^2y. \tag{113b}$$

3.4. Models with delayed differential systems

There are some different delayed models corresponding to vibrational resonance. A very simple example system is the overdamped bistable oscillator

$$\dot{x}+\omega_0^2x(t-\tau)+\beta x^3+r=s_{\mathrm{L}}(t)+s_{\mathrm{H}}(t). \tag{114}$$

The cases $r=0$ and $r\neq 0$ are considered in [29,33,36,45], respectively.

Vibrational resonance has been explored in the overdamped version of the delayed Duffing oscillator

$$\dot{x}+\omega_0^2x+\beta x^3+\gamma x(t-\tau)=s_{\mathrm{L}}(t)+s_{\mathrm{H}}(t), \tag{115}$$

and in underdamped version

$$\ddot{x}+\delta\dot{x}+\omega_0^2x+\beta x^3+\gamma x(t-\tau)=s_{\mathrm{L}}(t)+s_{\mathrm{H}}(t), \tag{116}$$

respectively [34]. In these two systems, the potential depends on the system parameters and may present in single-well, double-well or double-hump configuration.

The delayed harmonically trapped potential system is [43]

$$\ddot{x}+\delta\dot{x}+\omega_0^2x+\beta\sin x+rx(t-\tau)=s_{\mathrm{L}}(t)+s_{\mathrm{H}}(t). \tag{117}$$

The delayed coupled anharmonic oscillators are described by [15,30,31]

$$\dot{x} = a_1 x(t-\tau) - b_1 x^3 + \delta x y^2 + s_L(t) + s_H(t), \tag{118a}$$
$$\dot{y} = a_2 y - b_2 y^3 + \delta x^2 y \tag{118b}$$

and the globally coupled oscillators are given as [32]

$$\dot{x}_1 = x_1 - x_1^3 + \frac{\varepsilon}{N}\sum_{j=1}^{N}[x_j(t-\tau) - x_1] + s_L(t) + s_H(t), \tag{119a}$$
$$\dot{x}_i = x_i - x_i^3 + \frac{\varepsilon}{N}\sum_{j=1}^{N}[x_j(t-\tau) - x_i] + s_H(t),\ i = 2, 3, \ldots, N. \tag{119b}$$

Vibrational resonance was also investigated in the same coupled oscillators described by Eq. (118), albeit with excitations replaced by an amplitude-modulated signal, as studied in [31].

Considering multiple time delays [35], vibrational resonance was reported in a single Duffing oscillator

$$\ddot{x} + \delta\dot{x} + \omega_0^2 x + \beta x^3 + \frac{\gamma}{M}\sum_{m=1}^{M} x(t - m\tau) = s_L(t) + s_H(t) \tag{120}$$

and in coupled Duffing oscillators

$$\ddot{x}_1 + \delta\dot{x}_1 + \omega_0^2 x_1 + \beta x_1^3 = s_L(t) + s_H(t), \tag{121a}$$
$$\ddot{x}_i + \delta\dot{x}_i + \omega_0^2 x_i + \beta x_i^3 = \frac{\gamma}{M}\sum_{l=1}^{M} x_{i+1}(t - m\tau),\ i = 2, 3, \ldots, N. \tag{121b}$$

Vibrational resonance appears in the delayed single FitzHugh–Nagumo model [37,38]

$$\varepsilon\dot{x} = x - \frac{1}{3}x^3 - y, \tag{122a}$$
$$\dot{y} = x + a + K[y(t-\tau) - y] + s_L(t) + s_H(t), \tag{122b}$$

and in the delayed coupled FitzHugh–Nagumo model [39]

$$\varepsilon\dot{x}_1 = x_1 - \frac{1}{3}x_1^3 - y_1, \tag{123a}$$
$$\dot{y}_1 = x_1 + a + \frac{K}{N}\sum_{j=1}^{N}\left[y_j(t-\tau) - y_1\right] + s_L(t) + s_H(t), \tag{123b}$$
$$\varepsilon\dot{x}_i = x_i - \frac{1}{3}x_i^3 - y_i, \tag{123c}$$
$$\dot{y}_i = x_i + a + \frac{K}{N}\sum_{j=1}^{N}\left[y_j(t-\tau) - y_i\right] + s_H(t),\ i = 2, 3, \ldots, N. \tag{123d}$$

In [38], τ is time varying and $\tau = \tau_0 + \varepsilon_0 \sin\omega_0 t$. In [37,39], τ is a constant.

The delayed genetic toggle switch is [41]

$$\dot{u} = \frac{\alpha}{1+v^\beta} - u(t-\tau) + s_L(t) + s_H(t), \tag{124a}$$
$$\dot{v} = \frac{\alpha}{1+u^\beta} - v(t-\tau). \tag{124b}$$

Herein, u and v indicate the concentrations of two considered transcription factors. The excitations come from some factors such as the oscillating temperature, the experimental setting variation of the chemical inductor, etc.

The gene transcriptional regulatory system with a linear delayed term is modeled by [42]

$$\dot{x} = \frac{k_f x^2}{x^2 + K_d} - k_d x(t-\tau) + R_{bas} + s_L(t) + s_H(t). \tag{125}$$

When the delayed terms are in nonlinear form, the dynamical equation is

$$\dot{x} = \frac{k_f x^2(t-\tau)}{x^2(t-\tau) + K_d} - k_d x + R_{bas} + s_L(t) + s_H(t). \tag{126}$$

In the absence of time delay and external perturbations, the system's potential exhibits an asymmetric shape similar to the curve shown in Fig. 2(d).

Some systems also consider both fractional-order damping and time delay simultaneously. The fractional Duffing oscillators incorporating a time delay term are described in [59]

$$\frac{\mathrm{d}^{\alpha}x}{\mathrm{d}t^{\alpha}} + \omega_0^2 x + \beta x^3 + \gamma x(t-\tau) = s_{\mathrm{L}}(t) + s_{\mathrm{H}}(t), \tag{127}$$

and

$$\frac{\mathrm{d}^2x}{\mathrm{d}t^2} + \delta\frac{\mathrm{d}^{\alpha}x}{\mathrm{d}t^{\alpha}} - \omega_0^2 x + \beta x^3 + \gamma x(t-\tau) = s_{\mathrm{L}}(t) + s_{\mathrm{H}}(t), \tag{128}$$

and [262]

$$\frac{\mathrm{d}^{\alpha}x}{\mathrm{d}t^{\alpha}} + \omega_0^2 x + ax^2 + \beta x^3 + \gamma x(t-\tau) = s_{\mathrm{L}}(t) + s_{\mathrm{H}}(t). \tag{129}$$

The Duffing system with a generalized time delay term is [263]

$$\frac{\mathrm{d}^2x}{\mathrm{d}t^2} + \delta\frac{\mathrm{d}^{\alpha}x}{\mathrm{d}t^{\alpha}} + \omega_0 x + \beta x^3 + \gamma \mathrm{D}^{\alpha}x(t-\tau) = s_{\mathrm{L}}(t) + s_{\mathrm{H}}(t), \tag{130}$$

where $\mathrm{D}^{\alpha}x(t-\tau)$ is the delayed feedback in a generalized fractional-order differential form.

The fractional-order quintic oscillator with a linear time delay is investigated in the equation [264]

$$\frac{\mathrm{d}^2x}{\mathrm{d}t^2} + \delta\frac{\mathrm{d}^{\alpha}x}{\mathrm{d}t^{\alpha}} + \omega_0 x + \beta x^3 + \gamma x^5 + \xi x(t-\tau) = s_{\mathrm{L}}(t) + s_{\mathrm{H}}(t). \tag{131}$$

The fractional Mathieu–Duffing oscillator modeled with distributed time delay is [265]

$$\frac{\mathrm{d}^2x}{\mathrm{d}t^2} + \delta\frac{\mathrm{d}^{\alpha}x}{\mathrm{d}t^{\alpha}} + [a + s_{\mathrm{H}}(t)]x + bx^3 + \gamma\int_{-\infty}^{t} h(t-\tau)x(\tau)\mathrm{d}\tau = s_{\mathrm{L}}(t), \tag{132}$$

while with fixed time delay is

$$\frac{\mathrm{d}^2x}{\mathrm{d}t^2} + \delta\frac{\mathrm{d}^{\alpha}x}{\mathrm{d}t^{\alpha}} + [a + s_{\mathrm{H}}(t)]x + bx^3 + \gamma x(t-\tau) = s_{\mathrm{L}}(t). \tag{133}$$

The fractional Duffing oscillator with distributed time delay and excited by multi-frequency excitations is described as [266]

$$\begin{aligned} &m\ddot{x}(t) + c\dot{x}(t) + \delta\frac{d^{\alpha}x}{dt^{\alpha}} + kx(t) + s_{\mathrm{L1}}(t)x(t) + \beta x^3(t) \\ &+ r\int_{-\infty}^{t}\eta(t-\tau)x(\tau)d\tau = s_{\mathrm{L2}}(t) + s_{\mathrm{H}}(t). \end{aligned} \tag{134}$$

A generalized fractional Duffing–van der Pol oscillator with distributed time delay and excited by slow-varying external signal and fast-varying parametric signal was investigated in the following system [63]

$$\begin{aligned} &m\ddot{x}(t) + [c_1 + c_2x^2(t)]\dot{x}(t) + k_1x(t) + \delta_1 D_{0,t}^{q}x(t) + \alpha_1 x^3(t) \\ &+ \lambda_1\int_{-\infty}^{t} r(t-\tau)x(\tau)d\tau = s_{\mathrm{L}}(t) + x(t)s_{\mathrm{H}}(t), \end{aligned} \tag{135}$$

where $D_{0,t}^{q}x(t)$ is the fractional-order derivative with respect to the variable $x(t)$ in the Caputo definition.

3.5. Models with stochastic differential systems

Due to the significant influence of noise in various scenarios, we consider in this subsection the equation of vibrational resonance in the presence of noise.

3.5.1. Monostable systems

Vibrational resonance in a monostable system subjected to multiplicative noise in [134]

$$\dot{x} + \omega_0^2 x\xi(t) + \beta x^3 + r = \eta(t) + s_{\mathrm{L1}}(t) + s_{\mathrm{L2}}(t) + s_{\mathrm{H}}(t). \tag{136}$$

There are a fast-varying excitation, two slow-varying excitations, and two random excitations in the above equation, where $\xi(t)$ and $\eta(t)$ are uncorrelated Gaussian white noises and r is the bias parameter.

3.5.2. Bistable systems

The bistable system excited by both a slow- and fast-varying harmonic signals and a Gaussian white noise is given by [125,130]

$$\dot{x} + \omega_0^2 x + \beta x^3 = s_{\mathrm{L}}(t) + s_{\mathrm{H}}(t) + \xi(t). \tag{137}$$

The coupled piecewise linear system is a symmetric bistable system [124]

$$\dot{x}_i = f(x_i) + g(x_i)\xi_i(t) + \frac{D}{2d}\sum_{j\in nn(i)}(x_j - x_i) + s_{\mathrm{L}}(t) + s_{\mathrm{H}}(t) \tag{138a}$$

with

$$\langle \xi_i(t)\xi_j(t')\rangle = \sigma_m^2 \delta_{ij}\delta(t-t'), \tag{138b}$$

$$f(x) = \begin{cases} -G_b x - (G_a - G_b)B_{\mathrm{p}} & \text{if } x \le -B_p, \\ -G_a x & \text{if } |x| < B_{\mathrm{p}}, \\ -G_b x + (G_a - G_b)B_{\mathrm{p}} & \text{if } x \ge B_{\mathrm{p}}. \end{cases} \tag{138c}$$

The piecewise linear system can be viewed as an approximation of a typical bistable system. A similar topic was also investigated in the conventional globally coupled bistable system

$$\dot{x}_i = x_i - x_i^3 + \frac{\varepsilon}{N}\sum_{j=1}^{N}(x_j - x_i) + \sqrt{2D}\xi_i(t) + s_{\mathrm{L}}(t) + s_{\mathrm{H}}(t). \tag{139}$$

The effects of the noise and the bi-harmonic signal on the logical response of the system are investigated in the model [143]

$$\dot{x} + \omega_0^2 x(t) + \beta x^3(t) = I_1 + I_2 + r + \xi(t) + s_{\mathrm{L}}(t) + s_{\mathrm{H}}(t), \tag{140}$$

where I_1 and I_2 are two logical inputs, and $\xi(t)$ is a Gaussian white noise.

Vibrational ratchet which is very similar to vibrational resonance was investigated in the system [144–146]

$$\dot{x} = -V'(x) + s_{\mathrm{L}}(t) + s_{\mathrm{H}}(t) + \xi(t), \quad V(x) = d(1 - \cos x). \tag{141}$$

The model describes the dynamics of a Brownian particle diffusing on a one-dimensional periodic substrate. The case with

$$V(x) = \sum_{n=1}^{\infty} a_n \cos nx + \sum_{n=1}^{\infty} b_n \sin nx \tag{142}$$

has also been explored. The transport of the particle presents a vibrational ratchet effect with the cooperation of the system and the excitations. Certainly, vibrational resonance can also occur in this kind of systems.

3.5.3. The schmitt trigger circuit

The Schmitt trigger circuit is [267]

$$U_{\mathrm{out}} = \mathrm{sgn}\left[\Delta U - s_{\mathrm{L}}(t) - s_{\mathrm{H}}(t) - \xi(t)\right], \tag{143}$$

where $\Delta U = \frac{R_1}{R_1+R_2}U_{out}$ is the threshold value. U_{out} is either the positive or negative voltage $\pm U_0$ and adjusted by external signals. Here, $\xi(t)$ is a colored noise.

3.5.4. Neural models and complex networks

The role of noise on vibrational resonance was discussed in the FitzHugh–Nagumo model by adding the noise term $\xi(t)$ to the right-side of Eq. (70b) [66] and also in the FitzHugh–Nagumo model with different coupling [75]

$$\varepsilon\dot{x}_i = x_i - \frac{1}{3}x_i^3 - y_i - I_i^{\mathrm{syn}}, \tag{144a}$$

$$\dot{y}_i = x_i + a + s_{\mathrm{L}}(t) + s_{\mathrm{H}}(t) + \xi(t). \tag{144b}$$

Here, I_i^{syn} represents different kinds of coupling.

The feed-forward multilayer neural network corresponding to the Hodgkin–Huxley neuron model is governed by [84]

$$\begin{aligned} C_m\dot{V}_{i,j} = &-\left[g_k n_{i,j}^4\left(V_{i,j} - V_k\right) + g_{\mathrm{Na}}m_{i,j}^3 h_{i,j}\left(V_{i,j} - V_{\mathrm{Na}}\right) + g_l\left(V_{i,j} - V_l\right)\right] \\ &+ I_0 - I_{i,j}^{\mathrm{syn}} + a_{i,j}\left[s_{\mathrm{L}}(t) + s_{\mathrm{H}}(t)\right], \end{aligned} \tag{145a}$$

$$\dot{x}_{i,j} = \alpha_x(1 - x_{i,j}) - \beta_x x_{i,j} + \xi_{i,j}x_{i,j}, \quad x_{i,j} = m_{i,j}, n_{i,j}, h_{i,j}, \tag{145b}$$

where

$$\alpha_{m_{i,j}} = 0.1\left(V_{i,j}+40\right)/\left(1-\mathrm{e}^{-(V_{i,j}+40)/10}\right), \tag{145c}$$

$$\beta_{m_{i,j}} = 4\mathrm{e}^{-(V_{i,j}+65)/18}, \tag{145d}$$

$$\alpha_{n_{i,j}} = 0.01\left(V_{i,j}+55\right)/\left(1-\mathrm{e}^{-(V_{i,j}+55)/10}\right), \tag{145e}$$

$$\beta_{n_{i,j}} = 0.125\mathrm{e}^{-(V_{i,j}+65)/80}, \tag{145f}$$

$$\alpha_{h_{i,j}} = 0.07\mathrm{e}^{-(V_{i,j}+65)/20}, \tag{145g}$$

$$\beta_{h_{i,j}} = 1/\left(1+\mathrm{e}^{-(V_{i,j}+35)/10}\right), \tag{145h}$$

and $\xi_{i,j}(t)$ is a Gaussian white noise.

4. Performance metrics of vibrational resonance

In this section, we primarily provide performance metrics for different types of vibrational resonance. These frequently employed metrics encompass response amplitude and gain factor for harmonic component vibrational resonance, cross-correlation coefficient and bit error rate for binary aperiodic signal-induced vibrational resonance, cross-correlation coefficient and spectrum amplification factor for frequency-modulated signal-induced vibrational resonance, as well as success probability for logical vibrational resonance, among others.

4.1. Response amplitude

The response amplitude is used in measuring the response at a harmonic frequency. We label the response amplitude as Q. We extract the harmonic ω from the time series $x(t)$ by the Fourier series. The sine component Q_s and cosine component Q_c of $x(t)$ at the frequency ω are respectively calculated by

$$Q_s = \frac{2}{mT}\int_0^{mT} x(t)\sin(\omega t)\mathrm{d}t, \quad Q_c = \frac{2}{mT}\int_0^{mT} x(t)\cos(\omega t)\mathrm{d}t, \tag{146}$$

where m is a large enough positive number. Without a special explanation, $x(t)$ is a steady time series where the initial transient response has been removed. For a discrete series, the Fourier coefficients are

$$Q_s = \frac{2\Delta t}{mT}\sum_{i=1}^{mT/\Delta t} x(t_i)\sin(\omega t_i), \quad Q_c = \frac{2\Delta t}{mT}\sum_{i=1}^{mT/\Delta t} x(t_i)\cos(\omega t_i). \tag{147}$$

In Eq. (147), Δt is the time step for the numerical calculations, and T is the period of the low-frequency signal which is equal to $2\pi/\omega$. As a result, the response amplitude Q at the frequency ω is calculated by

$$Q = \sqrt{Q_s^2+Q_c^2}/A \tag{148}$$

where Q indicates the amplification of the weak low-frequency signal after is passes through the nonlinear system. Specifically, the low-frequency signal is improved Q times by the vibrational resonance.

Consider the system (16) with

$$s_{\mathrm{L}}(t) = A\cos(\omega t), \quad s_{\mathrm{H}}(t) = B\cos(\Omega t), \quad \omega \ll \Omega, \tag{149}$$

$\omega_0^2 < 0$ and $\beta > 0$. By numerical simulations, a typical vibrational resonance is shown in Fig. 3(a). With varying the amplitude B, the resonance on the $Q-B$ curve is clearly shown. Moreover, when we change the frequency Ω, we also find a vibrational resonance phenomenon, as given in Fig. 3(b). The critical value B_c at which Q becomes maximum and the corresponding maximum value $Q_{\max}$ are indicated in Fig. 3(a) for $\omega = 0.1$. The two signals in Eq. (149) are always used in the following analysis unless otherwise stated.

The output of the time series corresponding to the critical amplitude $B_c = 2.8$ for which $Q = Q_{\max} = 6.4$ is shown in Fig. 4 to present an intuitive understanding. While in Fig. 3 is given along with $s_{\mathrm{L}}(t)$ and $6.4(= Q_{\max})s_{\mathrm{L}}(t)$. In this figure, we find that the response amplitude at the low-frequency ω is greatly enhanced. It agrees with the results in Fig. 3. It presents the occurrence of vibrational resonance once again in the time domain. As illustrated by the results, the enhancement of the low-frequency characteristic signal is observed in both Fig. 3 and Fig. 4.

The response may vary depending on the initial conditions when a system has more than one stable state. Taking an asymmetric bistable system in an overdamped version as an example, the potential function is given in Eq. (22). The two harmonic excitations are $A\cos(\omega t)$ and $B\cos(\Omega t)$, respectively, where $\Omega \gg \omega$. The influence of the initial conditions on the response is illustrated in Fig. 5. Clearly, if the initial conditions differ, the response may also differ. Regarding the asymmetric bistable system, the difference is easily understandable. The tilt of the potential function causes the particle to move only in a high or a low potential well when the excitation is weak and there is no cross-well motion.

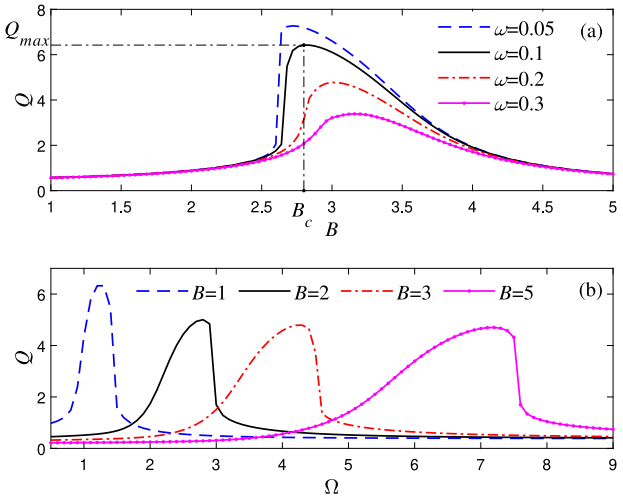

Fig. 3. Vibrational resonance induced by changing the amplitude B or the frequency Ω of the fast-varying auxiliary signal in the overdamped bistable system of Eq. (16). (a) The response amplitude Q versus the amplitude B presents vibrational resonance for four fixed values of ω. (b) The response amplitude Q versus the frequency Ω presents vibrational resonance for four fixed values of B. The parameters are $\omega_0^2 = -1$, $\beta = 1$, $A = 0.1$, $\Omega = 4$ in (a), and $\omega = 0.1$ in (b).

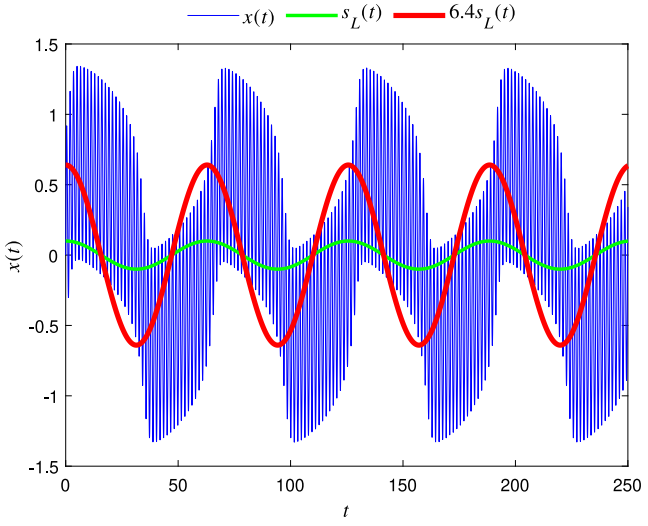

Fig. 4. Comparison of the time series of the optimal vibrational resonance response and the input low-frequency signal. The parameters are $\omega_0^2 = -1$, $\beta = 1$, $A = 0.1$, $\omega = 0.1$, $B = 2.8$, $\Omega = 4$.

Next, consider the FitzHugh–Nagumo neuron model in Eq. (70) [73], which is an excitable system subjected to biharmonic signals. The curve of Q versus B and some time series are depicted in Fig. 6. To display the periodic relationship between the signal $s_L(t)$ and the output $x(t)$ better, we give $20s_L(t)$ as a comparison in the figure. At the critical value $B = 0.058$, as shown in Fig. 6(a), $Q_{max} = 3.47$, the input signal $s_L(t)$ and the output $x(t)$ achieve the optimal synchronization. The weak slow-varying signal is amplified remarkably, and the spikes appear just in a half cycle of the slow-varying signal. For a smaller value of B, such as $B = 0.008$ in the figure, almost no spike emerges. For a larger value of B, e.g., $B = 0.075$, the spikes occur frequently. Although the output of the FitzHugh–Nagumo neuron model has a different form with the ordinary bistable system, the vibrational resonance still occurs when the system is excited by appropriate slow- and fast-varying signals. In fact, the vibrational resonance in the FitzHugh–Nagumo neuron model is complicated. It will produce the subthreshold and suprathreshold vibrational resonance. The bifurcation parameter a also influences the vibrational resonance pattern. In Fig. 6, the subthreshold vibrational resonance is shown. For other cases, a detailed discussion can be found in the work of [69].

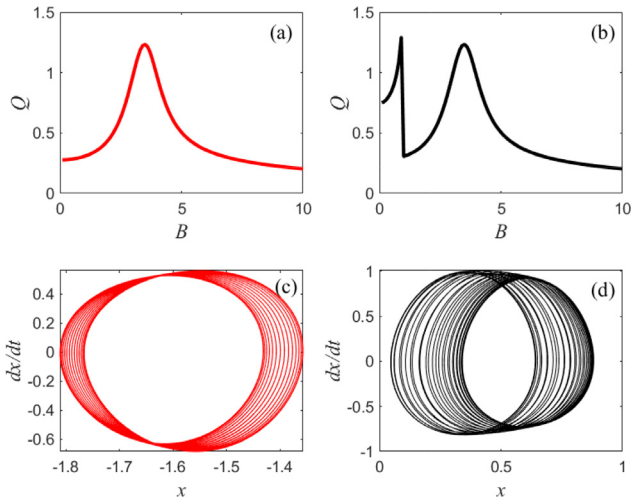

Fig. 5. Different initial conditions induce the change in the modal of vibrational resonance in the overdamped asymmetric bistable system with potential of Eq. (22). (a) The response amplitude Q versus the amplitude B of the fast-varying auxiliary signal presents single resonance. The initial condition is $x(0) = -1$. (b) The response amplitude Q versus the amplitude B of the fast-varying auxiliary signal presents double resonance. The initial condition is $x(0) = 1$. (c) The phase portrait oscillates in the left potential well under the conditions $x(0) = -1$ and $B = 0.9$. (d) The phase portrait oscillates in the right potential well under the conditions $x(0) = 1$ and $B = 0.9$. Other parameters are $\omega_0^2 = -1$, $\alpha = 1$, $\beta = 1$, $A = 0.1$, $\omega = 0.1$, $\Omega = 3$.

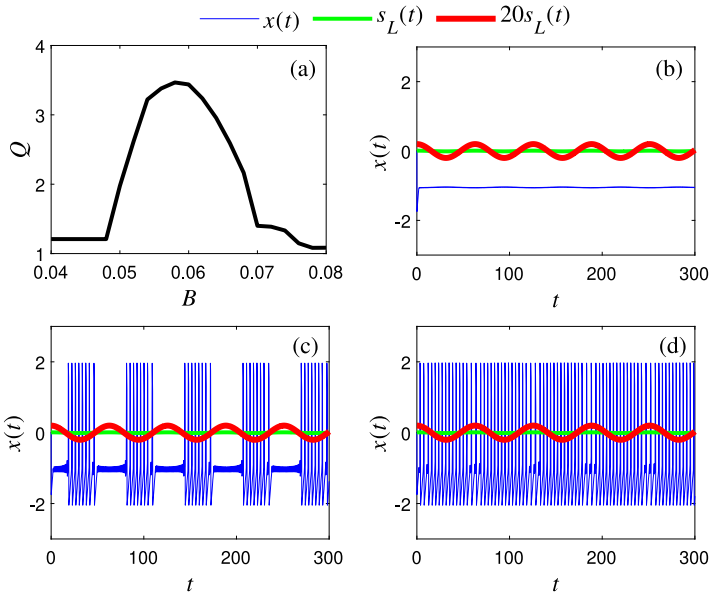

Fig. 6. The response of the FitzHugh–Nagumo neuron system of Eq. (70) to the slow-varying characteristic signal is influenced by the amplitude B of the fast-varying auxiliary signal. (a) The response amplitude Q versus the signal amplitude B presents vibrational resonance. (b)–(d) The time series of the response corresponding to different values of the signal amplitude B. The parameters are $\varepsilon = 0.01$, $a = 1.05$, $A = 0.01$, $\omega = 0.1$, $\Omega = 5$, and $B = 0.008$, 0.058, 0.075 in (b), (c), (d), respectively.

4.2. Gain factor

The phenomenon of vibrational resonance results from the interaction between the slow characteristic signal, the nonlinear system, and the fast auxiliary signal. However, a strong resonance can still occur if the system is solely driven by a single characteristic signal. This raises the question: What is the role of the fast auxiliary signal? Is it indispensable for amplifying the weak, slowly varying characteristic signal in a nonlinear system?

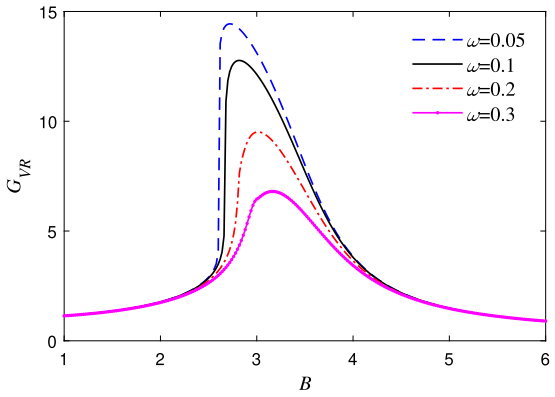

Fig. 7. The gain factor G_{VR} versus the amplitude B of the fast-varying auxiliary signal also presents vibrational resonance. All simulation parameters are the same as that in Fig. 3(a).

To reflect the role of the fast auxiliary signal on vibrational resonance directly, Chizhevsky and Giacomelli defined the gain factor of the response amplitude in their work [127,214]. The gain factor G_{VR} is calculated by

$$G_{\mathrm{VR}} = \frac{Q_{\mathrm{L}}(\omega)}{Q_0(\omega)}. \tag{150}$$

Herein, $Q_{\mathrm{L}}(\omega)$ and $Q_0(\omega)$ represent the response amplitude at the frequency of the slow-varying characteristic signal in the presence and absence of the fast-varying auxiliary signal, respectively. $Q_{\mathrm{L}}(\omega)$ and $Q_0(\omega)$ are calculated using Eq. (148). We continue to use the overdamped system in Eq. (16) as an example. The curve of G_{VR} is depicted in Fig. 7. The effect of the fast-varying auxiliary signal is clearly illustrated in the figure. Due to the presence of the auxiliary signal, similar to the results shown in Fig. 3, the weak slow-varying characteristic signal is notably amplified.

In fact, to investigate the role of the fast-varying auxiliary signal on vibrational resonance, one can consider introducing the concept of the gain factor as described in Eq. (150). Moreover, the response amplitude $Q(\omega)$ can be substituted with various other metrics such as signal-to-noise ratio (SNR), spectral amplification factor, cross-correlation coefficient, and so on, as deemed suitable.

4.3. Cross-correlation coefficient

When investigating vibrational resonance induced by an aperiodic binary signal, a commonly used metric is the cross-correlation coefficient between the system output and the input of a slowly-varying signal, as discussed in [110,115,116]. The cross-correlation coefficient is defined by

$$C_{sx} = \frac{\sum_{j=1}^{n} [s(j) - \bar{s}]\,[x(j) - \bar{x}]}{\sqrt{\sum_{j=1}^{n} [s(j) - \bar{s}]^2 \sum_{j=1}^{n} [x(j) - \bar{x}]^2}}, \tag{151}$$

where $\bar{s}$ and $\bar{x}$ are the average values of the input aperiodic signal and the output time series, respectively. The numerical value of C_{sx} lies in $[-1, 1]$. When vibrational resonance occurs, the cross-correlation coefficient usually reaches a maximum. Nevertheless, even though the cross-correlation coefficient is a large enough value, vibrational resonance does not necessarily occur. Specifically, the cross-correlation coefficient is the necessary but not sufficient condition for vibrational resonance. Thus, there is a need to establish novel metrics for assessing aperiodic vibrational resonance. Furthermore, recent studies have revealed that in cases where the system is subjected to a single aperiodic signal, the most pronounced aperiodic resonance can also manifest at the inflection point, where the correlation coefficient reaches its minimum, as reported in [268].

Here, we consider the system described by

$$\dot{x} + \omega_0^2 x + \beta x^3 = s(t) + B\mathrm{sgn}(\cos \Omega t) \tag{152}$$

where $s(t)$ is an aperiodic binary signal defined in Eq. (6). The fast-varying auxiliary signal is a periodic square signal with amplitude B. In Fig. 8, the cross-correlation coefficient corresponding to the amplitude of the fast-varying auxiliary signal is presented. At the maximal value $C_{\max}$, i.e., $B = B_c$, the response achieves the strongest aperiodic vibrational resonance. The response corresponding to the optimal aperiodic vibrational resonance is given in Fig. 9. The amplification of the weak aperiodic signal is evident.

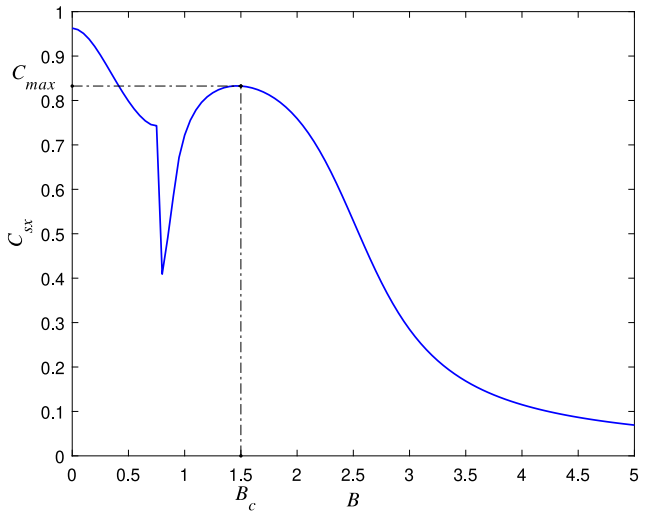

Fig. 8. The cross-correlation coefficient C_{sx} versus the amplitude B of the fast-varying auxiliary signal presents aperiodic vibrational resonance in the system of Eq. (152). The parameters are $\omega_0^2 = -1$, $\beta = 1$, $A = 0.3$, $T = 20$ and $\Omega = \pi$.

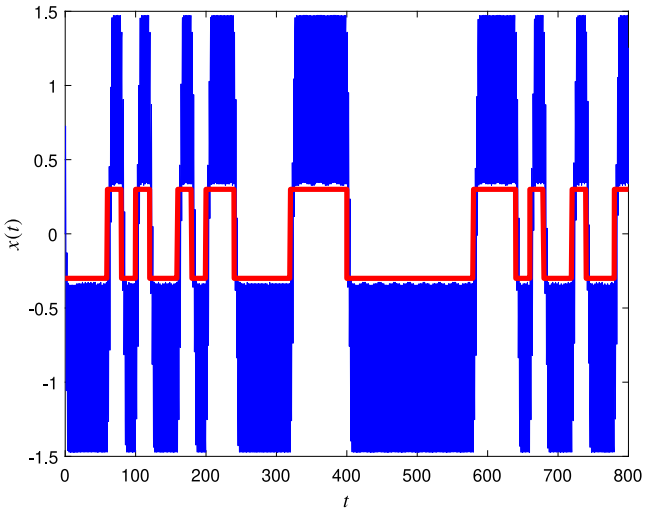

Fig. 9. Time series of the optimal aperiodic vibrational resonance caused by the binary signal in the system of Eq. (152). The thick line (red color) is the aperiodic binary characteristic signal. The thin line (blue color) is the output corresponding to the optimal aperiodic vibrational response. The parameters are $\omega_0^2 = -1$, $\beta = 1$, $A = 0.3$, $B = 1.5$, $T = 20$ and $\Omega = \pi$.

4.4. Bit error rate

The bit error rate is another commonly used metric to quantify the correctness of the output–input. The resonance occurs when the bit error rate reaches the minimum. The bit error rate has been successfully used in the stochastic resonance research [269–271]. Chizhevsky and Giacomelli introduced the bit error rate to quantify the occurrence of vibrational resonance induced by an aperiodic binary signal [110]. The bit error rate is the ratio of wrong received bits to the total number of transmitted bits. Specifically, it is the number of the received error bits divided by the total number of all transferred bits during the considered time interval. Usually, the bit error rate is a percentage number. As a result, it is important to define the correct or wrong received bits of the output. Here, there is a little difference to the conventional calculation of the bit error rate. As is well known, the response amplitude does not equal the input signal level in general. Hence, we consider that the output is correct if the absolute value of the discrete response value is greater than the given threshold value A_{th}, and vice versa. Apparently, the threshold value A_{th} is important. We still use the system in Eq. (152) as an example and give two values to plot the curves of the bit error rate versus the signal amplitude B in Fig. 10. Apparently, with the increase of the amplitude B, the minimal value of the bit error rate appears. It indicates the occurrence of aperiodic vibrational resonance. The bit error rate has the same effect as the cross-correlation coefficient.

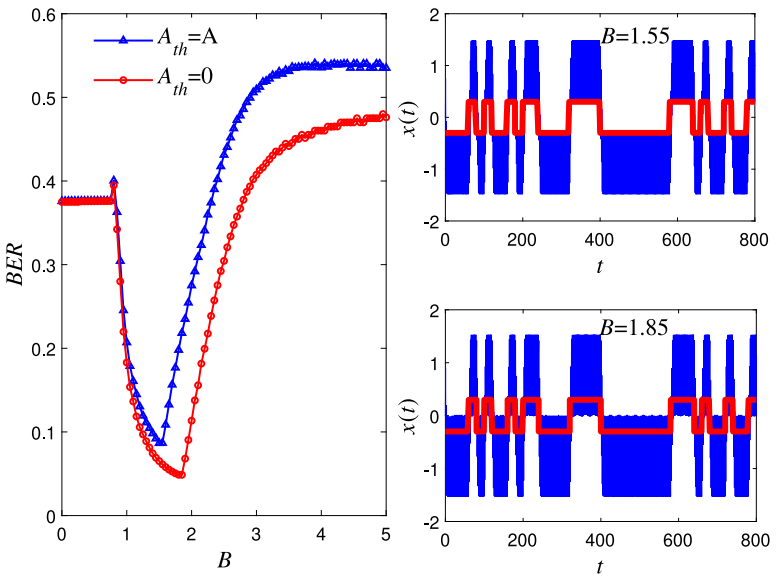

Fig. 10. The bit error rate versus the amplitude B of the fast-varying auxiliary signal presents aperiodic vibrational resonance in the system of Eq. (152) (left) and the optimal vibrational resonance response corresponding to the threshold value $A_{th} = A$ (right, top) and the threshold value $A_{th} = 0$(right, bottom), respectively. All simulation parameters are the same as those in Fig. 8.

For the case $A_{th} = 0$, it indicates that the received bit is correct if the output and the input signal have the same sign. For this case, the bit error rate achieves the minimum at $B = 1.85$. It is different from the optimal value B_c in Fig. 8. We also know that $B = 1.85$ cannot make the aperiodic vibrational resonance reach the strongest resonance output from the time series in Fig. 10. In addition, if we choose $A_{th} = A$, implies that the output amplitude is enhanced in comparison to the input level. Regarding to $A_{th} = A$, the critical value of B corresponding to the minimal of the bit error rate is $B = 1.55$. Compared with the result $B = 1.5$ in Fig. 8, there is only a minor error. This shows that using an error rate to measure resonance is also effective as long as the appropriate threshold is selected. The time series in Fig. 10 corresponding to $B = 1.55$ illustrates the feasibility of using the bit error rate as the measure of aperiodic vibrational resonance again.

4.5. Spectrum amplification factor

Consider the system [119]

$$\dot{x} - \omega_0^2 x + \beta x^3 = A\cos\left(\pi\gamma t^2 + 2\pi f t\right) + B\cos\left(k\pi\gamma t^2 + 2k\pi f t\right), \tag{153}$$

which is used to investigate vibrational resonance induced by the linear frequency modulated signal. In this equation, $A\cos\left(\pi\gamma t^2 + 2\pi f t\right)$ is the characteristic signal $s_{\mathrm{L}}(t)$, $B\cos\left(k\pi\gamma t^2 + 2k\pi f t\right)$ is the auxiliary signal $s_{\mathrm{H}}(t)$ with k is a positive number and $k \gg 1$. The instantaneous frequency of the auxiliary signal is much greater than that of the characteristic signal. We provide the plot of the characteristic signal, *i.e.*, the linear frequency modulated signal, in Fig. 11(a) and its corresponding spectrum in Fig. 11(b). Unlike the periodic signal, the spectrum of the linear frequency modulated signal is continuous. The spectrum of a periodic signal is discrete in some specific frequencies. In fact, when the frequency of the signal is varying with time, it is better to analyze the spectrum by using time–frequency analytical tools, such as the short-time Fourier transform [272], the fractional Fourier transform [273], and the empirical mode decomposition [274–276], *etc.*

For studying vibrational resonance induced by the linear frequency modulated signal, Jia et al. [119] proposed the spectrum amplification factor. At first, they used the cross-correlation coefficient to measure aperiodic vibrational resonance. Then, by a new spectrum amplification factor, they found that the new index is better for describing the vibrational resonance performance. The spectrum amplification factor η is defined by

$$\eta = \frac{\dfrac{1}{f_{\mathrm{end}} - f_{\mathrm{start}}}\displaystyle\int_{f_{\mathrm{start}}}^{f_{\mathrm{end}}} s_x\left(f_{\mathrm{in}}\right)\mathrm{d}f_{\mathrm{in}}}{\dfrac{1}{f_{\mathrm{end}} - f_{\mathrm{start}}}\displaystyle\int_{f_{\mathrm{start}}}^{f_{\mathrm{end}}} s_u\left(f_{\mathrm{in}}\right)\mathrm{d}f_{\mathrm{in}}} = \frac{\displaystyle\sum_{i=1}^{n} s_x(i)}{\displaystyle\sum_{i=1}^{n} s_u(i)}, \tag{154}$$

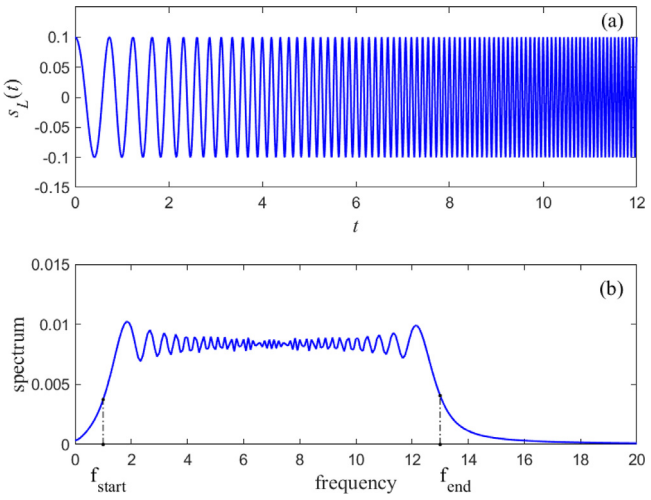

Fig. 11. The linear frequency modulated signal considered in the system of Eq. (153). (a) Time series of the input linear frequency modulated signal, (b) Spectrum of the input linear frequency modulated signal. The parameters are $A = 0.1$, $\gamma = 1$, $f = 1$.

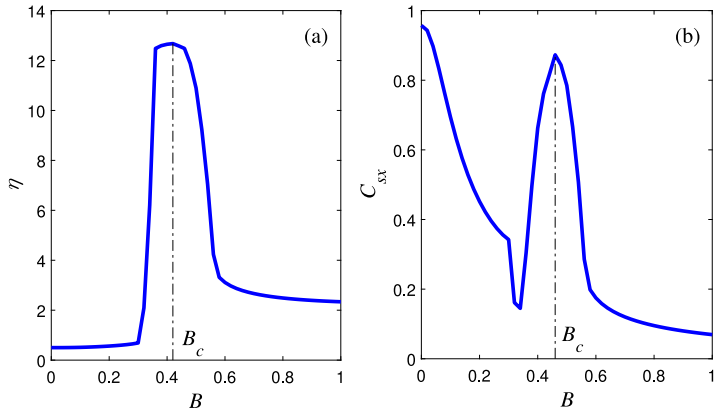

Fig. 12. Different characterizations of aperiodic vibrational resonance induced by the linear frequency modulated signal in the system of Eq. (153). (a) The spectrum amplification factor η versus the amplitude B of the fast-varying auxiliary signal presents aperiodic vibrational resonance. (b) The cross-correlation coefficient C_{sx} versus the amplitude B of the fast-varying auxiliary signal presents aperiodic vibrational resonance. The parameters are $\omega_0^2 = 300$, $\beta = 300$, $A = 0.1$, $\gamma = 1$, $f = 1$, $k = 10$.

where $s_u(\bullet)$ is the spectrum of the input linear frequency modulated signal, and $s_x(\bullet)$ is the spectrum of the system output. The spectrum amplification factor is an appropriate measure to quantify vibrational resonance in the case of driving forces considered in Eq. (153).

For the system Eq. (153), the spectrum amplification factor and the cross-correlation coefficient are given in Fig. 12(a) and Fig. 12(b), respectively. Apparently, there is only one maximal value corresponding to the peak value of the curve in Fig. 12(a). Although these two kinds of curves can prove the occurrence of vibrational resonance, in Fig. 12(b), the peak value of the curve does not correspond to the maximal value of the considered index C_{sx}. Due to the time modulation of the frequency, this kind of vibrational resonance is essentially an aperiodic vibrational resonance. It may occur at the peak of the $C_{sx} - B$ curve. For the spectrum amplification factor, the peak value of the $\eta - B$ curve corresponds to the maximal response of the system, *i.e.*, the aperiodic vibrational resonance. Besides, the spectrum amplification parameter can measure the degree of the amplification of the input characteristic signal. From the value of the optimal amplitude of the fast-varying auxiliary signal, in Fig. 12(a), at $B = 0.42$, η achieves the peak value 12.68. In Fig. 12(b), at $B = 0.46$, the peak value is $C_{sx} = 0.8729$. That is to say, the optimal amplitudes of B obtained from the two measures are approximately equal. To This method will be detailed in Section 5.4.

The response of the system corresponding to strong aperiodic vibrational resonance is illustrated in Fig. 13. To enhance clarity, we display the time series within the interval [0, 12] across four subplots. Upon comparison of the time series of $x(t)$, $s(t)$, and $12.68s(t)$, it becomes evident that the weak characteristic signal experiences significant amplification. Furthermore, the curve $12.68s(t)$ exhibits a magnitude nearly identical to that of the curve $x(t)$. This observation aligns with the peak value of the $\eta - B$ curve depicted in Fig. 12(a).

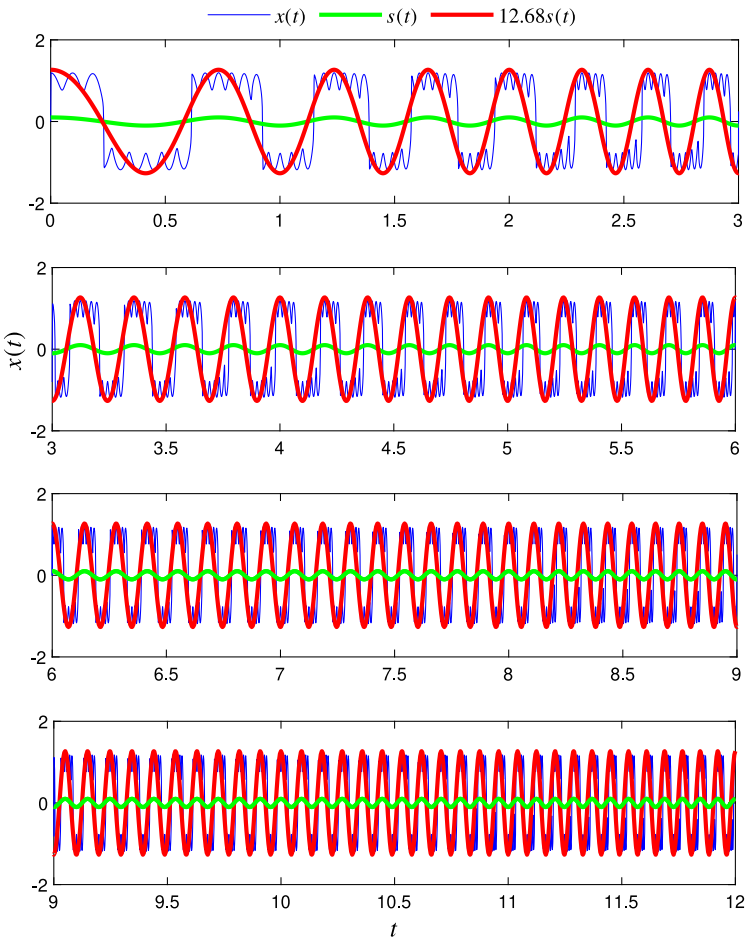

Fig. 13. Time series of the response when the optimal aperiodic vibrational resonance occurs in system of Eq. (153). The parameters are $A = 0.1$, $\gamma = 1$, $f = 1$, $B = 0.42$, $k = 10$.

Table 1
The logical calculation truth table.

Input set(I_1, I_2)	Value of $(I_1 + I_2)$	OR	AND	NOR	NAND	XOR	NXOR
(0, 0)	−1	0	0	1	1	0	1
(0, 1)/(1, 0)	0	1	0	0	1	1	0
(1, 1)	1	1	1	0	0	0	1

4.6. Success probability

We define P as the success probability, which serves as the index to measure the logical vibrational resonance

$$P = \frac{\text{The correct turns}}{\text{The total turns}}. \tag{155}$$

The specific process for obtaining the success probability P is given as follows.

1. Randomly arrange an array of four possible logical states (0,0), (0,1), (1,1), (1,0) and place it into the nonlinear system.
2. Drive the system by each logical state with the same time. Choose the total turns in a large number in the calculation. The turns mean all trajectories for the calculation.
3. Analyze the output based on the logical calculation truth table to obtain the success probability.

For the logical **OR**, **AND**, **NOR**, **NAND**, **XOR**, **NXOR**, the logical calculation truth values are given in Table 1.

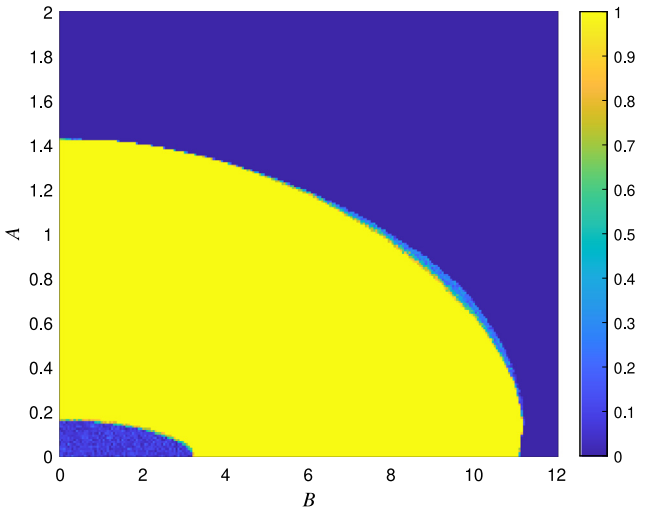

Fig. 14. There is an obvious logical vibrational resonance region corresponding to the **OR** logic operation in the two dimensional plane of the success probability with both A and B. The parameters are $\omega_0^2 = -2$, $\beta = 4$, $r = 0.5$, $\omega = 1$, $\Omega = 20$.

In the absence of noise, the logical computation in the system described by Eq. (140) involves two harmonic signals: $A\cos(\omega t)$ and $B\cos(\Omega t)$. Typically, the system output realizes **OR**, **NOR**, **AND**, and **NAND** logical calculations for $r > 0$ and $r < 0$, respectively. However, the bistable system cannot achieve **XOR** and **NXOR** calculations. To accomplish these operations using the response of a nonlinear system, it is suitable to employ a triple-well system [277]. Notably, the logical response exhibits a resonance region when varying the two harmonic signals, as depicted in Fig. 14. This phenomenon is *logical vibrational resonance*. In the simulation results shown in Fig. 14, $I_1, I_2 = -0.5$ corresponds to logic 0, and $I_1, I_2 = 0.5$ corresponds to logic 1. In this figure, for a weak slow-varying signal and a strong fast-varying signal, i.e., $B \gg A$, the logical vibrational resonance occurs. It is noteworthy that the same phenomenon occurs for a weak high-frequency signal and a strong low-frequency signal, i.e., $A \gg B$. This behavior is distinct from conventional vibrational resonance, where the amplitude of the slow-varying signal is typically very weak. In summary, appropriately chosen harmonic signals have a positive impact on the logical response of a nonlinear system.

To illustrate the logical vibrational resonance further, we show a time series plot in Fig. 15. In Figs. 15(a), (b), (d), the time series present a poor logical output. In Figs. 15(c), corresponding to the strong resonance (bright color region) in Fig. 14, the time series presents an excellent logical output.

5. Theoretical formulation of vibrational resonance

5.1. The linear response theory

The method of direct separation of motions either alone or in combination with other methods, serves as a valuable technique for analyzing the effects of a high-frequency excitation within a theoretical framework [278–291]. In this subsection, the method of direct separation of motions serves as the primary theoretical basis. Additionally, unless otherwise specified, we will consistently employ $A\cos(\omega t)$ and $B\cos(\Omega t)$ as the two excitations acting on the system.

5.1.1. Vibrational resonance in the bistable system

Taking the overdamped Duffing oscillator system Eq. (16) as an example, we introduce the method of direct separation of motions in detail. Letting

$$x(t) = X(t) + \Psi(t), \tag{156}$$

where, $X(t)$ is a slow variable with period $2\pi/\omega$, and $\Psi(\tau = \Omega t)$ is a fast variable with period 2π. Assuming the average of Ψ over the period is $\Psi_{\rm av} = (1/2\pi)\int_0^{2\pi} \Psi \mathrm{d}\tau = 0$, the equations for $X(t)$ and $\Psi(t)$ are

$$\dot{X} + \left(\omega_0^2 + 3\beta\Psi_{\rm av}^2\right)X + \beta\left(X^3 + \Psi_{\rm av}^3\right) + 3\beta X^2\Psi_{\rm av} = A\cos(\omega t), \tag{157a}$$

$$\dot{\Psi} + \omega_0^2\Psi + 3\beta X^2\left(\Psi - \Psi_{\rm av}\right) + 3\beta X\left(\Psi^2 - \Psi_{\rm av}^2\right) + \beta\left(\Psi^3 - \Psi_{\rm av}^3\right) = B\cos(\Omega t), \tag{157b}$$

where $\Psi_{\rm av}^n = (1/2\pi)\int_0^{2\pi} \Psi^n \mathrm{d}\tau$.

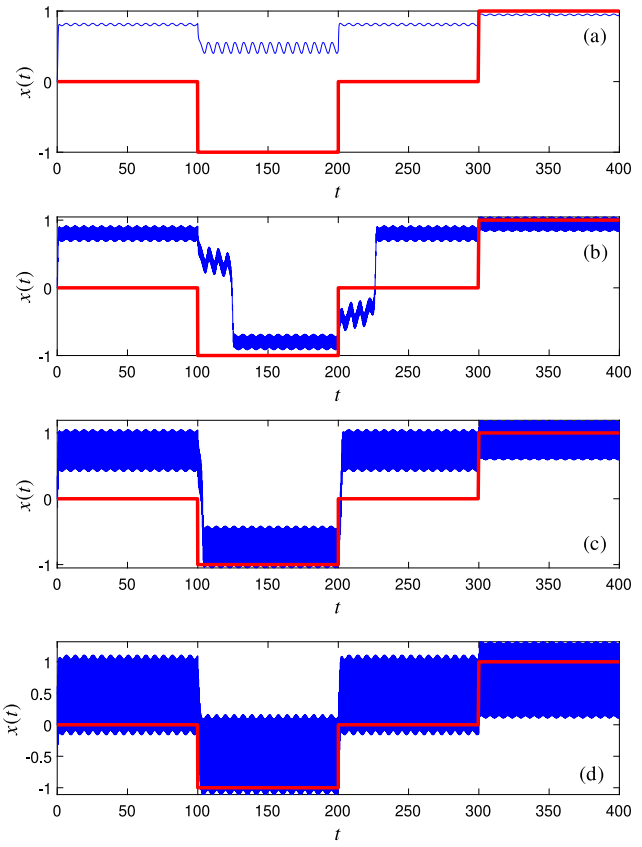

Fig. 15. Time series of the logic input $I_1 + I_2$ (thick line in red color) and logical output (thin line in blue color) of the system of Eq. (140) for different values of the amplitude B of the fast-varying auxiliary signal. The parameters are $\omega_0^2 = 2$, $\beta = 4$, $r = 0.5$, $A = 0.1$, $\omega = 1$, $\Omega = 20$, (a) $B = 0$, (b) $B = 2$, (c) $B = 6$, (d) $B = 12$.

As Ψ is fast varying, we neglect all nonlinear terms in Eq. (157b). Then, the solution of the linear equation in the limit of $t \to \infty$ is given by

$$\Psi = C\cos(\tau + \phi), \quad C = \frac{B}{\sqrt{\Omega^2 + (\omega_0^2)^2}}, \quad \phi = \tan^{-1}\left(-\frac{\Omega}{\omega_0^2}\right). \tag{158}$$

For $\Omega \gg \omega_0^2$, we can neglect the $(\omega_0^2)^2$ in the above equation and approximate the amplitude of Ψ as $g = B/\Omega$. Since $\Omega \gg \omega$, in the interval $[t, t + 2\pi/\Omega]$, $X(t)$ can be viewed as a constant. Using the Ψ given in Eq. (158), we find $\Psi_{\rm av} = 0$, $\Psi_{\rm av}^2 = C^2/2$ and $\Psi_{\rm av}^3 = 0$. Then, the equation for the slow variable (157a) becomes

$$\dot{X} + \mu X + \beta X^3 = A\cos(\omega t), \tag{159}$$

where $\mu = \frac{3}{2}\beta C^2 + \omega_0^2$.

For $\omega_0^2 < 0$ and $\beta > 0$ (bistable case), the equilibrium points of Eq. (159) when $A = 0$ are $X^* = 0$ and $X_\pm^* = \pm\sqrt{-\mu/\beta}$. In this scenario, a slow oscillation occurs around the stable equilibrium points. The parameters B and Ω are typically considered as control parameters for vibrational resonance. By adjusting these parameters, the equilibrium points and their stability can be naturally altered.

To determine the response amplitude at the frequency ω, we define $Y = X - X^*$ as the deviation of X from X^*, where X^* represents the stable equilibrium of the equivalent system (159). Then, we can derive the following expression

$$\dot{Y} + \omega_{\rm r} Y + 3\beta X^* Y^2 + \beta Y^3 = A\cos\omega t, \tag{160}$$

where $\omega_{\rm r} = \mu + 3\beta X^{*2}$. For a weak characteristic signal $A\cos\omega t$ with $A \ll 1$, $|Y| \ll 1$, making it reasonable to neglect all nonlinear terms in the equation. Then, the steady solution of the corresponding linear equation becomes $Y = A_{\rm L}\cos(\omega t + \phi)$, where

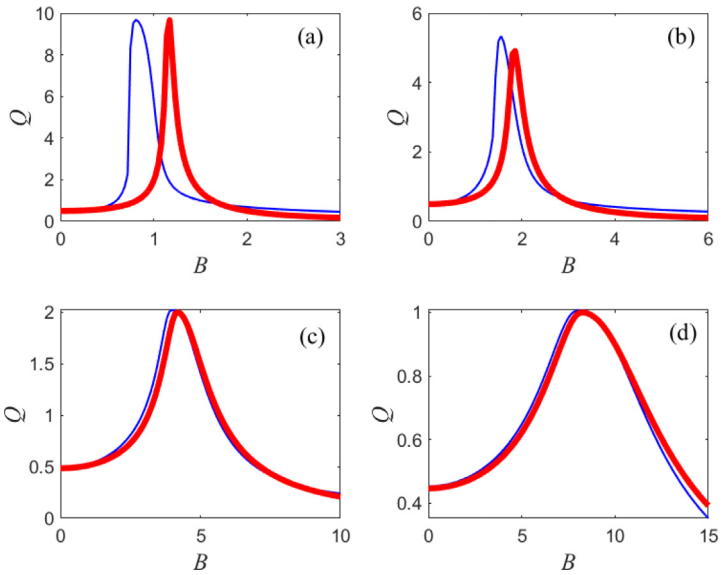

Fig. 16. Comparison between the analytical results (thick lines) and the numerical simulations (thin lines) of the response amplitude at the low-frequency ω in the system of Eq. (16). (a) $\omega = 0.1$, (b) $\omega = 0.2$, (c) $\omega = 0.5$, (d) $\omega = 1$. The parameters are $\omega_0^2 = -1$, $\beta = 1$, $A = 0.1$, $\Omega = 10\omega$.

$$A_{\mathrm{L}} = \frac{A}{\sqrt{\omega^2 + \omega_{\mathrm{r}}^2}}, \tag{161a}$$

$$\phi = \tan^{-1}\left(-\frac{\omega}{\omega_{\mathrm{r}}}\right). \tag{161b}$$

Apparently, the amplitude A_{L} is a nonlinear function of B and Ω. Then, the response amplitude Q is obtained as

$$Q = \frac{1}{\sqrt{\omega^2 + \omega_{\mathrm{r}}^2}}. \tag{162}$$

As mentioned in Section 1, the method of direct separation of motions is an approximate method that may introduce errors in certain cases. Blekhman and Landa addressed this issue in their work [6], focusing on vibrational resonance in the conventional bistable system in both overdamped, Eq. (16), and underdamped, Eq. (17), versions, respectively. In the overdamped bistable system, they compared analytical results with numerical results, as shown in Fig. 16. The curves illustrate that numerical results deviate more significantly from analytical results, especially when ω is very small. However, as ω increases, the analytical and numerical results gradually converge. Despite discrepancies in certain cases, the resonance phenomenon is clearly evident in each curve. Moreover, the errors typically remain within an acceptable range for $A \ll 1$. This analytical method, while simple, proves valuable in identifying and understanding the occurrence of vibrational resonance. Consequently, the method of direct separation of motions finds widespread use in vibrational resonance studies. Additionally, another similar linear response theory method is discussed in [292].

The resonance behavior can be obtained analytically by the expression of Q. We usually focus on the maximal value Q_{max} and the corresponding value B_{VR}. From Eq. (162), we note that Q will be maximum when ω_{r}^2 achieves a minimum. According to the formula of ω_{r} in Eq. (160), it is easy to get that $\omega_{\mathrm{r}}^2 = 0$ when $B = B_{VR} = B_{\mathrm{c}}$, and

$$B_{VR} = \sqrt{\frac{-2\omega_0^2\left[\Omega^2 + (\omega_0^2)\right]}{3\beta}}. \tag{163}$$

In addition, B_{c} denotes the pitchfork bifurcation point of Eq. (159). Specifically, when $B < B_{\mathrm{c}}$, the equivalent system has one unstable equilibrium point $X^* = 0$ and two stable equilibrium points $X_{\pm}^* = \pm\sqrt{-\mu/\beta}$. Conversely, when $B \geq B_c$, only one stable equilibrium point $X^* = 0$ exists in the equivalent system (159). Furthermore, ω_r behaves as a decreasing monotone function when $B < B_{\mathrm{c}}$ and as a monotone increasing function when $B \geq B_{\mathrm{c}}$. Consequently, the response amplitude Q monotonically increases when $B < B_{\mathrm{c}}$ and monotonically decreases when $B \geq B_{\mathrm{c}}$. Likewise, there is only one peak in the $Q - B$ curve at the pitchfork bifurcation $B = B_{\mathrm{VR}} = B_{\mathrm{c}}$, with the corresponding peak value being $Q = \frac{1}{\omega}$. These peak values are corroborated by Fig. 16 for various values of ω. It is noteworthy that double resonance peaks may emerge if the overdamped bistable system is in a fractional-order version, as in Eq. (103). Specifically, double resonance peaks may appear when the fractional order satisfies $\alpha > 1$ [48]. However, these double resonance peaks do not appear in the $Q - B$ curve of the ordinary differential system Eq. (16).

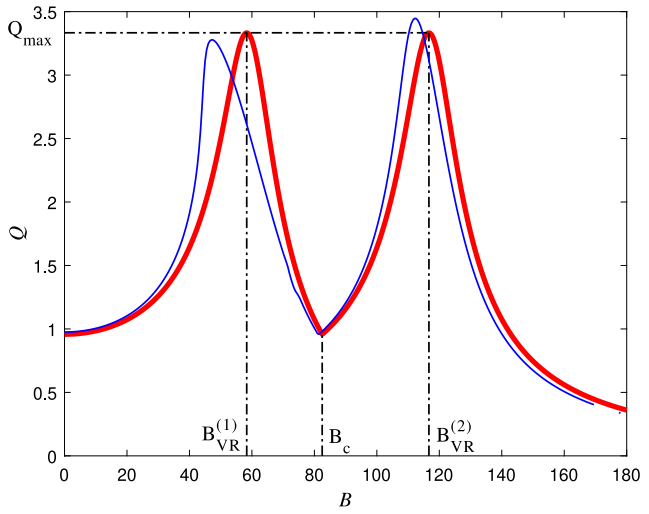

Fig. 17. The response amplitude Q versus the amplitude B of the fast-varying auxiliary signal presents double vibrational resonance in the underdamped bistable system of Eq. (17). The thick solid line is plotted by using analytical results and the thin solid line is plotted by using numerical results. The parameters are $\omega_0^2 = -1$, $\beta = 1$, $A = 0.1$, $\omega = 1$, $\Omega = 10$.

With regards to the underdamped Duffing oscillator system Eq. (17) excited by two cosine signals as another example, the analytical result of Q is

$$Q = \frac{1}{\sqrt{(\delta\omega)^2 + (\omega_r - \omega^2)^2}}, \tag{164}$$

where ω_r and X^* have the same expressions with that in the above overdamped system, but the amplitude of the fast variable is $C = \frac{B}{\sqrt{(\delta\Omega)^2+(\omega_0^2-\Omega^2)^2}}$. The pitchfork bifurcation of the equivalent system is

$$B_c = \sqrt{\frac{-2\omega_0^2\left[(\delta\Omega)^2 + (\omega_0^2 - \Omega^2)^2\right]}{3\beta}}. \tag{165}$$

When $B < B_c$, the equivalent system has two stable equilibrium points $X_{\pm}^* = \pm\sqrt{-\mu/\beta}$. When $B \geq B_c$, the equivalent system has one stable equilibrium point $X^* = 0$. According to the formula of ω_r in Eq. (160), we know that the equivalent system has a different mathematical expression when B is greater or less than B_c.

Solving $\omega_r = \omega^2$, when $0 < B < B_c$, the response amplitude achieves the peak at the location

$$B_{VR}^{(1)} = \sqrt{-\frac{2\omega_0^2 + \omega^2}{3\beta}\left[(\delta\Omega)^2 + (\omega_0^2 - \Omega^2)^2\right]}. \tag{166}$$

The corresponding peak value is $Q_{max}^{(1)} = \frac{1}{\delta\omega}$. When $B > B_c$, the resonance peak occurs at

$$B_{VR}^{(2)} = \sqrt{\frac{2(\omega^2 - \omega_0^2)}{3\beta}\left[(\delta\Omega)^2 + (\omega_0^2 - \Omega^2)^2\right]}. \tag{167}$$

The corresponding peak value is $Q_{max}^{(2)} = Q_{max}^{(1)} = \frac{1}{\delta\omega}$. Hence, at $B_{VR}^{(1)}$ and $B_{VR}^{(2)}$, the resonance corresponding to two different equivalent systems occurs. Further, at the bifurcation point $B = B_c$, there is a valley value $Q_{val} = \frac{1}{\sqrt{(\delta\omega)^2+\omega^4}}$. The specific resonance modal is presented in Fig. 17.

5.1.2. Vibrational resonance in the pendulum system

For the pendulum system with a periodical potential, taking Eq. (34) as an example, by the method of direct separation of motions, eliminating the fast variable, the equivalent system is [20,293]

$$\dot{X} + \frac{d\bar{V}(X)}{dX} = A\cos(\omega t). \tag{168}$$

The effective potential function $\bar{V}(X) = -J_0(F/\Omega)\cos X$, where $\omega_r = |J_0(B/\Omega)|$ and $J_0(\bullet)$ is the zero-order Bessel function of the first kind. The stable equilibrium points of Eq. (168) for $A = 0$ are $X^* = \pm 2n\pi$, $n = 1, 2, \ldots$. The response amplitude

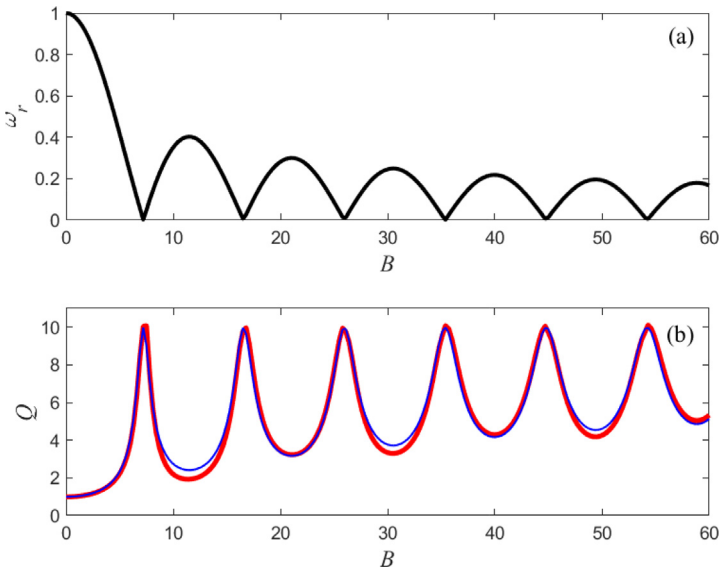

Fig. 18. The control parameter ω_r whose minimum value makes the resonance occur and the response amplitude Q changing with the amplitude B of the fast-varying auxiliary signal in the pendulum system of Eq. (34). (a) The minimum value of ω_r repeatedly appears as the signal amplitude B increases. (b) The response amplitude Q versus the signal amplitude B presents multiple vibrational resonance. The thick solid line is plotted by using analytical results and the thin solid line is plotted by using numerical results. The parameters are $A = 0.1$, $\omega = 0.1$, $\Omega = 3$.

at the excitation frequency ω is

$$Q = \frac{1}{\sqrt{\omega_r^2 + \omega^2}}. \tag{169}$$

As depicted in Fig. 18, peaks emerge whenever ω_r reaches local minima. Owing to the characteristics of the zero-order Bessel function of the first kind, a series of resonance peaks is observed in the graph. This differs from the resonance mode observed in the bistable system.

5.1.3. Vibrational resonance in coupled oscillators

It is noteworthy that the coupling in Eq. (68) is unidirectional. Interestingly, when the coupling strength is significantly high, vibrational resonance occurs whether high-frequency excitations are applied to all oscillators or only to the first oscillator while the others remain free from excitation, as discussed in [17]. In both scenarios, the response of the last oscillator at the frequency of the slowly varying excitation is notably robust, as depicted in Fig. 19. Apparently, there is a very wide resonance range in the subplot especially in Fig. 19b. Especially, for the case $\epsilon = 3$, the response amplitude Q versus the amplitude B almost presents a constant value in a large interval of B. In other words, a strong enough high-frequency signal makes the system achieve a saturated output of resonance in the corresponding interval. Here, we use the numerical simulation to obtain the results. According to the time series in [17], we find that the output of the *nth* oscillator is approximated to a square waveform when n is large enough. When using the method of direct separation of motions under these conditions, the deviation of slow motion from a harmonic waveform can result in a substantial error. Furthermore, when two excitations are exclusively applied to the first oscillator while leaving all others without excitation, the fast motion in the response of the nth oscillator is nearly negligible, and the slow motion predominates. Therefore, in this case, we present only the numerical results.

5.1.4. Vibrational resonance in the delayed system

For the delayed system of Eq. (115) with a bistable potential, $\omega_0^2 > 0$, $\beta > 0$ and $\gamma < -\omega_0^2$, by the method of direct separation of motions, it is easy to obtain the response amplitude at the frequency ω is

$$Q = \frac{1}{\sqrt{(\gamma \sin \omega\tau - \omega)^2 + (\gamma \cos \omega\tau + \omega_r)^2}}, \tag{170}$$

where μ and ω_r have the same expressions with that in Eqs. (159) and (160), but the equilibrium points are $X^* = 0$ and $X_\pm^* = \pm\sqrt{-(\mu+\gamma)/\beta}$. The amplitude of the fast motion is $C = \frac{B}{\sqrt{(\gamma \sin \Omega\tau - \Omega)^2 + (\gamma \cos \Omega\tau + \omega_0^2)^2}}$.

If we choose the parameter B to control the vibrational resonance, the resonance pattern depends on the feedback strength γ.

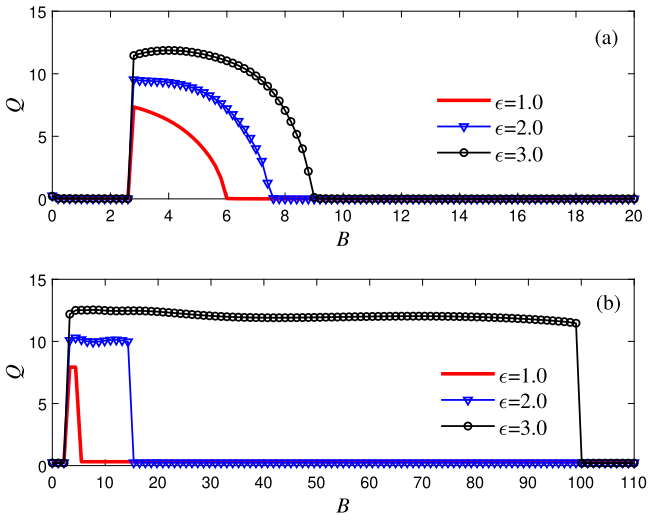

Fig. 19. Vibrational resonance of the last oscillator in the unidirectional coupled system of Eq. (68). (a) The high-frequency excitations are added to all oscillators. (b) The high-frequency excitation is added to the first oscillator only. The parameters are $a_1 = 1$, $b_1 = 1$, $A = 0.2$, $\omega = 0.1$, $\Omega = 5.0$. The total number of the oscillators is $n = 50$.

(1) $\gamma \leq 0$

The pitchfork bifurcation point is

$$B_c = \sqrt{-\frac{2(\gamma+\omega_0^2)}{3\beta}\left[(\gamma\sin\Omega\tau-\Omega)^2+(\gamma\cos\Omega\tau+\omega_0^2)^2\right]}. \tag{171}$$

At $B = B_c$, the response amplitude is

$$Q_c = \frac{1}{\sqrt{(\gamma\sin\omega\tau-\omega)^2+(\gamma\cos\omega\tau-\gamma)^2}}, \tag{172}$$

There is a single peak in the $Q - B$ curve, and the maximal value of the peak is $Q_{max} = Q_c$, as shown in Fig. 20(a).

(2) $0 < \gamma < -\omega_0^2$

The pitchfork bifurcation point is still given in Eq. (171). Solving $\gamma\cos\omega\tau + \omega_r = 0$, when $0 < B < B_c$, the resonance peak locates at

$$B_{VR}^{(1)} = \sqrt{\frac{(\gamma\cos\omega\tau-3\gamma-2\omega_0^2)}{3\beta}\left[(\gamma\sin\Omega\tau-\Omega)^2+(\gamma\cos\Omega+\omega_0^2)^2\right]}. \tag{173}$$

When $B > B_c$, the resonance peak occurs at

$$B_{VR}^{(2)} = \sqrt{-\frac{2(\gamma\cos\omega\tau+\omega_0^2)}{3\beta}\left[(\gamma\sin\Omega\tau-\Omega)^2+(\gamma\cos\Omega+\omega_0^2)^2\right]}. \tag{174}$$

The corresponding peak value is $Q_{\max} = Q_{\max}^{(1)} = Q_{\max}^{(2)} = \frac{1}{|\gamma\sin\omega\tau-\omega|}$. The double-resonance pattern is presented in Fig. 20(b). In addition, for the case $\tau = 0$ or $\gamma = 0$, i.e., when the time delay term is free, the system becomes the ordinary system, then we have $B_{VR}^{(1)} = B_{VR}^{(2)}$, and the double-peak disappear. Hence, the time delay is an important factor to induce the double-resonance pattern.

When utilizing the delay parameter τ as the control parameter while keeping the remaining parameters fixed, resonance occurs at τ_{VR}, which is the root of the equation $\frac{dQ}{d\tau} = 0$ and $\frac{d^2Q}{d\tau^2} < 0$. Obtaining an accurate analytical solution for this equation can be challenging, as it may have numerous (or infinite) roots. If the ratio ω/Ω is an irrational number, the delay τ will induce quasi-periodic vibrational resonance. Conversely, if the ratio ω/Ω is a rational number, the delay τ will induce periodic vibrational resonance. Furthermore, the curve exhibits two periods, namely $2\pi/\omega$ and $2\pi/\Omega$, as depicted in Fig. 21.

5.2. The nonlinear vibrational resonance

As mentioned in Section 1, different works on vibrational resonance at nonlinear frequencies have been carried out in different systems [26,94–99,254]. According to the linear response theory, the conventional vibrational resonance is

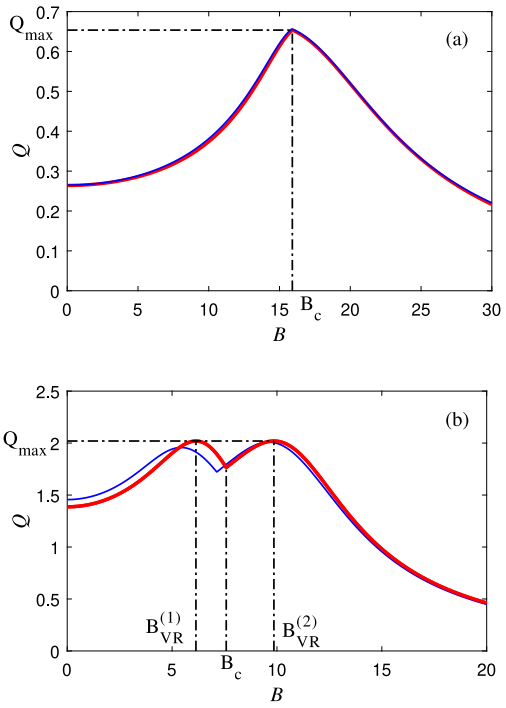

Fig. 20. Effect of the delayed strength γ on vibrational resonance modal in the system of Eq. (115). (a) The single vibrational resonance appears when $\gamma = -0.6$. (b) The double vibrational resonance appears when $\gamma = 0.6$. The thick solid line is plotted by using analytical results and the thin solid line is plotted by using numerical results. The parameters are $\omega_0^2 = -1$, $\beta = 1$, $\tau = 1$, $A = 0.1$, $\omega = 1$, $\Omega = 15$.

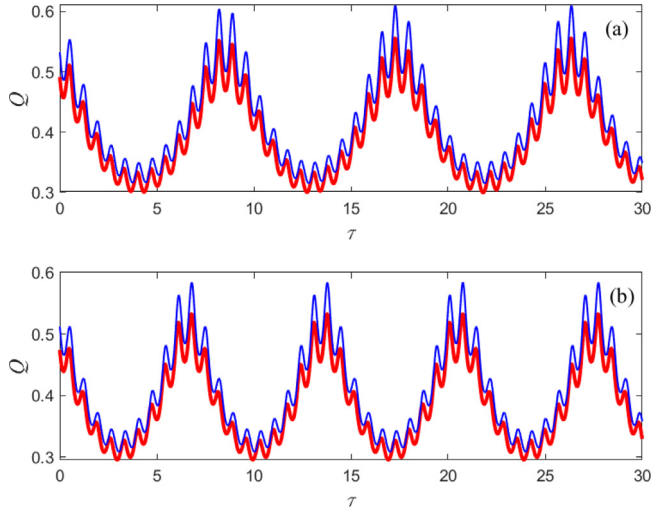

Fig. 21. Quasi-periodic or periodic vibrational resonance induced by the delay parameter τ in the system of Eq. (115). (a) The curve of $Q-\tau$ presents quasi-periodic vibrational resonance, $\omega = \sqrt{(2)}/2$. (b) The curve of $Q-\tau$ presents periodic vibrational resonance, $\omega = 0.9$. The thick solid line is plotted by using analytical results and the thin solid line is plotted by using numerical results. The parameters are $\omega_0^2 = -1$, $\beta = 1$, $\gamma = -0.6$, $A = 0.1$, $B = 6$, $\Omega = 9$.

obvious at the frequency of the characteristic signal. In addition, in Eq. (16), based on the nonlinear response theory, we know that there must be nonlinear frequencies in the response. Ghosh and Ray [94] first investigated vibrational resonance at the frequency 2ω. Yang et al. [98] expanded vibrational resonance to more nonlinear harmonic components, *i.e.*, subharmonic frequencies, superharmonic frequencies, or combined frequencies. Fig. 22 provides vibrational resonance at these frequencies. Especially in Fig. 22(b), the response amplitude at the subharmonic frequency component $\omega/3$ is much greater than that at ω. In Fig. 22(a), the combined frequency $\Omega - \omega$ is also a large value. In fact, in Fig. 22, we

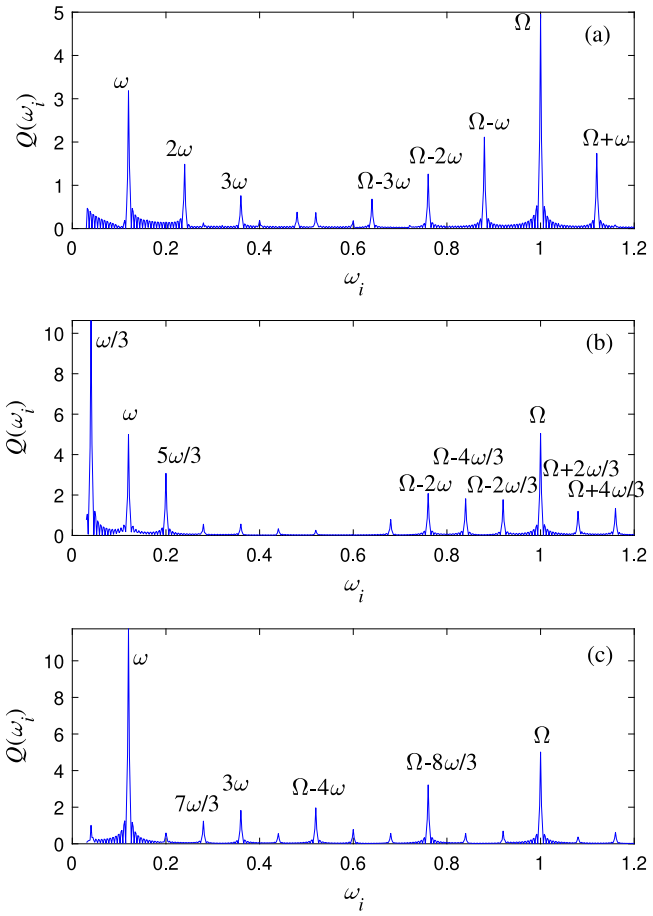

Fig. 22. Response amplitudes at different frequencies present nonlinear vibrational resonance in the system of Eq. (16) for different values of the amplitude B of the fast-varying auxiliary signal. (a) $B = 1.13$, (b) $B = 1.14$, (c) $B = 1.15$. The parameters are $\omega_0^2 = -1.5$, $\beta = 1$, $A = 0.1$, $\omega = 0.12$, $\Omega = 1$.

know that the nonlinear vibrational resonance can occur at more nonlinear frequencies. The frequencies in the output can be controlled by the fast-varying excitation. In addition, the nonlinear vibrational resonance is found by Das and Ray at combined frequencies $\omega - \omega_0$ and $\omega + \omega_0$ in the underdamped Duffing oscillator Eq. (17) [101].

5.3. Ultrasensitive vibrational resonance

Another peculiar resonance pattern emerges in the ultrasensitive response amplitude Q, induced by a phase space fractal structure [205]. The system employed here is Eq. (17). When $B = 0$, the response of the nonlinear system exhibits a basin of attraction, indicating a highly fractalized phase space. Upon introducing $B \neq 0$, the high-frequency perturbation leads to an ultrasensitive variation of Q. Within a very small range of B, this induces an ultrasensitive variation of Q, as depicted in Fig. 23. The response amplitude curve is characterized by multiple peaks in a fractal-like structure. Daza et al. [205] referred to this phenomenon as *ultrasensitive vibrational resonance*. Notably, ultrasensitive vibrational resonance occurs not only at the excitation frequency but also at various nonlinear frequencies. Moreover, the ultrasensitive response is highly dependent on initial conditions and calculation time. In Fig. 23, a total calculation time of $40T$ is used, with $T = 2\pi/\omega$, and the initial simulation conditions are set to $x(0) = 0$ and $\dot{x}(0) = 0$.

To further investigate whether ultrasensitive vibrational resonance is influenced by time, we present Fig. 24, which shows the patterns of ultrasensitive vibrational resonance at different time intervals. In these subplots, the ultrasensitive vibrational resonance always exists and the $Q - B$ curve becomes stable over time. Interestingly, while there are ultrasensitive vibrational resonance regions, there are also some non-ultrasensitive vibrational resonance regions in the figure.

Although ultrasensitive vibrational resonance persists indefinitely in Fig. 24, it may transition to a deterministic response for other parameter configurations, as illustrated in Fig. 25.

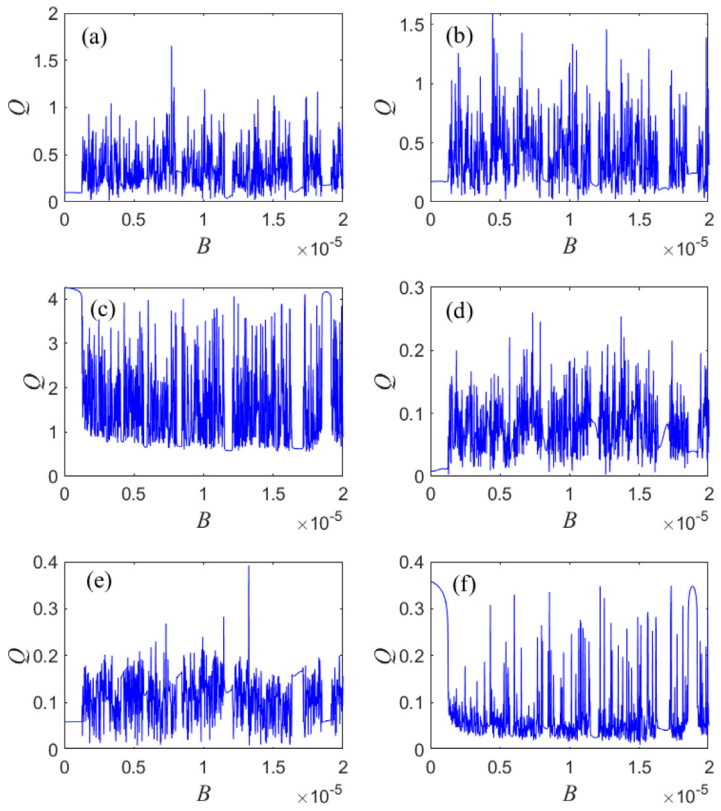

Fig. 23. The response amplitude Q at some given frequencies versus the amplitude B of the fast-varying auxiliary signal shows ultrasensitive vibrational resonance in a very small range of B in the system of Eq. (17). The response amplitude Q is calculated at the frequency $\omega/3$, $\omega/2$, ω, $5\omega/3$, 2ω and 3ω from (a)–(f) successively. The parameters are $\delta = 0.15$, $\omega_0^2 = -1$, $\beta = 1$, $A = 0.245$, $\omega = 0.9$ and $\Omega = 9.8$.

This transition occurs due to the system's response shifting from transient chaos to a periodic state over time. Such a phenomenon, where the system evolves from transient chaos to periodic behavior, has been extensively reported [294, 295]. However, as illustrated in Fig. 24, the response remains chaotic for an extended period, leading to the prolonged presence of ultrasensitive vibrational resonance.

Ultrasensitive vibrational resonance is not solely induced by high-frequency disturbances; rather, it can also arise from variations in the initial simulation conditions, as confirmed in Fig. 26. The presence of distinct regions of ultrasensitive vibrational resonance and nonsensitive responses is evident in the figure. Interestingly, the pattern of ultrasensitive vibrational resonance response remains largely consistent across different time intervals.

Different parameter choices have been explored to examine ultrasensitive vibrational resonance induced by initial conditions, as depicted in Fig. 27. Over time, the ultrasensitive vibrational resonance gradually diminishes until it transforms into a steady-state periodic response. The findings presented in Fig. 27 closely resemble those in Fig. 25, suggesting a transition from transient chaos to periodic behavior within the system.

Another instance of ultrasensitive vibrational resonance is observed in Eq. (67). The damping parameters γ_1 and γ_2 play a crucial role in shaping the vibrational resonance pattern. As depicted in Fig. 28(a), the $Q-B$ curve exhibits ultrasensitive vibrational resonance within certain ranges of B. Conversely, in Fig. 28(d), a trough-like feature is observed, which is referred to as *vibrational antiresonance* by Sarkar and Ray [16]. This phenomenon indicates that the strong fast-varying signal not only amplifies the weak low-frequency signal but also suppresses the response at the characteristic frequency to a significant extent. Figs. 28(b) and (c) illustrate the transition between ultrasensitive vibrational resonance and vibrational antiresonance. In Fig. 28(f), an intriguing observation is made where the response amplitude Q remains small despite the strong fast-varying signal. This occurrence is attributed to the damping effect, which effectively attenuates the vibration. It is worth noting that with time, the vibrational resonance pattern depicted in Fig. 28 under different simulation parameters may transition from ultrasensitive vibrational resonance to the traditional vibrational resonance.

In fact, ultrasensitive vibrational resonance presents a highly complex phenomenon. The regions and patterns of ultrasensitive resonance, along with conventional resonance, are unpredictable. Moreover, variations in the system parameters and different forms of external excitation can lead to extremely complex responses. To gain deeper insights into these phenomena, it is essential to integrate various aspects of nonlinear dynamics, including bifurcation, chaos,

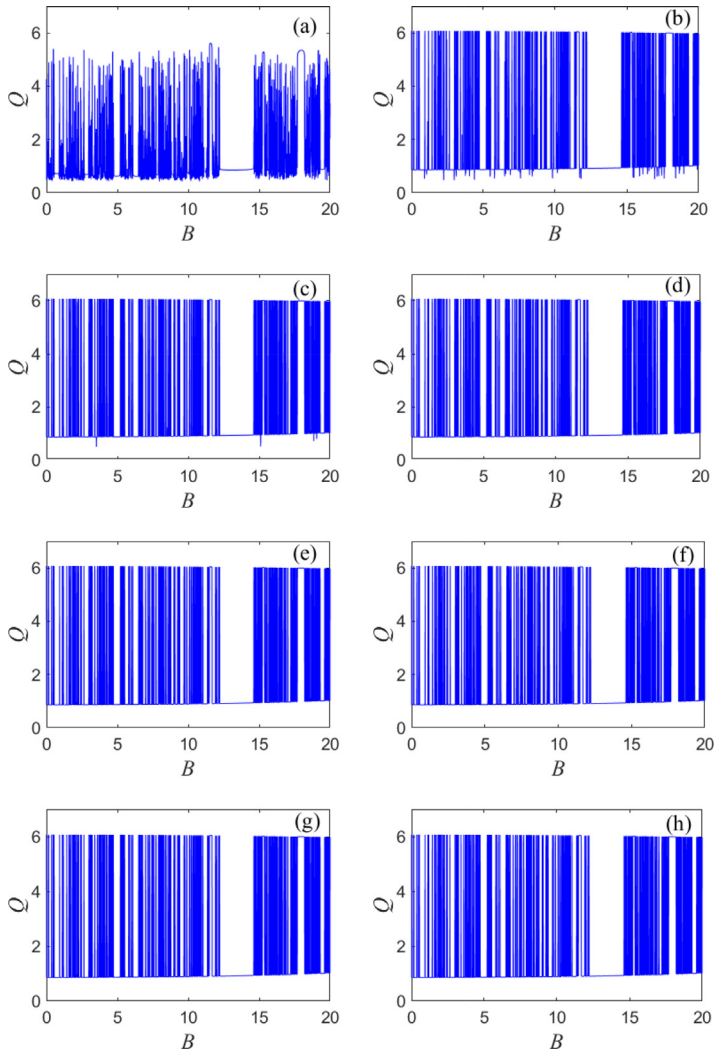

Fig. 24. The response amplitude Q at the excitation frequency ω versus the amplitude B of the fast-varying auxiliary signal shows ultrasensitive vibrational resonance in a relatively large range of B in system of Eq. (17) in different time intervals. The total calculation time starts from the very beginning of $(40m+1)T$ to the end of $40jT$, $m=j-1$ and $j=$ 1-8 in turn from (a)–(h). The parameters are $\delta=0.15$, $\omega_0^2=-1$, $\beta=1$, $A=0.245$, $\omega=0.9$ and $\Omega=9.8$. The initial conditions are $x(0)=0$, $\dot{x}(0)=0$.

fractals, and more. Investing further effort into studying ultrasensitive vibrational resonance holds promise for uncovering valuable insights and potential applications.

5.4. The re-scaled vibrational resonance

The conventional approach to vibrational resonance assumes that the frequency of the slow-varying excitation is $\omega \ll 1$, or that the smallest width of the aperiodic binary signal is far larger than 1. However, in many scientific and engineering applications, this assumption may not hold true. In such cases, achieving optimal vibrational resonance in the output becomes challenging because it is difficult to find a suitable correspondence between the characteristic signal and the system parameters. This challenge becomes even more pronounced when the characteristic signal takes on a complex frequency-modulated form. Identifying a matching parameter configuration that leads to vibrational resonance within the framework of conventional theory becomes nearly impossible. To address this issue, Liu et al. [111] proposed the normalized transformation method, while Yang et al. [112] introduced the generalized transformation method. These methods involve scale transformations that convert the fast-varying characteristic signal into a slow-varying signal. This transformation makes it easier for vibrational resonance to occur in the output. Through the scale transformations, the fast-varying characteristic signal can be transformed to a slow-varying signal, making it easy the vibrational resonance to occur in the output. The concept of re-scaled vibrational resonance draws inspiration from the re-scaled stochastic

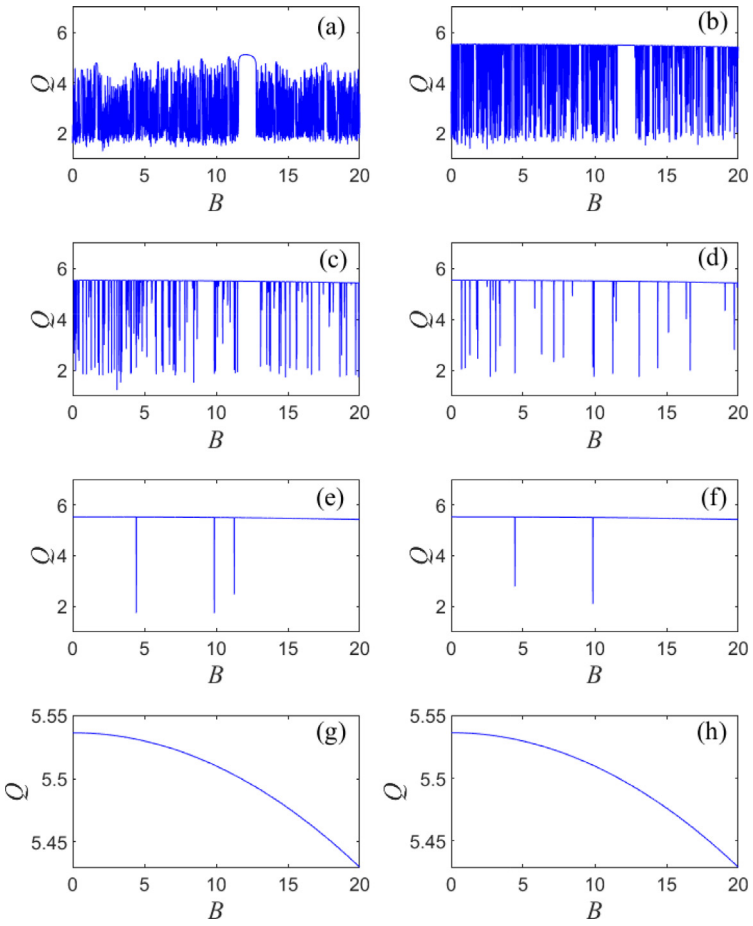

Fig. 25. The ultrasensitive vibrational resonance caused by the signal amplitude B at the excitation frequency ω gradually disappears with the increase of time in the system of Eq. (17). The total calculation time starts from the very beginning of $(40m+1)T$ to the end of $40jT$, $m = j-1$ and $j =$ 1-8 in turn from (a)–(h). The parameters are $\delta = 0.15$, $\omega_0^2 = -0.6$, $\beta = 1$, $A = 0.245$, $\omega = 0.9$ and $\Omega = 9.8$. The initial conditions are $x(0) = 0$, $\dot{x}(0) = 0$.

resonance method [296–299], which has been explored in various studies. By employing these transformation methods, researchers can overcome the limitations of conventional vibrational resonance theory and enhance their ability to achieve resonance in real-world applications.

First, we still take the overdamped Duffing oscillator in Eq. (16) as an example. The difference is the frequency of the characteristic signal $\omega \gg 1$. If we do not use the re-scaled vibrational resonance theory, it is difficult to find that the system parameter matches the frequency ω.

Introducing the generalized scale transformation

$$t_s = \kappa t, x(t) = z(t_s), \tag{175}$$

herein, κ is the scale parameter and t_s is the new time scale. Then, we obtain the equation in the new time scale

$$\frac{dz(t_s)}{dt_s} + \frac{\omega_0^2}{\kappa} z(t_s) + \frac{\beta}{\kappa} z^3(t_s) = \frac{A}{\kappa} \cos\left(\frac{\omega t_s}{\kappa}\right) + \frac{B}{\kappa} \cos\left(\Omega \frac{t_s}{\kappa}\right). \tag{176}$$

Let

$$a = \frac{\omega_0^2}{\kappa},\ b = \frac{\beta}{\kappa},\ \omega_1 = \frac{\omega}{\kappa},\ \Omega_1 = \frac{\Omega}{\kappa} \tag{177}$$

and recover the signals to the original magnitude, then Eq. (176) turns to

$$\frac{dz(t_s)}{dt_s} + az(t_s) + bz^3(t_s) = A\cos(\omega_1 t_s) + B\cos(\Omega_1 t_s). \tag{178}$$

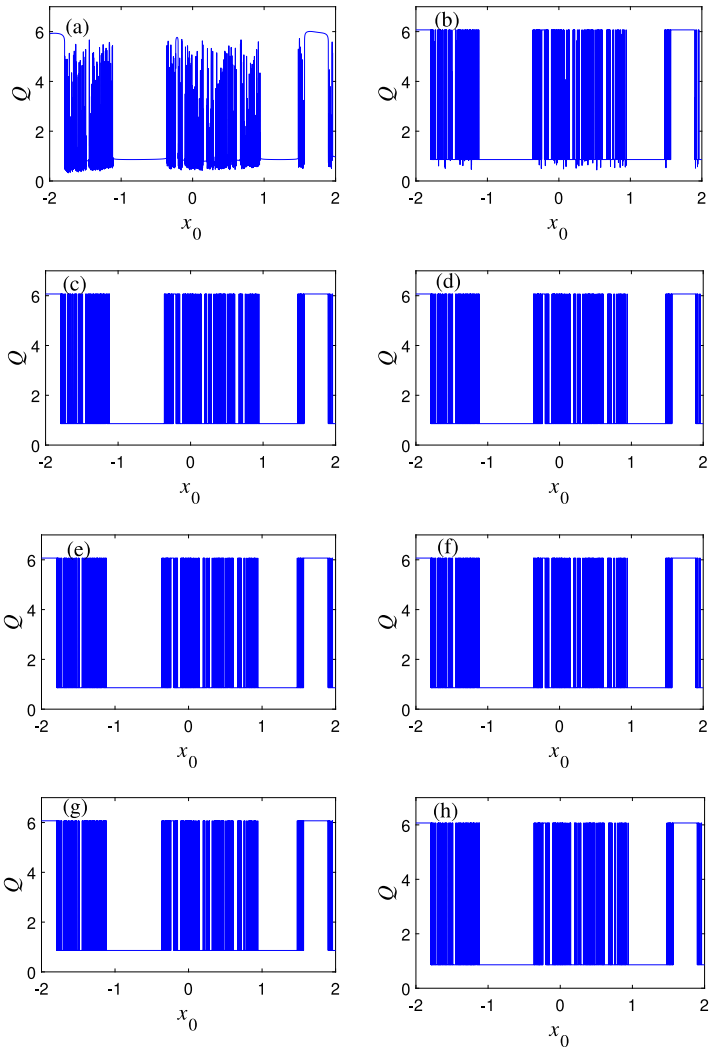

Fig. 26. The ultrasensitive vibrational resonance caused by the change of the initial condition x_0 at the excitation frequency ω in system of Eq. (17) in different time intervals. The total calculation time starts from the very beginning of $(40m+1)T$ to the end of $40jT$, $m=j-1$ and $j=$ 1-8 in turn from (a)–(h). The parameters are $\delta=0.15$, $\omega_0^2=-1$, $\beta=1$, $A=0.245$, $\omega=0.9$, $B=2$ and $\Omega=9.8$.

In Eq. (178), if we choose an appropriate scale parameter, we can make the frequency of the characteristic signal to be small enough to make the vibrational resonance to occur. Then, the analysis of vibrational resonance of Eq. (178) can be carried out by the method of direct separation of motions.

Furthermore, for the numerical simulations, the original equation turns to the form

$$\frac{dx}{dt}+\omega_0^2 x+\beta x^3=\kappa A\cos(\omega t)+\kappa B\cos(\Omega t). \tag{179}$$

Herein, ω_0^2 and β are large parameters with $\omega_0^2=a\kappa$, $\beta=b\kappa$. a and b are small parameters in the order of 1. ω and Ω are large parameters. The relationship between the conventional vibrational resonance and the re-scaled vibrational resonance is shown in Fig. 29. When $\kappa=1$, the re-scaled equation degenerates to the conventional vibrational resonance equation.

In Fig. 30, we provide the analytical results and the corresponding numerical results of the re-scaled vibrational resonance. Because $\kappa=6000$, the re-scaled frequency is $\omega_1=0.5$. The response amplitude at $\omega=1500$ in Eq. (179) is the same as the response amplitude at $\omega_1=0.5$ in Eq. (178), i.e., Eq. (16) when $\omega=0.5$. As a result, the curves in Fig. 30 are the same as the ones in Fig. 16 although their ω values are in huge difference.

The re-scaled vibrational resonance theory can be used not only in the periodic characteristic signal case, but also in the aperiodic characteristic signal case, such as the aperiodic binary signal [115,116], the linear frequency modulated signal [118,119], among others. Especially, if the characteristic signal is a frequency-modulated signal, the piecewise

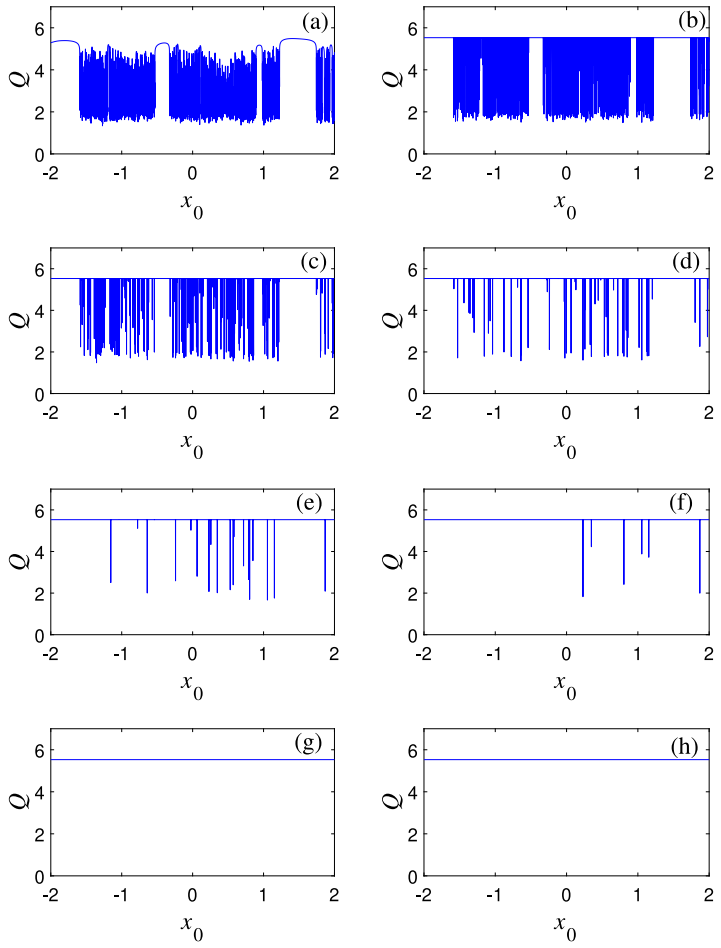

Fig. 27. The ultrasensitive vibrational resonance caused by the change of the initial condition x_0 at the excitation frequency ω gradually disappears with the increase of time in the system of Eq. (17). The total calculation time starts from the very beginning of $(40m + 1)T$ to the end of $40jT$, $m = j$-1 and $j =$ 1-8 in turn from (a)–(h). The parameters are $\delta = 0.15$, $\omega_0^2 = -0.6$, $\beta = 1$, $A = 0.245$, $\omega = 0.9$, $B = 2$ and $\Omega = 9.8$.

idea should be introduced with the re-scaled treatment simultaneously. This is because the instantaneous frequency at a different time may vary greatly. Hence, fixed system parameters cannot always match the instantaneous frequency. In each segment, the instantaneous frequency varies within a small range. Fixed system parameters can match the instantaneous frequency corresponding to this segment. In other segment, we need to change the system parameters to different values to match the instantaneous frequency approximately. Certainly, the number of the segments will influence the vibrational resonance output. A new method needs to be developed to deal with complex frequency-modulated signals, such as the real-time scale transformation method [300–302].

Another method similar to the re-scaled vibrational resonance is the twice-sampling method. The twice-sampling method was first used in studying stochastic resonance induced by a high-frequency characteristic signal in the bearing fault diagnosis field [303,304]. It was introduced in vibrational resonance analysis of the fast-varying characteristic signal case [113,115,116,155]. The results of the two methods are compared in detail in the above four references. These two different methods can achieve the same goal. For twice-sampling vibrational resonance, the following procedure is performed [113].

1. Sampling the excitations by the first sampling frequency f_s.
2. For the sampled signal in the first step, sampling the new time series by the twice-sampling frequency f_s/γ once more. Then, the frequency of the reconstructed signal will be γ times of the original frequency. Here, γ is the frequency reduced ratio.
3. Input the reconstructed signal in the nonlinear system. Then, the time series of the output are obtained.
4. Recovering the output to the first sampling frequency f_s according to the frequency reduced ratio γ.
5. Calculating the index and tuning the control signal to make vibrational resonance occur.

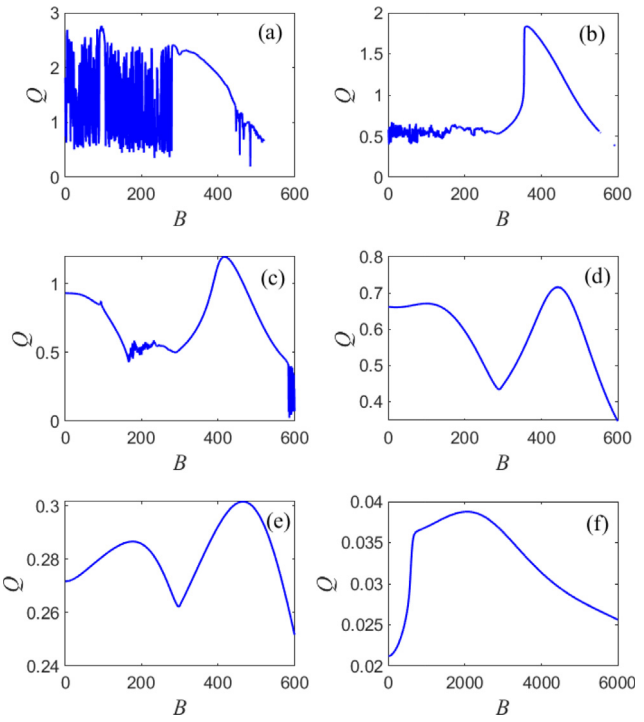

Fig. 28. The response amplitude of the first oscillator at the excitation frequency ω versus the signal amplitude B presents ultrasensitive vibrational resonance and traditional vibrational resonance for different values of γ_1 and γ_2. In (a) - (f), $\gamma_1 = \gamma_2 = 0.05$, 0.2, 0.3, 0.5, 1.2 and 10 in turn. The parameters are $g_1 = g_2 = 0.05$, $\beta_1 = \beta_2 = 0.1$, $\omega_1 = \omega_2 = 1.1$, $A = 2$, $\omega = 1.4$ and $\Omega = 10$.

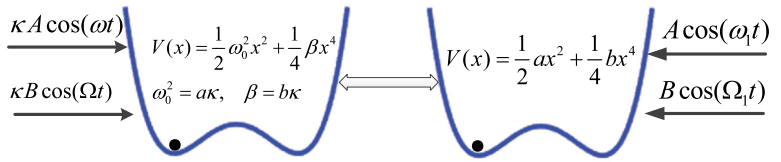

Fig. 29. The relationship between the re-scaled vibrational resonance and the conventional vibrational resonance.

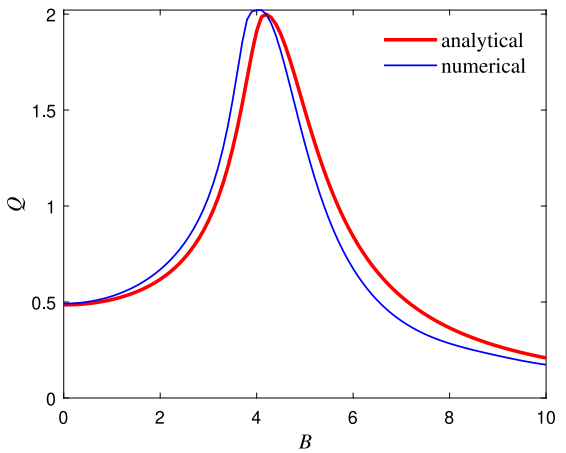

Fig. 30. The analytical and numerical results of the re-scaled vibrational resonance facilitated by a fast-varying characteristic signal and a faster-varying auxiliary signal. The parameters are $\omega = 1500$, $\Omega = 10\omega$, $A = 0.1$, $\kappa = 3000$, $\omega_0^2 = -1$, $\beta = 1$.

These two methods can handle not only the nonlinear system excited by two determined signals but also the system excited by a characteristic signal with different types of noise. Re-scaled vibrational resonance requires a system with large parameters to manage the mixed signal after amplifying it to a large amplitude. Conversely, the twice-sampling method necessitates converting the mixed fast-varying signal into a slow-varying one initially, followed by reverting the output to the original time scale through another sampling process. Both the re-scaled and twice-sampling methods have demonstrated good performance, albeit they may lack rigorous mathematical treatment.

5.5. Role of noise on vibrational resonance

In a nonlinear system excited by a bi-harmonic signal and noise simultaneously, an interplay between vibrational resonance and stochastic resonance typically occurs. In this subsection, we describe the role of noise in a bistable system, beginning with a pendulum system. Subsequently, we elucidate the impact of noise on logical vibrational resonance. We model the noise using Gaussian white noise denoted as $\xi(t)$, characterized by statistical properties $\langle \xi(t) \rangle = 0$ and $\langle \xi(t)\xi(0) \rangle = 2D\delta(t)$.

Baltanás et al. [125], Lin and Huang [130] investigated stochastic resonance controlled by vibrational resonance in Eq. (137). Applying the method of direct separation of motions and assuming that the statistical properties of noise are invariant in the period $[0, 2\pi/\Omega]$, the equivalent equation for the slow variable X is obtained as

$$\dot{X} + \mu X + \beta X^3 = A\cos(\omega t) + \xi(t). \tag{180}$$

The parameter μ shares the same expression as in Eq. (159). Consequently, both the Signal-to-Noise Ratio (SNR) and the spectrum amplification factor can be determined using stochastic resonance theory, regardless of whether the equivalent system described in Eq. (180) is bistable or monostable. The next step involves employing stochastic resonance theory to analyze various stochastic resonance measures of the output. Given the extensive literature on stochastic resonance [2], we refrain from delving further into the analysis of the influence of the fast-varying auxiliary signal on stochastic resonance. In fact, Eq. (180) indicates that the fundamental reason for stochastic resonance being controlled by vibrational resonance lies in the direct dependence of the equivalent system's parameter on the fast-varying auxiliary signal. Consequently, adjusting the fast-varying auxiliary signal is equivalent to tuning the system parameter in Eq. (137). Furthermore, controlling stochastic resonance through the fast-varying auxiliary signal offers additional advantages. For instance, if we were to control stochastic resonance by adjusting the system parameters using a hardware circuit, we would need to modify the values of the circuit elements. However, by leveraging vibrational resonance, we simply need to adjust the fast-varying auxiliary signal at the input, a task easily accomplished using a signal generator.

Baltanás et al. [125] investigated the phenomena of stochastic resonance and vibrational resonance in a forced bistable system. According to their findings, in the absence of the auxiliary signal, conventional stochastic resonance occurs. For low noise intensities, there is a noticeable vibrational resonance. When the noise is not overly strong, vibrational resonance can enhance the stochastic resonance effect. Specifically, an appropriate value of B improves the maximal value of Q. However, in cases of strong noise, both vibrational resonance and stochastic resonance vanish. In such scenarios, the strongest resonance state can be achieved through the re-scaled method or the twice sampling method. Evidently, the auxiliary signal assists in adjusting the parameters of the equivalent system, thereby effectively controlling the strongest resonance through vibrational resonance. Chizhevsky and Giacomelli [128,214] observed that the mechanism of vibrational resonance results in a higher Signal-to-Noise Ratio (SNR) compared to stochastic resonance.

Considering the role of noise in the pendulum system described by Eq. (141), Fig. 31 illustrates that the response amplitude Q is augmented by noise, particularly evident at the valleys of the curve. At these points, stochastic resonance enhances vibrational resonance, underscoring the beneficial effect of noise. Conversely, at the peaks of the curves, the response amplitude undergoes minimal alteration, indicating the limited influence of vibrational resonance. Naturally, excessive noise weakens the response amplitude at the frequency ω. Specifically, strong noise disrupts the coherence of the output, leading to a loss of order. This phenomenon is intuitively comprehensible, and thus we omit providing an example for this case here.

The role of noise on logical vibrational resonance, as described by Eq. (140), is depicted in Fig. 32. Notably, both logical stochastic resonance and logical vibrational resonance are evident simultaneously in the figure. With the presence of a small noise, logical resonance occurs at smaller values of B. Even when logical stochastic resonance is observed, logical vibrational resonance persists across a wide range of B. However, strong noise disrupts the phenomenon of logical vibrational resonance. Through logical vibrational resonance, effective control over logical stochastic resonance can be achieved. In addition, if a chaotic signal replaces the fast-varying signal, the output will manifest a logical chaotic signal [305–307].

6. Applications of vibrational resonance

In this section, we show applications of vibrational resonance to image perception enhancement and bearing fault diagnosis.

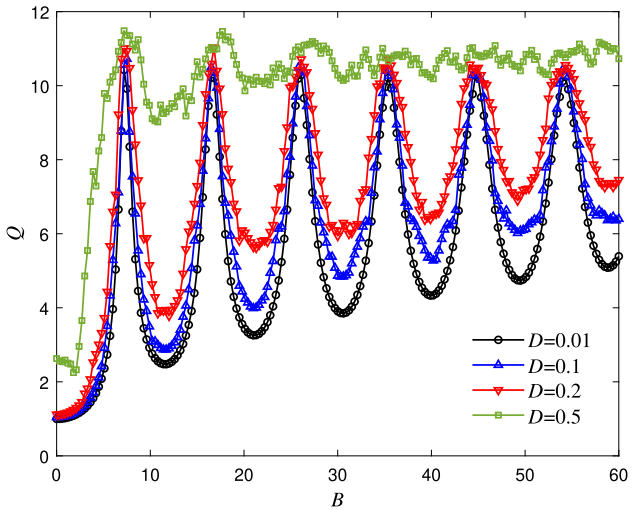

Fig. 31. The effect of noise on the multiple vibrational resonance in the pendulum system of Eq. (141). The parameters are $A = 0.1$, $\omega = 0.1$, $\Omega = 3$.

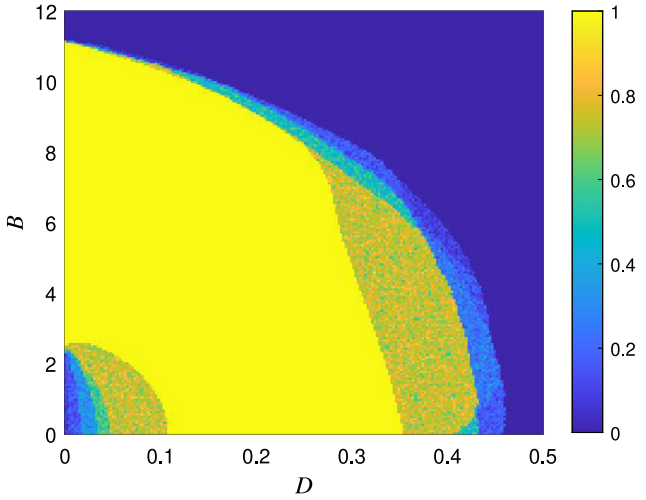

Fig. 32. The region of the logical vibrational resonance (**OR** operation) in the two-dimensional plane of the success probability with the noise intensity D and the signal amplitude B in the system of Eq. (140). The color coding represents the success probability. The parameters are $\omega_0^2 = -2$, $\beta = 4$, $r = 0.5$, $A = 0.1$, $\omega = 1$, $\Omega = 20$.

6.1. Vibrational resonance applied in image perception

In a recent study, Morfu et al. [158,159] explored the application of vibrational resonance in image perception. They devised a resonant threshold detector based on stochastic resonance and vibrational resonance principles to process images. In this approach, a specific image serves as the characteristic signal input to the system. The choice of either noise or a high-frequency sinusoidal signal as the auxiliary signal determines the nature of the detector: when noise is selected, it operates as a stochastic resonance-based detector, whereas employing a high-frequency sinusoidal signal transforms it into a vibrational resonance-based detector. Given that images inherently contain noise, this process essentially represents a vibrational resonance-enhanced stochastic resonance phenomenon. The detector's operation mode can be toggled between stochastic resonance and vibrational resonance through switch control. The effectiveness of the detector is evaluated using the cross-correlation coefficient between the output image and the noise-free source image. Maximal values of the cross-correlation coefficient indicate optimal noise reduction, particularly in the most significant regions of the image, potentially leading to improved perception of image contours.

For a noisy image, the grey levels of the pixels of coordinates $P_{i,j}$ are given by

$$P_{i,j} = I_{i,j} + \sigma \eta_{i,j}, \quad i = 1 \cdots M, \quad j = 1 \cdots N, \tag{181}$$

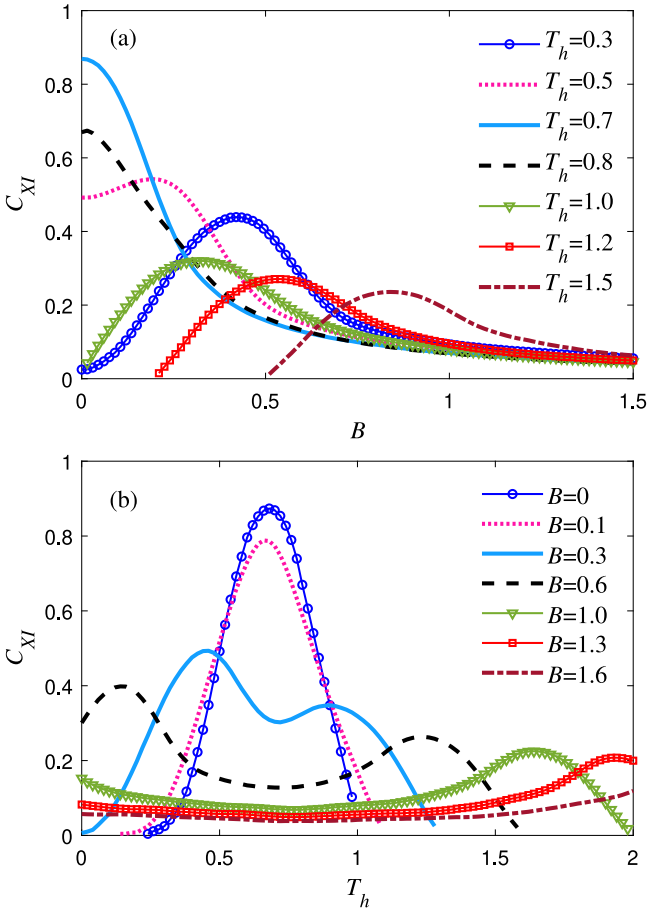

Fig. 33. The cross-correlation coefficient C_{XI} between the output image and the pure original image. (a) C_{XI} versus the signal amplitude B under different values of threshold value T_h. (b) C_{XI} versus the threshold value T_h under different values of the signal amplitude B. The parameters are $\sigma = 0.1$, $D = 10$.

where $I_{i,j}$ is the pure image without noise, $\eta_{i,j}$ is noise with strength σ, M and N denote the image size. Image noise may have different types for different backgrounds. Here, for simplicity, we choose the standard Gaussian white noise. For a given image, we use the vibrational resonance detector as below

$$X_{i,j} = P_{i,j} + B\cos\left(\frac{2\pi ij\Omega \times 0.5(M+N)}{M \times N} + \varphi_{i,j}\right), \quad i = 1\cdots M, \quad j = 1\cdots N, \tag{182}$$

where $X_{i,j}$ is the output image processed by the vibrational resonance detector, B and Ω are the amplitude and frequency of the high-frequency perturbation, $\varphi_{i,j}$ is the noise added to the detector, and $\varphi_{i,j} = \sqrt{2D}\xi(t)$ with $\xi(t)$ is a standard Gaussian white noise.

Once we have the value of $X_{i,j}$, we compare it to a threshold value, T_h. If $X_{i,j}$ exceeds this threshold ($X_{i,j} > T_h$), we set it to $X_{i,j} = 1$, representing the white level. Otherwise, if $X_{i,j}$ is less than or equal to the threshold ($X_{i,j} \le T_h$), we set it to $X_{i,j} = 0$, indicating the black level. Evidently, the final output, X, is strongly influenced by the chosen threshold value.

As an index to measure the aperiodic vibrational resonance, the cross-correlation coefficient C_{XI} between the final output X and the original pure image source without noise can be calculated to observe the resonance phenomenon. In Fig. 33(a), for different values of T_h, the cross-correlation coefficient C_{XI} versus the amplitude of the fast-varying perturbation B is shown. The image for calculation in Fig. 33 is a weld flaw detection image, which is given in Fig. 34(a). Again in Fig. 33, for $T_h = 0.7$ and $T_h = 0.8$, C_{XI} decreases monotonously with the increase of B. The cross-correlation coefficient C_{XI} is large due to the dither phenomenon here [308,309]. Especially for $T_h = 1.2$ and $T_h = 1.5$, it is found that the values of the cross-correlation coefficient disappear. It is because $X_{i,j} = 0$ is zero for a large value of T_h. If the denominator of the cross-correlation coefficient formula in Eq. (151) becomes zero, it renders the coefficient undefined, thereby making its interpretation meaningless. Incidentally, to get a better perceived image, in addition to the cross-correlation coefficient, we also suggest using some other specific metrics of the image. To further investigate the effect of the threshold value on the cross-correlation coefficient, we provide Fig. 33(b) which illustrates the dependence of

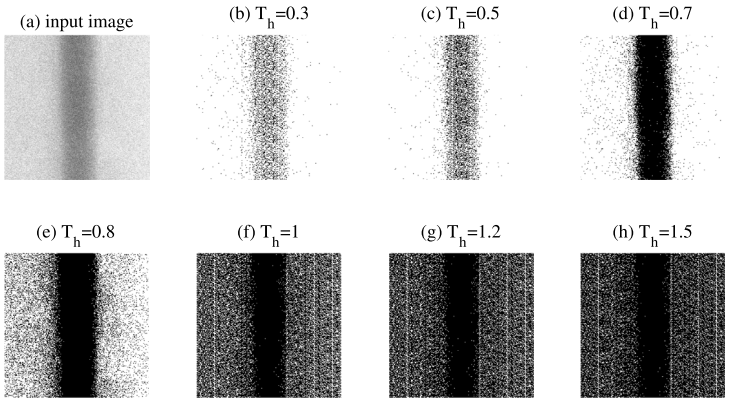

Fig. 34. The image contour perception based on the vibrational resonance detector of the noisy image under different threshold values. (a) The input noisy image, (b)–(h) The extraction effect of the weld seam image contour. The parameters are $\sigma = 0.1$, $D = 10$, and $B = 0.43$, 0.2, 0, 0, 0.32, 0.54 and 0.84 from (b) to (h) successively.

the cross-correlation coefficient on the threshold value directly. Generally, the cross-correlation coefficient versus the threshold value presents a nonlinear correlation. For different values of B, there is always an optimal threshold to make the cross-correlation coefficient to achieve the maximum. There is also "single-resonance" or "double-resonance" in Fig. 33(b). The curves in Fig. 33 highlight the importance of the threshold selection. In fact, from Fig. 33, we find that the dither phenomenon cannot be ignored. It may bring a better perception effect. The selection of a threshold value can make the image darker or whiter, which is meaningful in image contour detection.

Corresponding to the maximal value of each curve in Fig. 33(a), we present the images processed by the vibrational resonance detector in Fig. 34(b) - (h) respectively. The effective perception of image contours is facilitated by vibrational resonance or dithering techniques. By analyzing the curves in Fig. 33, we can identify the optimal amplitude of B for different values of T_h. Utilizing the peaks of the cross-correlation coefficient curve, we obtain the optimal output image corresponding to the specific threshold value. Notably, the weld contour becomes more distinct in some images of Fig. 34(b)–(h). Vibrational resonance plays a crucial role in enhancing the perception of feature contours in noisy images, particularly for certain values of T_h. It is essential to recognize that T_h dictates the black-and-white degree of the image, consequently impacting the efficacy of vibrational resonance processing in contour perception. Therefore, selecting appropriate thresholds is vital for refining image features in specific applications. Clearly, the choice of threshold significantly influences the contour of the weld seam area in Fig. 34.

To illustrate the advantages of using vibrational resonance to process noisy images, we employ two commonly used image quality evaluation indicators: the mean absolute error and the peak signal-to-noise ratio. The mean absolute error (MAE) is defined as follows

$$MAE = \frac{\sum_{i=1}^{M}\sum_{j=1}^{N}|I(i,j) - X(i,j)|}{M \times N}. \tag{183}$$

The peak signal-to-noise ratio (PSNR) is calculated by

$$PSNR = 10\log_{10}[\frac{255^2 \times M \times N}{\sum_{i=1}^{M}\sum_{j=1}^{N}[I(i,j) - X(i,j)]^2}]. \tag{184}$$

A smaller value of the mean absolute error indicates a smaller deviation from the original image, implying better image quality. Conversely, a higher value of the peak signal-to-noise ratio signifies better image quality.

The results of the mean absolute error and the peak signal-to-noise ratio before and after processing by vibrational resonance are presented in Table 2. The original noisy signal is depicted in image in Fig. 34(a), while Figs. 34(b) - (h) show images processed by vibrational resonance.

Analysis of Table 2 reveals that vibrational resonance processing effectively improves both the mean absolute error and the peak signal-to-noise ratio, enhancing image quality and perceptibility. Selecting appropriate thresholds based on the specific characteristics of the image can significantly improve image perception, particularly regarding contour features.

The analysis presented above highlights that the primary role of vibrational resonance in image processing extends beyond conventional noise reduction. Instead, it introduces a novel approach for extracting image contour features, a crucial aspect of image processing. While noise reduction remains an essential component, vibrational resonance offers a distinctive mechanism for enhancing image perception and facilitating feature extraction.

Table 2
Results of the mean absolute error and the peak signal-to-noise ratio for noisy images in Fig. 34(a) and images processed by vibrational resonance in Fig. 34 (b) – (h).

	(a)	(b)	(c)	(d)	(e)	(f)	(g)	(h)
MAE	198.464	26.352	26.296	26.133	26.234	26.717	26.736	26.736
PSNR	2.062	17.848	17.878	17.948	17.937	17.856	17.852	17.852

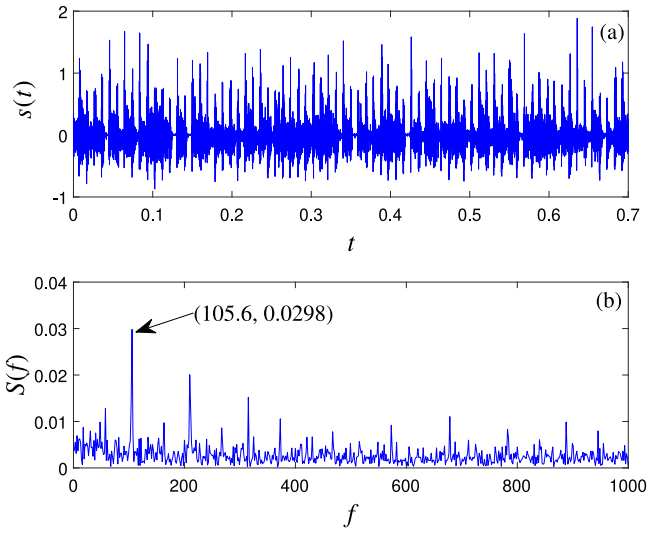

Fig. 35. Vibration signal of a bearing with a scratch fault in the outer ring. (a) The time domain waveform. (b) The amplitude spectrum versus the frequency of the signal.

6.2. Vibrational resonance applied in fault diagnosis

As a successful application example, the re-scaled vibrational resonance method in the bearing fault diagnosis field has been used in several studies [152–157].

For a vibration signal obtained from an experimental system of a bearing test rig, Fig. 35 presents both the time series in the time domain and the corresponding amplitude spectrum. The characteristic frequency, observed at 105.6 Hz, exhibits a weak amplitude. However, alongside the characteristic frequency, numerous other interference frequency components are evident in the spectrum, rendering the signal considerably complicated, what may pose challenges in realizing vibrational resonance.

Using a classic overdamped bistable model to process the vibration signal, the excitation in the system contains the vibration signal of the bearing and a harmonic auxiliary signal with frequency 2500 Hz. The re-scaled vibrational resonance is achieved by adjusting the amplitude of high-frequency auxiliary signal, as is shown in Fig. 36. Although the input signal has complex frequency components as shown in Fig. 35, the characteristic frequency is amplified to a great extent when the re-scaled vibrational resonance occurs in Fig. 36. In addition, the parameters herein used are $a = 0.02$, $b = 0.0001$, $\kappa = 100\,000$, and the meanings of these parameters are given in Eq. (177).

Fig. 37 gives the time series and the amplitude spectrum of the system output corresponding to the peak in Fig. 36. In Figs. 35–37, the amplitude is calculated by Eq. (148) without dividing by the amplitude A. From Fig. 37, the amplification of the characteristic frequency is verified once again. More importantly, compared with Fig. 35, we find that the interference frequency components are suppressed. The advantage of employing the vibrational resonance method is its capability to amplify a complex signal containing multiple interference frequency components. In contrast, when using a signal amplifier, all signal components are amplified simultaneously.

In this subsection, the vibrational resonance is applied successfully in the bearing fault diagnosis under the constant speed condition. In addition, this method can also be used in bearing fault diagnosis under the time-varying speed condition, such as the vibration signal in Fig. 1(l). For this special case, there are two ways to realize the vibrational resonance. The one is using the aperiodic vibrational resonance directly to deal with the engineering signal which has a frequency-modulated characteristic. The other one is using some technology such as order analysis to transmit from the non-stationary signal (corresponding to the time-varying speed condition) to a stationary signal (corresponding to the constant speed condition) [310,311]. Then, the re-scaled vibrational resonance is used to enhance or extract the characteristic frequency of the bearing fault.

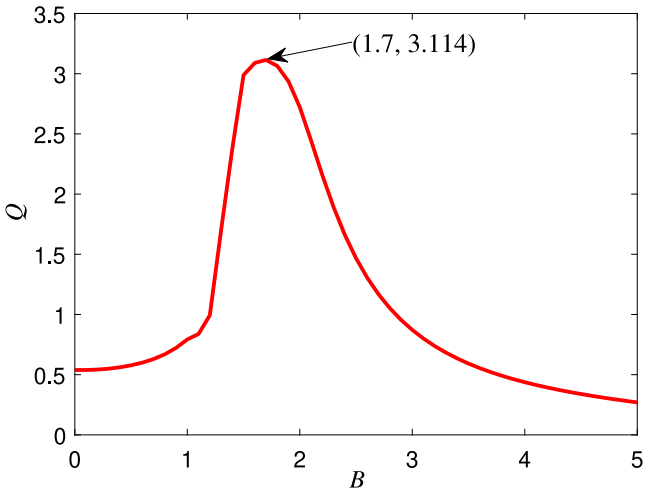

Fig. 36. The response amplitude at the characteristic frequency versus the amplitude B of the fast-varying auxiliary signal presents the re-scaled vibrational resonance phenomenon.

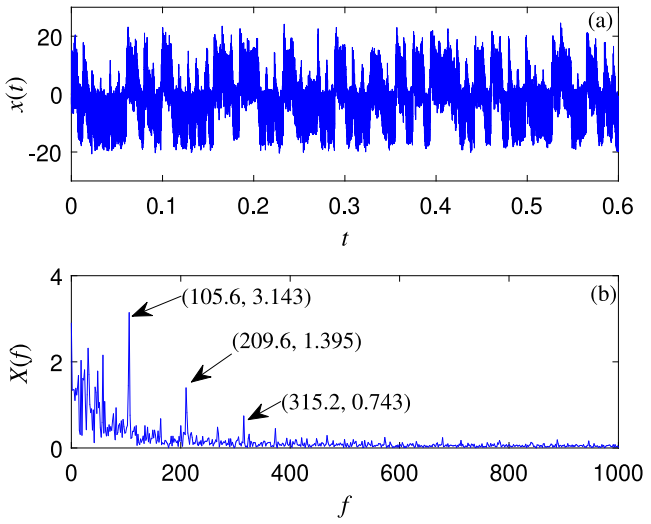

Fig. 37. The energy improves greatly at the characteristic frequency of the output corresponding to the optimal re-scaled vibrational resonance. (a) The time domain waveform. (b) The amplitude spectrum versus the frequency of the output.

7. Conclusions and outlooks

In this review, we provide a broad overview of the vibrational resonance phenomenon, theory, applications and related topics. Vibrational resonance was proposed twenty years ago and focused on the response of a nonlinear system driven by a slow-varying characteristic signal and fast-varying auxiliary signal. With the development of vibrational resonance, it has been extended from the conventional vibrational resonance to the aperiodic vibrational resonance, the nonlinear vibrational resonance, the ultrasensitive vibrational resonance, the re-scaled vibrational resonance, the twice-sampling vibrational resonance, the logical vibrational resonance, etc. Furthermore, the vibrational resonance theory and related topics is still developing rapidly.

At present, there are a large number of nonlinear models for studying vibrational resonance. In this review paper, we have summarized the nonlinear models into five categories. The models described by ordinary differential equations, maps, fractional differential equations, delayed systems, and stochastic systems. Each category, contains nonlinear models associated to numerous disciplines.

In the field of signal processing, the purpose of the vibrational resonance research is to process the characteristic signal. The form of the characteristic signal is one of the most important factors in the study of vibrational resonance. We have given some typical types of the characteristic signal. Among them, vibrational resonance when the characteristic

signal in a simple harmonic signal or an aperiodic binary signal have been widely studied in the past two decades. Some complex signals, such as a frequency-modulated signal, bearing vibration signal are also introduced. While certain typical characteristic signals have been used in research, they are insufficient to address the requirements of complex signal processing in engineering. Complex signals often comprise numerous intricate frequency components that can evolve over time. Moreover, the rules governing these changes may be uncertain. When a nonlinear system is subjected to such complex signals, it exhibits considerably more intricate and diverse dynamical phenomena. Achieving vibrational resonance under the influence of such complex signals is a challenging yet significant and pressing issue to address. This necessitates the application of advanced signal processing techniques. Achieving this objective is demanding using only conventional methods for vibrational resonance research. In certain situations, the presence of strong noise makes it challenging to determine the weak characteristic signal in advance. In this situation, the stochastic resonance and vibrational resonance may be combined to realize the optimal resonance in the future. Corresponding to different characteristic signals, the choice of auxiliary signals determines the quality of the system output. If we blindly choose a harmonic signal or a periodic signal as an auxiliary signal, we may not get the strongest resonance output. These are also problems worth of study. With regards to the characteristic signal, we hope to pay much more attention to the complex signal especially for the signals acquired from real systems.

For studying vibrational resonance by using analytical tools, the method of direct separation of motions is mainly used. Needless to say, further new methods are necessary to develop to identify the vibrational resonance occurring at the subharmonic, superharmonic, or combined frequencies.

In the past studies, we have only paid attention to the forward problem. We know the nonlinear system and the characteristic signal and the auxiliary signal at first, then we investigate the occurrence of vibrational resonance. However, in applied science, there are a lot of inverse problems. Specifically, if we know the nonlinear system and the response, or we know the characteristic signal and the output, how to solve the unknown factor? The inverse problems have been studied in dynamics for decades. Whereas, the vibrational resonance theory is different from the general vibration formulation. The vibrational resonance focuses on the response of a nonlinear system with a very weak signal. It may solve the inverse problem corresponding to some special issues, such as the very small fault feature recognition and dynamic evolution of characteristic signals in machinery fault diagnosis applications, among others.

To conclude, the vibrational resonance investigations in the last decades have been mainly focused on analyzing nonlinear systems with simple characteristic signals in order to study the resonance response. In the future, much attention needs to be paid to find new nonlinear models, complex characteristic signals, and the corresponding inverse problems. Especially, key aspects of the research should be the study of vibrational resonance in experimental settings along with physical and engineering applications.

CRediT authorship contribution statement

Jianhua Yang: Writing – review & editing, Writing – original draft, Funding acquisition, Conceptualization. **S. Rajasekar:** Writing – review & editing, Conceptualization. **Miguel A.F. Sanjuán:** Writing – review & editing, Funding acquisition, Conceptualization.

Declaration of competing interest

The authors declare the following financial interests/personal relationships which may be considered as potential competing interests: Jianhua Yang reports financial support was provided by National Natural Science Foundation of China (Grant Nos. 12072362 and 12311530053). Miguel A. F. Sanjuan reports financial support was provided by State Agency of Research. If there are other authors, they declare that they have no known competing financial interests or personal relationships that could have appeared to influence the work reported in this paper.

Acknowledgments

The project was supported by the National Natural Science Foundation of China (Grant Nos. 12072362 and 12311530053), the Priority Academic Program Development of Jiangsu Higher Education Institutions, China, the Spanish State Research Agency (AEI) and the European Regional Development Fund (ERDF, EU) under Project No. PID2019- 105554GB-I00 (MCIN/AEI/10.13039/501100011033). We thank Prof. Chenggui Yao in Jiaxing University and Dr. Jinjie Zhu in Nanjing University of Aeronautics and Astronautics for their useful discussions. We also thank the graduate students Shengping Huang and Tao Gong in CUMT for some numerical calculations.

Appendix

The fractional-order derivative of a function $f(t)$ usually has a fractional order $\alpha \in R^+$. For the Riemann–Liouville definition of the fractional-order derivative, it is given as

$$ {}_{RL}D^{\alpha}f(t) \triangleq \frac{d^m}{dt^m}\left[\frac{1}{\Gamma(m-\alpha)}\int_0^t \frac{f(\tau)}{(t-\tau)^{\alpha-m+1}}d\tau\right]. \tag{A.1}$$

For the Caputo definition of the fractional-order derivative, it is defined as

$$ {}_{C}D^{\alpha}f(t) \triangleq \frac{1}{\Gamma(m-\alpha)}\int_0^t \frac{f^{(m)}(\tau)}{(t-\tau)^{\alpha-m+1}}d\tau. \tag{A.2} $$

In Eqs. (A.1) and (A.2), $\Gamma(\bullet)$ is the Gamma function, and $m-1<\alpha<m$, $m\in N$.

The Grünwald–Letnikov definition of the fractional-order derivative facilitates discretization of numerical calculations and is described in the form

$$ D^{\alpha}f(t)|_{t=kh} = \lim_{h\to 0}\frac{1}{h^{\alpha}}\sum_{j=0}^{k}(-1)^{j}\binom{\alpha}{j}f(kh-jh), \tag{A.3} $$

where $\binom{\alpha}{j}$ is the binomial coefficients.

More details for the three fractional-order derivative definitions mentioned above are given in [261].

References

[1] P.S. Landa, P.V.E. McClintock, Vibrational resonance, J. Phys. A: Math. Gen. 33 (2000) L433–L438, http://dx.doi.org/10.1088/0305-4470/33/45/103.

[2] L. Gammaitoni, P. Hañggi, P. Jung, F. Marchesoni, Stochastic resonance, Rev. Modern Phys. 70 (1998) 223–287, http://dx.doi.org/10.1103/RevModPhys.70.223.

[3] T. Wellens, V. Shatokhin, A. Buchleitner, Stochastic resonance, Rep. Progr. Phys. 67 (2003) 45–105, http://dx.doi.org/10.1088/0034-4885/67/1/R02.

[4] M. Rosenblum, P.V.E. McClintock, In memoriam-polina S. Landa (15 1931-21 2022), Chaos 32 (2022) 120401, http://dx.doi.org/10.1063/5.0136898.

[5] M. Gitterman, Bistable oscillator driven by two periodic fields, J. Phys. A: Math. Gen. 34 (2001) L355–L357, http://dx.doi.org/10.1088/0305-4470/34/24/101.

[6] I.I. Blekhman, P.S. Landa, Conjugate resonances and bifurcations in nonlinear systems under biharmonical excitation, Int. J. Nonlin. Mech. 39 (2004) 421–426, http://dx.doi.org/10.1016/S0020-7462(02)00201-9.

[7] J.J. Thomsen, Vibrations and Stability: Advanced Theory, Analysis, and Tools, third ed., Springer Nature, Switzerland, 2021, pp. 387–447, http://dx.doi.org/10.1007/978-3-030-68045-9.

[8] I.I. Blekhman, Vibrational Mechanics: Nonlinear Dynamic Effects, General Approach, Applications, World Scientific, Singapore, 2000, http://dx.doi.org/10.1142/4116.

[9] I.I. Blekhman, Selected Topics in Vibrational Mechanics, World Scientific, Singapore, 2004, http://dx.doi.org/10.1142/5013.

[10] A.H. Nayfeh, B. Balachandran, Applied Nonlinear Dynamics: Analytical, Computational, and Experimental Methods, Wiley-Vch Verlag GmbH & Co. KGaA, Weinheim, 2008, pp. 209–212.

[11] S. Jeyakumari, V. Chinnathambi, S. Rajasekar, M.A.F. Sanjuán, Single and multiple vibrational resonance in a quintic oscillator with monostable potentials, Phys. Rev. E 80 (2009) 046608, http://dx.doi.org/10.1103/PhysRevE.80.046608.

[12] S. Jeyakumari, V. Chinnathambi, S. Rajasekar, M.A.F. Sanjuán, Analysis of vibrational resonance in a quintic oscillator, Chaos 19 (2009) 043128, http://dx.doi.org/10.1063/1.3272207.

[13] Y.F. Yang, C.J. Wang, Theory and numerics of double-vibrational resonance in the overdamped oscillator, Chinese J. Phys. 51 (2013) 728–737, http://dx.doi.org/10.6122/CJP.51.728.

[14] C.J. Wang, Vibrational resonance in an overdamped system with a sextic double-well potential, Chinese Phys. Lett. 28 (2011) 090504, http://dx.doi.org/10.1088/0256-307X/28/9/090504.

[15] C.J. Fang, X.B. Liu, Theoretical analysis on the vibrational resonance in two coupled overdamped anharmonic oscillators, Chinese Phys. Lett. 29 (2012) 050504, http://dx.doi.org/10.1088/0256-307X/29/5/050504.

[16] P. Sarkar, D.S. Ray, Vibrational antiresonance in nonlinear coupled systems, Phys. Rev. E 99 (2019) 052221, http://dx.doi.org/10.1103/PhysRevE.99.052221.

[17] C. Yao, M. Zhan, Signal transmission by vibrational resonance in one-way coupled bistable systems, Phys. Rev. E 81 (2010) 061129, http://dx.doi.org/10.1103/PhysRevE.81.061129.

[18] J.A. Laoye, T.O. Roy-Layinde, K.A. Omoteso, O.O. Popoola, U.E. Vincent, Vibrational resonance in a higher-order nonlinear damped oscillator with rough potential, Pramana 93 (2019) 1–10, http://dx.doi.org/10.1007/s12043-019-1865-5.

[19] O. Kolebaje, O.O. Popoola, U.E. Vincent, Occurrence of vibrational resonance in an oscillator with an asymmetric toda potential, Physica D 419 (2021) 132853, http://dx.doi.org/10.1016/j.physd.2021.132853.

[20] S. Rajasekar, K. Abirami, M.A.F. Sanjuán, Novel vibrational resonance in multistable systems, Chaos 21 (2011) 033106, http://dx.doi.org/10.1063/1.3610213.

[21] L.C. Du, W.H. Song, W. Guo, D.C. Mei, Multiple current reversals and giant vibrational resonance in a high-frequency modulated periodic device, Europhys. Lett. 115 (2016) 40008, http://dx.doi.org/10.1209/0295-5075/115/40008.

[22] T.O. Roy-Layinde, J.A. Laoye, O.O. Popoola, U.E. Vincent, P.V.E. McClintock, Vibrational resonance in an inhomogeneous medium with periodic dissipation, Phys. Rev. E 96 (2017) 032209, http://dx.doi.org/10.1103/PhysRevE.96.032209.

[23] T.O. Roy-Layinde, K.A. Omoteso, O.T. Kolebaje, F.O. Ogunmefun, R.A. Fasasi, J.A. Laoye, U.E. Vincent, Vibrational resonance in a multistable system with position-dependent mass, Commun. Theor. Phys. 75 (2023) 115602, http://dx.doi.org/10.1088/1572-9494/acf20e.

[24] S. Ghosh, D.S. Ray, Optical Bloch equations in a bichromatic field; vibrational resonance, Eur. Phy. J. B 88 (2015) 23, http://dx.doi.org/10.1140/epjb/e2014-50306-y.

[25] O.I. Olusola, O.P. Shomotun, U.E. Vincent, P.V.E. McClintock, Quantum vibrational resonance in a dual-frequency-driven Tietz-Hua quantum well, Phys. Rev. E 101 (2020) 052216, http://dx.doi.org/10.1103/PhysRevE.101.052216.

[26] S. Paul, D.S. Ray, Vibrational resonance in a driven two-level quantum system, linear and nonlinear response, Philos. T. R. Soc. A 379 (2021) 20200231, http://dx.doi.org/10.1098/rsta.2020.0231.

[27] A. Chowdhury, M.G. Clerc, S. Barbay, I. Robert-Philip, R. Braive, Weak signal enhancement by nonlinear resonance control in a forced nano-electromechanical resonator, Nature Commun. 11 (2020) 1–9, http://dx.doi.org/10.1038/s41467-020-15827-3.

[28] A.V. Monwanou, A.A. Koukpémédji, C. Ainamon, P.R. Nwagoum Tuwa, C.H. Miwadinou, J.B. Chabi Orou, Nonlinear dynamics in a chemical reaction under an amplitude-modulated excitation: hysteresis, vibrational resonance, multistability, and chaos, Complexity 2020 (2020) 8823458, http://dx.doi.org/10.1155/2020/8823458.
[29] J.H. Yang, X.B. Liu, Delay induces quasi-periodic vibrational resonance, J. Phys. A 43 (2010) 122001, http://dx.doi.org/10.1088/1751-8113/43/12/122001.
[30] J.H. Yang, X.B. Liu, Controlling vibrational resonance in a multistable system by time delay, Chaos 20 (2010) 033124, http://dx.doi.org/10.1063/1.3481343.
[31] J.H. Yang, X.B. Liu, Controlling vibrational resonance in a delayed multistable system driven by an amplitude-modulated signal, Phys. Scr. 82 (2010) 025006, http://dx.doi.org/10.1088/0031-8949/82/02/025006.
[32] J.H. Yang, X.B. Liu, Delay-improved signal propagation in globally coupled bistable systems, Phys. Scr. 83 (2011) 065008, http://dx.doi.org/10.1088/0031-8949/83/06/065008.
[33] J.H. Yang, X.B. Liu, Analysis of periodic vibrational resonance induced by linear time delay feedback, Acta Phys. Sin. 61 (2012) 010505, http://dx.doi.org/10.7498/aps.61.010505.
[34] C. Jeevarathinam, S. Rajasekar, M.A.F. Sanjuán, Theory and numerics of vibrational resonance in duffing oscillators with time-delayed feedback, Phys. Rev. E 83 (2011) 066205, http://dx.doi.org/10.1103/PhysRevE.83.066205.
[35] C. Jeevarathinam, S. Rajasekar, M.A.F. Sanjuán, Effect of multiple time-delay on vibrational resonance, Chaos 23 (2013) 013136, http://dx.doi.org/10.1063/1.4793542.
[36] X.N. Yang, Y.F. Yang, Vibrational resonance in an asymmetric bistable system with time-delay feedback, Acta Phys. Sin. 64 (2015) 070507, http://dx.doi.org/10.7498/aps.64.070507.
[37] D. Hu, J. Yang, X. Liu, Delay-induced vibrational multiresonance in FitzHugh–nagumo system, Commun. Nonlinear Sci. Numer. Simul. 17 (2012) 1031–1035, http://dx.doi.org/10.1016/j.cnsns.2011.05.041.
[38] D.L. Hu, J.H. Yang, X.B. Liu, Vibrational resonance in the FitzHugh–Nagumo system with time-varying delay feedback, Comput. Biol. Med. 45 (2014) 80–86, http://dx.doi.org/10.1016/j.compbiomed.2013.11.022.
[39] D.L. Hu, X.B. Liu, Delay-enhanced signal transmission in a coupled excitable system, Neurocomputing 135 (2014) 268–272, http://dx.doi.org/10.1016/j.neucom.2013.12.021.
[40] C. Wang, K. Yang, S. Qu, Vibrational resonance in a discrete neuronal model with time delay, Internat. J. Modern Phys. B 28 (2014) 1450103, http://dx.doi.org/10.1142/S0217979214501033.
[41] A. Daza, A. Wagemakers, S. Rajasekar, M.A.F. Sanjuán, Vibrational resonance in a time-delayed genetic toggle switch, Commun. Nonlinear Sci. Numer. Simul. 18 (2013) 411–416, http://dx.doi.org/10.1016/j.cnsns.2012.07.010.
[42] L. Ning, Z. Chen, Vibrational resonance analysis in a gene transcriptional regulatory system with two different forms of time-delays, Physica D 401 (2020) 132164, http://dx.doi.org/10.1016/j.physd.2019.132164.
[43] Z. Yang, L. Ning, Vibrational resonance in a harmonically trapped potential system with time delay, Pramana 92 (2019) 89, http://dx.doi.org/10.1007/s12043-019-1750-2.
[44] J.H. Yang, M.A.F. Sanjuán, H.G. Liu, Signal generation and enhancement in a delayed system, Commun. Nonlinear Sci. Numer. Simul. 22 (2015) 1158–1168, http://dx.doi.org/10.1016/j.cnsns.2014.08.005.
[45] M.L. Lv, G. Shen, H.L. Wang, J.H. Yang, Is the high-frequency signal necessary for the resonance in the delayed system? Chinese Phys. Lett. 32 (2015) 010501, http://dx.doi.org/10.1088/0256-307X/32/1/010501.
[46] S. Yanchuk, P. Perlikowski, Delay and periodicity, Phys. Rev. E 79 (2009) 046221, http://dx.doi.org/10.1103/PhysRevE.79.046221.
[47] M.D. Ortigueira, An introduction to the fractional continuous-time linear systems: the 21st century systems, IEEE Circuits Syst. Mag. 8 (2008) 19–26, http://dx.doi.org/10.1109/MCAS.2008.928419.
[48] J.H. Yang, H. Zhu, Vibrational resonance in duffing systems with fractional-order damping, Chaos 22 (2012) 013112, http://dx.doi.org/10.1063/1.3678788.
[49] L. Zhang, T.T. Xie, M.K. Luo, Vibrational resonance in a duffing system with fractional-order external and intrinsic dampings driven by two-frequency signal, Acta Phys. Sin. 63 (2014) 010506, http://dx.doi.org/10.7498/aps.63.010506.
[50] Z. Yan, X. Liu, Effect of parametric excitation on a bifractional-order damped system with a fractional-power nonlinearity, Chaos 30 (2020) 023109, http://dx.doi.org/10.1063/1.5133810.
[51] T. Qin, T. Xie, M. Luo, K. Deng, Vibrational resonance in fractional-order overdamped multistable systems, Chinese J. Phys. 55 (2017) 546–555, http://dx.doi.org/10.1016/j.cjph.2016.11.005.
[52] J.H. Yang, Vibrational resonance in fractional-order anharmonic oscillators, Chinese Phys. Lett. 29 (2012) 104501, http://dx.doi.org/10.1088/0256-307X/29/10/104501.
[53] Z. Yan, W. Wang, X. Liu, Analysis of a quintic system with fractional damping in the presence of vibrational resonance, Appl. Math. Comput. 321 (2018) 780–793, http://dx.doi.org/10.1016/j.amc.2017.11.028.
[54] T.L.M.D. Mbong, M.S. Siewe, C. Tchawoua, The effect of the fractional derivative order on vibrational resonance in a special fractional quintic oscillator, Mech. Res. Commun. 78 (2016) 13–19, http://dx.doi.org/10.1016/j.mechrescom.2016.10.004.
[55] W. Guo, L. Ning, Vibrational resonance in a fractional order quintic oscillator system with time delay feedback, Int. J. Bifurcation Chaos 30 (2020) 2050025, http://dx.doi.org/10.1142/S021812742050025X.
[56] P. Fu, C.J. Wang, K.L. Yang, X.B. Li, B. Yu, Reentrance-like vibrational resonance in a fractional-order birhythmic biological system, Chaos Solitons Fractals 155 (2022) 111649, http://dx.doi.org/10.1016/j.chaos.2021.111649.
[57] J. Wang, R. Zhang, J. Liu, Vibrational resonance analysis in a fractional order toda oscillator model with asymmetric potential, Int. J. Nonlin. Mech. 148 (2023) 104258, http://dx.doi.org/10.1016/j.ijnonlinmec.2022.104258.
[58] J.H. Yang, Bifurcation and Resonance in Fractional-Order Systems, Science Press, Beijing, 2017, in Chinese.
[59] J.H. Yang, M.A.F. Sanjuán, W. Xiang, H. Zhu, Pitchfork bifurcation and vibrational resonance in a fractional-order duffing oscillator, Pramana 81 (2013) 943–957, http://dx.doi.org/10.1007/s12043-013-0621-5.
[60] J.H. Yang, H. Zhu, Bifurcation and resonance induced by fractional-order damping and time delay feedback in a duffing system, Commun. Nonlinear Sci. Numer. Simul. 18 (2013) 1316–1326, http://dx.doi.org/10.1016/j.cnsns.2012.09.023.
[61] J.H. Yang, M.A.F. Sanjuán, H.G. Liu, Bifurcation and resonance in a fractional mathieu-duffing oscillator, Eur. Phys. J. B 88 (2015) 310, http://dx.doi.org/10.1140/epjb/e2015-60315-y.
[62] J.H. Yang, H.G. Liu, G. Cheng, The pitchfork bifurcation and vibrational resonance in a quintic oscillator, Acta Phys. Sin. 62 (2013) 180503, http://dx.doi.org/10.7498/aps.62.180503.
[63] Y. Zhang, J. Li, S. Zhu, H. Zhao, Bifurcation and chaos detection of a fractional duffing-van der pol oscillator with two periodic excitations and distributed time delay, Chaos 33 (2023) 083153, http://dx.doi.org/10.1063/5.0160812.
[64] J.H. Yang, M.A.F. Sanjuán, F. Tian, H.F. Yang, Saddle–node bifurcation and vibrational resonance in a fractional system with an asymmetric bistable potential, In. J. Bifurcat. Chaos 25 (2015) 1550023, http://dx.doi.org/10.1142/S0218127415500236.
[65] J.H. Yang, M.A.F. Sanjuán, H.G. Liu, G. Cheng, Bifurcation transition and nonlinear response in a fractional-order system, J. Comput. Nonlin. Dyn. 10 (2015) 061017, http://dx.doi.org/10.1115/1.4029512.

[66] E. Ullner, A. Zaikin, J. García-Ojalvo, R. Báscones, J. Kurths, Vibrational resonance and vibrational propagation in excitable systems, Phys. Lett. A 312 (2003) 348–354, http://dx.doi.org/10.1016/S0375-9601(03)00681-9.
[67] D. Cubero, J.P. Baltanás, J. Casado-Pascual, High-frequency effects in the FitzHugh–Nagumo neuron model, Phys. Rev. E 73 (2006) 061102, http://dx.doi.org/10.1103/PhysRevE.73.061102.
[68] L. Yang, W. Liu, M. Yi, C. Wang, Q. Zhu, X. Zhan, Y. Jia, Vibrational resonance induced by transition of phase-locking modes in excitable systems, Phys. Rev. E 86 (2012) 016209, http://dx.doi.org/10.1103/PhysRevE.86.016209.
[69] J. Zhu, C. Kong, X. Liu, Subthreshold and suprathreshold vibrational resonance in the FitzHugh–Nagumo neuron model, Phys. Rev. E 94 (2016) 032208, http://dx.doi.org/10.1103/PhysRevE.94.032208.
[70] S. Morfu, M. Bordet, On the correlation between phase-locking modes and vibrational resonance in a neuronal model, Commun. Nonlinear Sci. Numer. Simul. 55 (2018) 277–286, http://dx.doi.org/10.1016/j.cnsns.2017.07.023.
[71] S. Morfu, M. Bordet, On the propagation of a low frequency excitation in a perturbed FitzHugh–Nagumo system: Simulation and experiments, Chaos Solitons Fractals 103 (2017) 205–212, http://dx.doi.org/10.1016/j.chaos.2017.06.006.
[72] M. Bordet, S. Morfu, Experimental and numerical enhancement of vibrational resonance in neural circuit, Electron. Lett. 48 (2012) 903–905, http://dx.doi.org/10.1049/el.2012.1343.
[73] B. Deng, J. Wang, X. Wei, H. Yu, H. Li, Theoretical analysis of vibrational resonance in a neuron model near a bifurcation point, Phys. Rev. E 89 (2014) 062916, http://dx.doi.org/10.1103/PhysRevE.89.062916.
[74] B. Deng, J. Wang, X. Wei, K.M. Tsang, W.L. Chan, Vibrational resonance in neuron populations, Chaos 20 (2010) 013113, http://dx.doi.org/10.1063/1.3324700.
[75] B. Deng, J. Wang, X. Wei, Effect of chemical synapse on vibrational resonance in coupled neurons, Chaos 19 (2009) 013117, http://dx.doi.org/10.1063/1.3076396.
[76] M. Ge, L. Lu, Y. Xu, R. Mamatimin, Q. Pei, Y. Jia, Vibrational mono-/bi-resonance and wave propagation in FitzHugh–Nagumo neural systems under electromagnetic induction, Chaos Solitons Fractals 133 (2020) 109645, http://dx.doi.org/10.1016/j.chaos.2020.109645.
[77] A. Calim, A. Longtin, M. Uzuntarla, Vibrational resonance in a neuron-astrocyte coupled model, Philos. T. R. Soc. A 379 (2021) 20200267, http://dx.doi.org/10.1098/rsta.2020.0267.
[78] X. Li, X. Xue, D. Liu, T. Yu, Q. He, G. Xu, Effects of electric field on vibrational resonances in hindmarsh-rose neuronal systems for signal detection, Chinese Phys. B 32 (2023) 048701, http://dx.doi.org/10.1088/1674-1056/ac9cc0.
[79] H. Yu, J. Wang, C. Liu, B. Deng, X. Wei, Vibrational resonance in excitable neuronal systems, Chaos 21 (2011) 043101, http://dx.doi.org/10.1063/1.3644390.
[80] H. Yu, J. Wang, J. Sun, H. Yu, Effects of hybrid synapses on the vibrational resonance in small-world neuronal networks, Chaos 22 (2012) 033105, http://dx.doi.org/10.1063/1.4729462.
[81] H. Yu, X. Guo, J. Wang, B. Deng, X. Wei, Vibrational resonance in adaptive small-world neuronal networks with spike-timing-dependent plasticity, Physica A 436 (2015) 170–179, http://dx.doi.org/10.1016/j.physa.2015.05.037.
[82] M. Xue, J. Wang, B. Deng, X. Wei, Vibrational resonance in feedforward neuronal network with unreliable synapses, Eur. Phy. J. B 86 (2013) 122, http://dx.doi.org/10.1140/epjb/e2013-30782-3.
[83] M. Uzuntarla, E. Yilmaz, A. Wagemakers, M. Ozer, Vibrational resonance in a heterogeneous scale free network of neurons, Commun. Nonlinear Sci. Numer. Simul. 22 (2015) 367–374, http://dx.doi.org/10.1016/j.cnsns.2014.08.040.
[84] C. Yao, J. Ma, Z. He, Y. Qian, L. Liu, Transmission and detection of biharmonic envelope signal in a feed-forward multilayer neural network, Physica A 523 (2019) 797–806, http://dx.doi.org/10.1016/j.physa.2019.02.053.
[85] C. Yao, Z. He, T. Nakano, Y. Qian, J. Shuai, Inhibitory-autapse-enhanced signal transmission in neural networks, Nonlinear Dynam. 97 (2019) 1425–1437, http://dx.doi.org/10.1007/s11071-019-05060-z.
[86] J. Sun, B. Deng, C. Liu, H. Yu, J. Wang, X. Wei, J. Zhao, Vibrational resonance in neuron populations with hybrid synapses, Appl. Math. Model. 37 (2013) 6311–6324, http://dx.doi.org/10.1016/j.apm.2013.01.007.
[87] Y. Qin, J. Wang, C. Men, B. Deng, X.L. Wei, Vibrational resonance in feedforward network, Chaos 21 (2011) 023133, http://dx.doi.org/10.1063/1.3603818.
[88] Y.M. Qin, J. Wang, C. Men, W.L. Chan, X.L. Wei, B. Deng, Control of synchronization and spiking regularity by heterogenous aperiodic high-frequency signal in coupled excitable systems, Commun. Nonlinear Sci. Numer. Simul. 18 (2013) 2775–2782, http://dx.doi.org/10.1016/j.cnsns.2013.02.010.
[89] C. Han, Y. Qin, Q. Qin, R. Wang, M. Lu, J. Zhao, Y. Che, Vibrational resonance without tuning in a neuronal parallel array, Physica A 523 (2019) 204–210, http://dx.doi.org/10.1016/j.physa.2019.02.042.
[90] S.N. Agaoglu, A. Calim, P. Hövel, M. Ozer, Vibrational resonance in a scale-free network with different coupling schemes, Neurocomputing 325 (2019) 59–66, http://dx.doi.org/10.1016/j.neucom.2018.09.070.
[91] J. Shi, C. Huang, T. Dong, X. Zhang, High-frequency and low-frequency effects on vibrational resonance in a synthetic gene network, Phys. Biol. 7 (2010) 036006, http://dx.doi.org/10.1088/1478-3975/7/3/036006.
[92] V. Baysal, E. Yilmaz, Effects of electromagnetic induction on vibrational resonance in single neurons and neuronal networks, Physica A 537 (2020) 122733, http://dx.doi.org/10.1016/j.physa.2019.122733.
[93] A. Calim, T. Palabas, M. Uzuntarla, Stochastic and vibrational resonance in complex networks of neurons, Philos. T. R. Soc. A 379 (2021) 20200236, http://dx.doi.org/10.1098/rsta.2020.0236.
[94] S. Ghosh, D.S. Ray, Nonlinear vibrational resonance, Phys. Rev. E 88 (2013) 042904, http://dx.doi.org/10.1103/PhysRevE.88.042904.
[95] V.N. Chizhevsky, Vibrational higher-order resonances in an overdamped bistable system with biharmonic excitation, Phys. Rev. E 90 (2014) 042924, http://dx.doi.org/10.1103/PhysRevE.90.042924.
[96] R. Lin, T.Y. Ng, Z. Fan, New type of spectral nonlinear resonance enhances identification of weak signals, Sci. Rep. 9 (2019) 14125, http://dx.doi.org/10.1038/s41598-019-50767-z.
[97] R.Z. Sun, Z.Z. Wang, M.S. Wang, J.Q. Zhang, Vibrational resonance and nonlinear vibrational resonance in square-lattice neural system, Acta Phys. Sin. 64 (2015) 110501, http://dx.doi.org/10.7498/aps.64.110501.
[98] J.H. Yang, M.A.F. Sanjuán, H.G. Liu, Vibrational subharmonic and superharmonic resonances, Commun. Nonlinear Sci. Numer. Simul. 30 (2016) 362–372, http://dx.doi.org/10.1016/j.cnsns.2015.07.002.
[99] P. Sarkar, S. Paul, D.S. Ray, Controlling subharmonic generation by vibrational and stochastic resonance in a bistable system, J. Stat. Mech. 2019 (2019) 063211, http://dx.doi.org/10.1088/1742-5468/ab2532.
[100] S. Roy, A. Ray, A.R. Chowdhury, Controlling subharmonic resonance and chaos by a fast forcing in a van der pol-duffing oscillator with parametrically excited damping, Chaos Solitons Fractals 174 (2023) 113857, http://dx.doi.org/10.1016/j.chaos.2023.113857.
[101] D. Das, D.S. Ray, Enhancement of nonlinear response using vibrational resonance in a nonlinear oscillator; sum and difference frequency generation, Eur. Phy. J. B 91 (2018) 279, http://dx.doi.org/10.1140/epjb/e2018-90349-4.
[102] S. Rajamani, S. Rajasekar, M.A.F. Sanjuán, Ghost-vibrational resonance, Commun. Nonlinear Sci. Numer. Simul. 19 (2014) 4003–4012, http://dx.doi.org/10.1016/j.cnsns.2014.04.006.

[103] K. Abirami, S. Rajasekar, M.A.F. Sanjuán, Vibrational and ghost-vibrational resonances in a modified chua's circuit model equation, Int. J. Bifurcation Chaos 24 (2014) 1430031, http://dx.doi.org/10.1142/S0218127414300316.
[104] B.I. Usama, S. Morfu, P. Marquie, Vibrational resonance and ghost-vibrational resonance occurrence in chua's circuit models with specific nonlinearities, Chaos Solitons Fractals 153 (2021) 111515, http://dx.doi.org/10.1016/j.chaos.2021.111515.
[105] R. Samikkannu, M. Ramasamy, S. Kumarasamy, K. Rajagopal, Studies on ghost-vibrational resonance in a periodically driven anharmonic oscillator, Eur. Phy. J. B 96 (2023) 56, http://dx.doi.org/10.1140/epjb/s10051-023-00527-w.
[106] P. Balenzuela, H. Braun, D.R. Chialvo, The ghost of stochastic resonance: an introductory review, Contemp. Phys. 53 (2012) 17–38, http://dx.doi.org/10.1080/00107514.2011.639605.
[107] L. Du, R. Han, J. Jiang, W. Guo, Entropic vibrational resonance, Phys. Rev. E 102 (2020) 012149, http://dx.doi.org/10.1103/PhysRevE.102.012149.
[108] J. Jiang, J. Liu, W. Guo, L. Du, Energetic and entropic vibrational resonance with a time-delayed feedback, Chinese J. Phys. 78 (2022) 1–12, http://dx.doi.org/10.1016/j.cjph.2022.05.002.
[109] P.S. Burada, G. Schmid, D. Reguera, M.H. Vainstein, J.M. Rubi, P. Hänggi, Entropic stochastic resonance, Phys. Rev. Lett. 101 (2008) 130602, http://dx.doi.org/10.1103/PhysRevLett.101.130602.
[110] V.N. Chizhevsky, G. Giacomelli, Vibrational resonance and the detection of aperiodic binary signals, Phys. Rev. E 77 (2008) 051126, http://dx.doi.org/10.1103/PhysRevE.77.051126.
[111] H.G. Liu, X.L. Liu, J.H. Yang, M.A.F. Sanjuán, G. Cheng, Detecting the weak high-frequency character signal by vibrational resonance in the duffing oscillator, Nonlinear Dynam. 89 (2017) 2621–2628, http://dx.doi.org/10.1007/s11071-017-3610-2.
[112] J.H. Yang, M.A.F. Sanjuán, H.G. Liu, Enhancing the weak signal with arbitrary high-frequency by vibrational resonance in fractional-order duffing oscillators, J. Comput. Nonlin. Dyn. 12 (2017) 051011, http://dx.doi.org/10.1115/1.4036479.
[113] J.R. Yang, C.J. Wu, J.H. Yang, H.G. Liu, On the weak signal amplification by twice sampling vibrational resonance method in fractional duffing oscillators, J. Comput. Nonlin. Dyn. 13 (2018) 031009, http://dx.doi.org/10.1115/1.4038778.
[114] P. Jia, J. Yang, H. Liu, E. Hu, Improving amplitude-modulated signals by re-scaled and twice sampling vibrational resonance methods, Pramana 91 (2018) 38, http://dx.doi.org/10.1007/s12043-018-1617-y.
[115] P.X. Jia, C.J. Wu, J.H. Yang, M.A.F. Sanjuán, G.X. Liu, Improving the weak aperiodic signal by three kinds of vibrational resonance, Nonlinear Dynam. 91 (2018) 2699–2713, http://dx.doi.org/10.1007/s11071-017-4040-x.
[116] J.H. Yang, Q. Ma, C.J. Wu, H.G. Liu, Aperiodic vibrational resonance in the fractional-order bistable system, Acta Phys. Sin. 67 (2018) 054501, http://dx.doi.org/10.7498/aps.67.20172046.
[117] P. Jia, Y. Leng, J. Yang, On the aperiodic signal amplification by rescaled vibrational resonance in fractional-order duffing oscillators, J. Comput. Nonlin. Dyn. 15 (2020) 071001, http://dx.doi.org/10.1115/1.4046936.
[118] P. Jia, J. Yang, C. Wu, M.A.F. Sanjuán, Amplification of the LFM signal by using piecewise vibrational methods, J. Vib. Control 25 (2019) 141–150, http://dx.doi.org/10.1177/107754631877225.
[119] P. Jia, J. Yang, X. Zhang, M.A.F. Sanjuán, On the LFM signal improvement by piecewise vibrational resonance using a new spectral amplification factor, IET Signal Process. 13 (2018) 65–69, http://dx.doi.org/10.1049/iet-spr.2018.5101.
[120] C. Yang, J. Yang, D. Zhou, S. Zhang, G. Litak, Adaptive stochastic resonance in bistable system driven by noisy NLFM signal: phenomenon and application, Philos. T. R. Soc. A 379 (2021) 20200239, http://dx.doi.org/10.1098/rsta.2020.0239.
[121] P. Jia, J. Yang, Y. Leng, The echo chirp signal amplification by the vibrational information fusion method, Internat. J. Modern Phys. B 34 (2020) 2050041, http://dx.doi.org/10.1142/S0217979220500411.
[122] Y. Zhai, J. Yang, S. Zhang, H. Liu, Linear frequency modulated signal induced aperiodic resonance, Phys. Scr. 95 (2020) 065213, http://dx.doi.org/10.1088/1402-4896/ab825a.
[123] P.S. Landa, P.V.E. McClintock, Nonlinear systems with fast and slow motions. Changes in the probability distribution for fast motions under the influence of slower ones, Phys. Rep. 532 (2013) 1–26, http://dx.doi.org/10.1016/j.physrep.2013.06.002.
[124] A.A. Zaikin, L. Lopez, J.P. Baltanás, J. Kurths, M.A.F. Sanjuán, Vibrational resonance in a noise-induced structure, Phys. Rev. E 66 (2002) 011106, http://dx.doi.org/10.1103/PhysRevE.66.011106.
[125] J.P. Baltanás, L. Lopez, I.I. Blechman, P.S. Landa, A. Zaikin, J. Kurths, M.A.F. Sanjuán, Experimental evidence, numerics, and theory of vibrational resonance in bistable systems, Phys. Rev. E 67 (2003) 066119, http://dx.doi.org/10.1103/PhysRevE.67.066119.
[126] J. Casado-Pascual, J.P. Baltanás, Effects of additive noise on vibrational resonance in a bistable system, Phys. Rev. E 69 (2004) 046108, http://dx.doi.org/10.1103/PhysRevE.69.046108.
[127] V.N. Chizhevsky, G. Giacomelli, Experimental and theoretical study of the noise-induced gain degradation in vibrational resonance, Phys. Rev. E 70 (2004) 062101, http://dx.doi.org/10.1103/PhysRevE.70.062101.
[128] V.N. Chizhevsky, G. Giacomelli, Improvement of SNR ratio in a bistable optical system: comparison between vibrational and stochastic resonance, Phys. Rev. A 71 (2005) 011801, http://dx.doi.org/10.1103/PhysRevA.71.011801.
[129] V.N. Chizhevsky, Noise-induced suppression of nonlinear distortions in a bistable system with biharmonic excitation in vibrational resonance, Phys. Rev. E 92 (2015) 032902, http://dx.doi.org/10.1103/PhysRevE.92.032902.
[130] M. Lin, Y. Huang, Stochastic resonance control based on vibration resonance, Acta Phys. Sin. 56 (2007) 6173–6177, http://dx.doi.org/10.7498/aps.56.6173.
[131] C. Stan, C.P. Cristescu, D. Alexandroaei, M. Agop, Stochastic resonance and vibrational resonance in an excitable system: The golden mean barrier, Chaos Solitons Fractals 41 (2009) 727–734, http://dx.doi.org/10.1016/j.chaos.2008.03.004.
[132] C. Yao, Y. Liu, M. Zhan, Frequency-resonance-enhanced vibrational resonance in bistable systems, Phys. Rev. E 83 (2011) 061122, http://dx.doi.org/10.1103/PhysRevE.83.061122.
[133] Z.Y. He, Y.R. Zhou, Vibrational and stochastic resonance in the FitzHugh–Nagumo neural model with multiplicative and additive noise, Chinese Phys. Lett. 28 (2011) 110505, http://dx.doi.org/10.1088/0256-307X/28/11/110505.
[134] F. Guo, Multiplicative noise-induced vibrational resonance in a monostable system with one high-frequency and two low-frequency forces, Phys. Scr. 83 (2011) 025008, http://dx.doi.org/10.1088/0031-8949/83/02/025008.
[135] M. Bordet, S. Morfu, Experimental and numerical study of noise effects in a FitzHugh–Nagumo system driven by a biharmonic signal, Chaos Solitons Fractals 54 (2013) 82–89, http://dx.doi.org/10.1016/j.chaos.2013.05.020.
[136] F. Duan, F. Chapeau-Blondeau, D. Abbott, Double-maximum enhancement of signal-to-noise ratio gain via stochastic resonance and vibrational resonance, Phys. Rev. E 90 (2014) 022134, http://dx.doi.org/10.1103/PhysRevE.90.022134.
[137] Y. Ren, Y. Pan, F. Duan, F. Chapeau-Blondeau, D. Abbott, Exploiting vibrational resonance in weak-signal detection, Phys. Rev. E 96 (2017) 022141, http://dx.doi.org/10.1103/PhysRevE.96.022141.
[138] Y. Ren, F. Duan, Theoretical and experimental implementation of vibrational resonance in an array of hard limiters, Physica A 456 (2016) 319–326, http://dx.doi.org/10.1016/j.physa.2016.03.073.
[139] Y. Ren, Y. Pan, F. Duan, Generalized energy detector for weak random signals via vibrational resonance, Phys. Lett. A 382 (2018) 806–810, http://dx.doi.org/10.1016/j.physleta.2018.01.015.
[140] S.B. Jiao, D. Sun, D. Liu, G. Xie, Y.L. Wu, Q. Zhang, Vibrational resonance in a periodic potential system with alpha stable noise, Acta Phys. Sin. 66 (2017) 100501, http://dx.doi.org/10.7498/aps.66.100501.

[141] J. Zhao, J. Yang, J. Zhang, C. Wu, D. Huang, Improving the stochastic resonance in a bistable system with the bounded noise excitation, J. Stat. Phys. 173 (2018) 1688–1697, http://dx.doi.org/10.1007/s10955-018-2145-3.
[142] H. Liu, J. Yang, H. Liu, S. Shi, Different fast excitations on the improvement of stochastic resonance in bounded noise excited system, Internat. J. Modern Phys. B 34 (2020) 2050238, http://dx.doi.org/10.1142/S0217979220502380.
[143] R. Gui, Y. Wang, Y. Yao, G. Cheng, Enhanced logical vibrational resonance in a two-well potential system, Chaos Solitons Fractals 138 (2020) 109952, http://dx.doi.org/10.1016/j.chaos.2020.109952.
[144] M. Borromeo, F. Marchesoni, Vibrational ratchets, Phys. Rev. E 73 (2006) 016142, http://dx.doi.org/10.1103/PhysRevE.73.016142.
[145] M. Borromeo, F. Marchesoni, Mobility oscillations in high-frequency modulated devices, Europhys. Lett. 72 (2005) 362, http://dx.doi.org/10.1209/epl/i2005-10246-4.
[146] M. Borromeo, P. Hänggi, F. Marchesoni, Transport by bi-harmonic drives: from harmonic to vibrational mixing, J. Phys.: Condens. Matter 17 (2005) S3709, http://dx.doi.org/10.1088/0953-8984/17/47/005.
[147] J. Liu, C. Li, H. Gao, L. Du, Vibrational resonance in globally-coupled bistable systems under the noise background, Chinese Phys. B 32 (2023) 070502, http://dx.doi.org/10.1088/1674-1056/acc05f.
[148] M. Coccolo, G. Litak, J.M. Seoane, M.A.F. Sanjuán, Energy harvesting enhancement by vibrational resonance, Int. J. Bifurcation Chaos 24 (2014) 1430019, http://dx.doi.org/10.1142/S0218127414300195.
[149] I.A. Khovanov, The response of a bistable energy harvester to different excitations: the harvesting efficiency and links with stochastic and vibrational resonance, Philos. T. R. Soc. A 379 (2021) 20200245, http://dx.doi.org/10.1098/rsta.2020.0245.
[150] T. Zhang, Y. Jin, Y. Xu, X. Yue, Dynamical response and vibrational resonance of a tri-stable energy harvester interfaced with a standard rectifier circuit, Chaos 32 (2022) 093150, http://dx.doi.org/10.1063/5.0105337.
[151] Z. Chen, F. Chen, Bifurcation behaviors and bursting regimes of a piezoelectric buckled beam harvester under fast-slow excitation, Nonlinear Dynam. 111 (2023) 4121–4139, http://dx.doi.org/10.1007/s11071-022-08046-6.
[152] S. Wang, B. Lu, Detecting the weak damped oscillation signal in the agricultural machinery working environment by vibrational resonance in the duffing system, J. Mech. Sci. Technol. 36 (2022) 5925–5937, http://dx.doi.org/10.1007/s12206-022-1109-3.
[153] L. Xiao, X. Zhang, S. Lu, T. Xia, L. Xi, A novel weak-fault detection technique for rolling element bearing based on vibrational resonance, J. Sound Vib. 438 (2019) 490–505, http://dx.doi.org/10.1016/j.jsv.2018.09.039.
[154] J. Gao, J. Yang, D. Huang, H. Liu, S. Liu, Experimental application of vibrational resonance on bearing fault diagnosis, J. Braz. Soc. Mech. Sci. Eng. 41 (2019) 6, http://dx.doi.org/10.1007/s40430-018-1502-0.
[155] J. Zhang, J. Yang, G. Litak, E. Hu, Feature extraction under bounded noise background and its application in low speed bearing fault diagnosis, J. Mech. Sci. Technol. 33 (2019) 3193–3204, http://dx.doi.org/10.1007/s12206-019-0614-5.
[156] L. Xiao, J. Tang, X. Zhang, T. Xia, Weak fault detection in rotating machineries by using vibrational resonance and coupled varying-stable nonlinear systems, J. Sound Vib. 478 (2020) 115355, http://dx.doi.org/10.1016/j.jsv.2020.115355.
[157] L. Xiao, R. Bajric, J. Zhao, J. Tang, X. Zhang, An adaptive vibrational resonance method based on cascaded varying stable-state nonlinear systems and its application in rotating machine fault detection, Nonlinear Dynam. 103 (2021) 715–739, http://dx.doi.org/10.1007/s11071-020-06143-y.
[158] S. Morfu, B.I. Usama, P. Marquié, Perception enhancement of subthreshold noisy image with vibrational resonance, Electron. Lett. 55 (2019) 650–652, http://dx.doi.org/10.1049/el.2018.8059.
[159] S. Morfu, B.I. Usama, P. Marquié, On some applications of vibrational resonance on image perception: The role of the perturbation parameters, Philos. T. R. Soc. A 379 (2021) 20200240, http://dx.doi.org/10.1098/rsta.2020.0240.
[160] U.E. Vincent, P.V.E. McClintock, I.A. Khovanov, S. Rajasekar, Vibrational and stochastic resonances in driven nonlinear systems, Philos. T. R. Soc. A 379 (2021) 20200226, http://dx.doi.org/10.1098/rsta.2020.0226.
[161] U.E. Vincent, P.V.E. McClintock, I.A. Khovanov, S. Rajasekar, Vibrational and stochastic resonances in driven nonlinear systems - part 2, Philos. T. R. Soc. A 379 (2021) 20210003, http://dx.doi.org/10.1098/rsta.2021.0003.
[162] V.N. Chizhevsky, Amplification of optical signals in a bistable vertical-cavity surface-emitting laser by vibrational resonance, Philos. T. R. Soc. A 379 (2021) 20200241, http://dx.doi.org/10.1098/rsta.2020.0241.
[163] Y. Pan, F. Duan, F. Chapeau-Blondeau, L. Xu, D. Abbott, Study of vibrational resonance in nonlinear signal processing, Philos. T. R. Soc. A 379 (2021) 20200235, http://dx.doi.org/10.1098/rsta.2020.0235.
[164] T.O. Roy-Layinde, U.E. Vincent, S.A. Abolade, O.O. Popoola, J.A. Laoye, P.V.E. McClintock, Vibrational resonances in driven oscillators with position-dependent mass, Philos. T. R. Soc. A 379 (2021) 20200227, http://dx.doi.org/10.1098/rsta.2020.0227.
[165] K. Murali, S. Rajasekar, M.V. Aravind, V. Kohar, W.L. Ditto, S. Sinha, Construction of logic gates exploiting resonance phenomena in nonlinear systems, Philos. T. R. Soc. A 379 (2021) 20200238, http://dx.doi.org/10.1098/rsta.2020.0238.
[166] V. Sorokin, I. Demidov, On representing noise by deterministic excitations for interpreting the stochastic resonance phenomenon, Philos. T. R. Soc. A 379 (2021) 20200229, http://dx.doi.org/10.1098/rsta.2020.0229.
[167] E. Kremer, The effect of high-frequency stochastic actions on the low-frequency behaviour of dynamic systems, Philos. T. R. Soc. A 379 (2021) 20200242, http://dx.doi.org/10.1098/rsta.2020.0242.
[168] A.H. Alhadidi, S. Khazaaleh, M.F. Daqaq, Suppression of galloping oscillations by injecting a high-frequency excitation, Philos. T. R. Soc. A 379 (2021) 20200244, http://dx.doi.org/10.1098/rsta.2020.0244.
[169] S. Rajasekar, M.A.F. Sanjuán, Nonlinear Resonances, Springer International Publishing, Switzerland, 2016, http://dx.doi.org/10.1007/978-3-319-24886-8.
[170] V.M. Gandhimathi, S. Rajasekar, J. Kurths, Effects of the shape of periodic forces on stochastic resonance, Int. J. Bifurcation Chaos 18 (2008) 2073–2088, http://dx.doi.org/10.1142/S0218127408021579.
[171] V.M. Gandhimathi, K. Murali, S. Rajasekar, Stochastic resonance with different periodic forces in overdamped two coupled anharmonic oscillators, Chaos Solitons Fractals 30 (2006) 1034–1047, http://dx.doi.org/10.1016/j.chaos.2005.09.046.
[172] J. Zhang, J. Yang, Z. Zhu, G. Shen, M.A.F. Sanjuán, Effects of different fast periodic excitations on the pitchfork bifurcation and vibrational resonance, Int. J. Bifurcation Chaos 30 (2020) 2050092, http://dx.doi.org/10.1142/S0218127420500923.
[173] V. Ravichandran, V. Chinnathambi, S. Rajasekar, Effect of various periodic forces on duffing oscillator, Pramana 67 (2006) 351–356, http://dx.doi.org/10.1007/s12043-006-0079-9.
[174] M.S. Meenakshi, S. Athisayanathan, V. Chinnathambi, S. Rajasekar, Effect of fractional damping in double-well duffing-van der pol oscillator driven by different sinusoidal forces, Int. J. Nonlin. Sci. Num. 20 (2019) 115–124, http://dx.doi.org/10.1515/ijnsns-2016-0165.
[175] K. Srinivasan, K. Thamilmaran, A. Venkatesan, Classification of bifurcations and chaos in chua's circuit with effect of different periodic forces, Int. J. Bifurcation Chaos 19 (2009) 1951–1973, http://dx.doi.org/10.1142/S0218127409023846.
[176] K. Srinivasan, K. Thamilmaran, A. Venkatesan, Effect of nonsinusoidal periodic forces in duffing oscillator: Numerical and analog simulation studies, Chaos Solitons Fractals 40 (2009) 319–330, http://dx.doi.org/10.1016/j.chaos.2007.07.090.
[177] C. Cheng, B. Zhou, X. Gao, M.D. McDonnell, M-ary suprathreshold stochastic resonance in multilevel threshold systems with signal-dependent noise, Physica A 479 (2017) 48–56, http://dx.doi.org/10.1016/j.physa.2017.03.010.
[178] M.D. McDonnell, X. Gao, M-ary suprathreshold stochastic resonance: Generalization and scaling beyond binary threshold nonlinearities, Europhys. Lett. 108 (2015) 60003, http://dx.doi.org/10.1209/0295-5075/108/60003.

[179] B. Zhou, X. Wang, Q. Qi, Optimal weights decoding of M-ary suprathreshold stochastic resonance in stochastic pooling network, Chinese J. Phys. 56 (2018) 1718–1726, http://dx.doi.org/10.1016/j.cjph.2018.06.010.
[180] Y.J. Zheng, C. Zhang, C.J. Li, Z.X. Zhu, F. Wang, Fractional Fourier transform of ultrasonic chirp signal for range measurement, in: The 54th Annual Conference of the Society of Instrument and Control Engineers of Japan, SICE, IEEE, 2015, pp. 140–144, http://dx.doi.org/10.1109/SICE.2015.7285568.
[181] Y.K. Chan, M.Y. Chua, V.C. Koo, Sidelobes reduction using simple two and tri-stages non linear frequency modulation (NLFM), Prog. Electromagn. Res. 98 (2009) 33–52, http://dx.doi.org/10.2528/PIER09073004.
[182] J. Song, Y. Gao, D. Gao, Analysis and detection of S-shaped NLFM signal based on instantaneous frequency, J. Commun. 10 (2015) 976–982, http://dx.doi.org/10.12720/jcm.10.12.976-982.
[183] I.C. Vizitiu, Some aspects of sidelobe reduction in pulse compression radars using NLFM signal processing, Prog. Electromag. Res. 47 (2014) 119–129, http://dx.doi.org/10.2528/PIERC14010605.
[184] Y. Yang, Z.K. Peng, G. Meng, W.M. Zhang, Spline-kernelled chirplet transform for the analysis of signals with time-varying frequency and its application, IEEE T. Ind. Electron. 59 (3) (2011) 1612–1621, http://dx.doi.org/10.1109/TIE.2011.2163376.
[185] J. Yang, S. Zhang, M.A.F. Sanjuán, H. Liu, Time-frequency analysis of a new aperiodic resonance, Commun. Nonlinear Sci. Numer. Simul. 85 (2020) 105258, http://dx.doi.org/10.1016/j.cnsns.2020.105258.
[186] V.M. Gandhimathi, S. Rajasekar, Vibrational and stochastic resonances in two coupled overdamped anharmonic oscillators driven by an amplitude modulated force, Phys. Scr. 76 (2007) 693, http://dx.doi.org/10.1088/0031-8949/76/6/019.
[187] V. Chinnathambi, S. Rajasekar, M.A.F. Sanjuán, Enhanced vibrational resonance by an amplitude-modulated force, in: J. Awrejcewicz, S. Rajasekar, M. Ragulskis (Eds.), Recent Trends in Chaotic, Nonlinear and Complex Dynamics, World Scientific Publishing Company, Singapore, 2022, pp. 15–39, http://dx.doi.org/10.1142/9789811221903_0002.
[188] B. Bhuvaneshwari, K. Amutha, V. Chinnathambi, S. Rajasekar, Enhanced vibrational resonance by an amplitude modulated signal in a nonlinear dissipative two-fluid plasma model, Contrib. Plasm. Phys. 62 (2022) e202100099, http://dx.doi.org/10.1002/ctpp.202100099.
[189] O.T. Kolebaje, U.E. Vincent, B.E. Benyeogor, P.V.E. McClintock, Effect of a modulated acoustic field on the dynamics of a vibrating charged bubble, Ultrasonics 135 (2023) 107110, http://dx.doi.org/10.1016/j.ultras.2023.107110.
[190] C. Adéyèmi, F.Y.J. Kpomahou, J.K. Agbélélé, A.J. Adéchinan, A.E. Yamadjako, Effects of periodic parametric damping and amplitude-modulated signal on vibrational resonance and torus-doubling bifurcations occurrence in an asymmetric mixed Rayleigh-liénard oscillator, Phys. Scr. 98 (2023) 105204, http://dx.doi.org/10.1088/1402-4896/acf3ad.
[191] S. Lu, Q. He, H. Zhang, F. Kong, Enhanced rotating machine fault diagnosis based on time-delayed feedback stochastic resonance, J. Vib. Acoust. 137 (2015) 051008, http://dx.doi.org/10.1115/1.4030346.
[192] D. Ho, R.B. Randall, Optimisation of bearing diagnostic techniques using simulated and actual bearing fault signals, Mech. Syst. Signal Pr. 14 (2000) 763–788, http://dx.doi.org/10.1006/mssp.2000.1304.
[193] J. Antoni, R.B. Randall, A stochastic model for simulation and diagnostics of rolling element bearings with localized faults, J. Vib. Acoust. 125 (2003) 282–289, http://dx.doi.org/10.1115/1.1569940.
[194] J. Antoni, F. Bonnardot, A. Raad, M. El Badaoui, Cyclostationary modelling of rotating machine vibration signals, Mech. Syst. Signal Pr. 18 (2004) 1285–1314, http://dx.doi.org/10.1016/S0888-3270(03)00088-8.
[195] J. Antoni, R.B. Randall, Differential diagnosis of gear and bearing faults, J. Vib. Acoust. 124 (2002) 165–171, http://dx.doi.org/10.1115/1.1456906.
[196] J. Yang, C. Wu, Z. Shan, H. Liu, C. Yang, Extraction and enhancement of unknown bearing fault feature in the strong noise under variable speed condition, Meas. Sci. Technol. 32 (2021) 105021, http://dx.doi.org/10.1088/1361-6501/ac0d78.
[197] R. Gui, H. Zhang, G. Cheng, Y. Yao, Set-reset latch logic operation in a bistable system under suprathreshold and subthreshold signals, Chaos 30 (2020) 023119, http://dx.doi.org/10.1063/1.5134888.
[198] R. Gui, Y. Yang, Y. Yao, G. Cheng, Noise-free logic and set-reset latch operation in a triple-well potential system, Chinese J. Phys. 68 (2020) 178–190, http://dx.doi.org/10.1016/j.cjph.2020.09.009.
[199] S. Huang, J. Zhang, J. Yang, H. Liu, M.A.F. Sanjuán, Logical vibrational resonance in a symmetric bistable system: Numerical and experimental studies, Commun. Nonlinear Sci. Numer. Simul. 119 (2023) 107123, http://dx.doi.org/10.1016/j.cnsns.2023.107123.
[200] P.R. Venkatesh, A. Venkatesan, Vibrational resonance and implementation of dynamic logic gate in a piecewise-linear Murali-Lakshmanan-Chua circuit, Commun. Nonlinear Sci. Numer. Simul. 39 (2016) 271–282, http://dx.doi.org/10.1016/j.cnsns.2016.03.009.
[201] Y. Yao, J. Ma, Logical stochastic and vibrational resonances induced by periodic force in the FitzHugh–Nagumo neuron, Eur. Phys. J. Plus 137 (2022) 1214, http://dx.doi.org/10.1140/epjp/s13360-022-03423-x.
[202] I.I. Blekhman, V.S. Sorokin, On a deterministic explanation of the stochastic resonance phenomenon, Nonlinear Dynam. 93 (2018) 767–778, http://dx.doi.org/10.1007/s11071-018-4225-y.
[203] V.N. Chizhevsky, Analytical study of vibrational resonance in an overdamped bistable oscillator, Int. J. Bifurcation Chaos 18 (2008) 1767–1773, http://dx.doi.org/10.1142/S021812740802135X.
[204] S. Rajasekar, S. Jeyakumari, V. Chinnathambi, M.A.F. Sanjuán, Role of depth and location of minima of a double-well potential on vibrational resonance, J. Phys. A 43 (2010) 465101, http://dx.doi.org/10.1088/1751-8113/43/46/465101.
[205] A. Daza, A. Wagemakers, M.A.F. Sanjuán, Strong sensitivity of the vibrational resonance induced by fractal structures, Int. J. Bifurcation Chaos 23 (2013) 1350129, http://dx.doi.org/10.1142/S0218127413501290.
[206] A. Abusoua, M.F. Daqaq, Experimental evidence of vibrational resonance in a mechanical bistable twin-well oscillator, J. Comput. Nonlinear Dyn. 13 (2018) 061002, http://dx.doi.org/10.1115/1.4039839.
[207] I.S. Sawkmie, D. Kharkongor, Theoretical and numerical study of vibrational resonance in a damped softening duffing oscillator, Int. J. Nonlin. Mech. 144 (2022) 104055, http://dx.doi.org/10.1016/j.ijnonlinmec.2022.104055.
[208] C. Gan, Noise-induced chaos and basin erosion in softening duffing oscillator, Chaos Solitons Fractals 25 (2005) 1069–1081, http://dx.doi.org/10.1016/j.chaos.2004.11.070.
[209] J. Yang, D. Huang, M.A.F. Sanjuán, H. Liu, Vibrational resonance in an overdamped system with a fractional order potential nonlinearity, Int. J. Bifurcation Chaos 28 (2018) 1850082, http://dx.doi.org/10.1142/S0218127418500827.
[210] C.A.K. Kwuimy, B.R.N. Nbendjo, Active control of horseshoes chaos in a driven Rayleigh oscillator with fractional order deflection, Phys. Lett. A 375 (2011) 3442–3449, http://dx.doi.org/10.1016/j.physleta.2011.07.049.
[211] C.A.K. Kwuimy, G. Litak, C. Nataraj, Nonlinear analysis of energy harvesting systems with fractional order physical properties, Nonlinear Dynam. 80 (2015) 491–501, http://dx.doi.org/10.1007/s11071-014-1883-2.
[212] H. Li, X. Liao, S. Ullah, L. Xiao, Analytical proof on the existence of chaos in a generalized duffing-type oscillator with fractional-order deflection, Nonlinear Anal.: Real 13 (2012) 2724–2733, http://dx.doi.org/10.1016/j.nonrwa.2011.12.028.
[213] S. Jeyakumari, V. Chinnathambi, S. Rajasekar, M.A.F. Sanjuán, Vibrational resonance in an asymmetric duffing oscillator, Int. J. Bifurcation Chaos 21 (2011) 275–286, http://dx.doi.org/10.1142/S0218127411028416.
[214] V.N. Chizhevsky, G. Giacomelli, Experimental and theoretical study of vibrational resonance in a bistable system with asymmetry, Phys. Rev. E 73 (2006) 022103, http://dx.doi.org/10.1103/PhysRevE.73.022103.

[215] Z.X. Zhou, K.L. Yang, C.J. Wang, B. Yu, X.B. Li, Y.W. Su, Theory and numerics of vibrational resonance in a three-level atomic optical bistable system, Chaos Solitons Fractals 170 (2023) 113355, http://dx.doi.org/10.1016/j.chaos.2023.113355.
[216] C. Jeevarathinam, S. Rajasekar, M.A.F. Sanjuán, Vibrational resonance in groundwater-dependent plant ecosystems, Ecol. Complex. 15 (2013) 33–42, http://dx.doi.org/10.1016/j.ecocom.2013.02.003.
[217] A. Abusoua, M.F. Daqaq, Changing the nonlinear resonant response of an asymmetric mono-stable oscillator by injecting a hard high-frequency harmonic excitation, J. Sound Vib. 436 (2018) 262–272, http://dx.doi.org/10.1016/j.jsv.2018.08.027.
[218] K. Abirami, S. Rajasekar, M.A.F. Sanjuán, Vibrational resonance in the morse oscillator, Pramana 81 (2013) 127–141, http://dx.doi.org/10.1007/s12043-013-0546-z.
[219] S. Liu, Y. Sun, Y. Kang, A novel E-exponential stochastic resonance model and weak signal detection method for steel wire rope, IEEE T. Ind. Electron. 69 (2021) 7428–7440, http://dx.doi.org/10.1109/TIE.2021.3095802.
[220] Z. Xu, Z. Wang, J. Yang, M.A.F. Sanjuán, B. Sun, S. Huang, Aperiodic stochastic resonance in a biased monostable system excited by different weak aperiodic pulse signals and strong noise, Eur. Phys. J. Plus 138 (2023) 1–12, http://dx.doi.org/10.1140/epjp/s13360-023-03985-4.
[221] Z. Chen, L. Ning, Impact of depth and location of the wells on vibrational resonance in a triple-well system, Pramana 90 (2018) 49, http://dx.doi.org/10.1007/s12043-018-1539-8.
[222] A. Wickenbrock, P.C. Holz, N.A.A. Wahab, P. Phoonthong, D. Cubero, F. Renzoni, Vibrational mechanics in an optical lattice: Controlling transport via potential renormalization, Phys. Rev. Lett. 108 (2012) 020603, http://dx.doi.org/10.1103/PhysRevLett.108.020603.
[223] B.I. Usama, S. Morfu, P. Marquié, Numerical analyses of the vibrational resonance occurrence in a nonlinear dissipative system, Chaos Solitons Fractals 127 (2019) 31–37, http://dx.doi.org/10.1016/j.chaos.2019.06.028.
[224] K. Abirami, S. Rajasekar, M.A.F. Sanjuán, Vibrational resonance in a harmonically trapped potential system, Commun. Nonlinear Sci. Numer. Simul. 47 (2017) 370–378, http://dx.doi.org/10.1016/j.cnsns.2016.12.002.
[225] U.E. Vincent, T.O. Roy-Layinde, O.O. Popoola, P.O. Adesina, P.V.E. McClintock, Vibrational resonance in an oscillator with an asymmetrical deformable potential, Phys. Rev. E 98 (2018) 062203, http://dx.doi.org/10.1103/PhysRevE.98.062203.
[226] T.L.M.D. Mbong, M.S. Siewe, C. Tchawoua, Controllable parametric excitation effect on linear and nonlinear vibrational resonances in the dynamics of a buckled beam, Commun. Nonlinear Sci. Numer. Simul. 54 (2018) 377–388, http://dx.doi.org/10.1016/j.cnsns.2017.06.019.
[227] P.K. Sahoo, S. Chatterjee, High-frequency vibrational control of principal parametric resonance of a nonlinear cantilever beam: Theory and experiment, J. Sound Vib. 505 (2021) 116138, http://dx.doi.org/10.1016/j.jsv.2021.116138.
[228] S. Roy, D. Das, D. Banerjee, Vibrational resonance in a bistable van der pol-mathieu-duffing oscillator, Int. J. Nonlin. Mech. 135 (2021) 103771, http://dx.doi.org/10.1016/j.ijnonlinmec.2021.103771.
[229] T.O. Roy-Layinde, K.A. Omoteso, B.A. Oyero, J.A. Laoye, U.E. Vincent, Vibrational resonance of ammonia molecule with doubly singular position-dependent mass, Eur. Phys. J. B 95 (2022) 1–11, http://dx.doi.org/10.1140/epjb/s10051-022-00342-9.
[230] R. Kabilan, M. Sathish Aravindh, A. Venkatesan, M. Lakshmanan, Vibrational resonance in a damped and two-frequency driven system of particle on a rotating parabola, Eur. Phys. J. Plus 138 (2023) 500, http://dx.doi.org/10.1140/epjp/s13360-023-04017-x.
[231] R. Kabilan, A. Venkatesan, Vibrational resonance in a damped bi-harmonic driven Mathews-Lakshmanan oscillator, J. Vib. Eng. Technol. (2023) http://dx.doi.org/10.1007/s42417-023-00897-6.
[232] U.E. Vincent, O. Kolebaje, Introduction to the dynamics of driven nonlinear systems, Contemp. Phys. 61 (2020) 169–192, http://dx.doi.org/10.1080/00107514.2020.1850003.
[233] T.O. Roy-Layinde, J.A. Laoye, O.O. Popoola, U.E. Vincent, Analysis of vibrational resonance in bi-harmonically driven plasma, Chaos 26 (2016) 093117, http://dx.doi.org/10.1063/1.4962403.
[234] T.L.M.D. Mbong, M.S. Siewe, C. Tchawoua, The effect of nonlinear damping on vibrational resonance and chaotic behavior of a beam fixed at its two ends and prestressed, Commun. Nonlinear Sci. Numer. Simul. 22 (2015) 228–243, http://dx.doi.org/10.1016/j.cnsns.2014.10.001.
[235] P.K. Sahoo, S. Chatterjee, Vibrational control and resonance of a nonlinear tilted cantilever beam under multi-harmonic low and high-frequency excitations, Commun. Nonlinear Sci. Numer. Simul. 125 (2023) 107386, http://dx.doi.org/10.1016/j.cnsns.2023.107386.
[236] K.A. Omoteso, T.O. Roy-Layinde, J.A. Laoye, U.E. Vincent, P.V.E. McClintock, Acoustic vibrational resonance in a Rayleigh-Plesset bubble oscillator, Ultrason. Sonochem. 70 (2021) 105346, http://dx.doi.org/10.1016/j.ultsonch.2020.105346.
[237] K.S. Oyeleke, O.I. Olusola, U.E. Vincent, D. Ghosh, P.V.E. McClintock, Parametric vibrational resonance in a gyroscope driven by dual-frequency forces, Phys. Lett. A 387 (2021) 127040, http://dx.doi.org/10.1016/j.physleta.2020.127040.
[238] K. Abirami, S. Rajasekar, M.A.F. Sanjuán, Vibrational resonance in a system with a signum nonlinearity, Discontin. Nonlinear. Complexity 5 (2016) 43–58, http://dx.doi.org/10.5890/DNC.2016.03.006.
[239] E. Pennestrí, V. Rossi, P. Salvini, P.P. Valentini, Review and comparison of dry friction force models, Nonlinear Dynam. 83 (2016) 1785–1801, http://dx.doi.org/10.1007/s11071-015-2485-3.
[240] E.J. Berger, Friction modeling for dynamic system simulation, Appl. Mech. Rev. 55 (2002) 535–577, http://dx.doi.org/10.1115/1.1501080.
[241] J.J. Thomsen, Some general effects of strong high-frequency excitation: stiffening, biasing and smoothening, J. Sound Vib. 253 (2002) 807–831, http://dx.doi.org/10.1006/jsvi.2001.4036.
[242] P.K. Sahoo, S. Chatterjee, Effect of high-frequency excitation on friction induced vibration caused by the combined action of velocity-weakening and mode-coupling, J. Vib. Control 26 (2020) 735–746, http://dx.doi.org/10.1177/107754631988.
[243] J.J. Thomsen, K.L. Ebbehøj, Strong nonlinearity and external high-frequency forcing for controlling effective mechanical stiffness: theory and experiment, Nonlinear Dynam. 111 (2023) 6985–7003, http://dx.doi.org/10.1007/s11071-023-08255-7.
[244] M.P. Asir, A. Jeevarekha, P. Philominathan, Multiple vibrational resonance and antiresonance in a coupled anharmonic oscillator under monochromatic excitation, Pramana 93 (2019) 43, http://dx.doi.org/10.1007/s12043-019-1802-7.
[245] V.M. Gandhimathi, S. Rajasekar, J. Kurths, Vibrational and stochastic resonances in two coupled overdamped anharmonic oscillators, Phys. Lett. A 360 (2006) 279–286, http://dx.doi.org/10.1016/j.physleta.2006.08.051.
[246] M. Gosak, M. Perc, S. Kralj, The impact of static disorder on vibrational resonance in a ferroelectric liquid crystal, Mol. Cryst. Liq. Cryst. 553 (2012) 13–20, http://dx.doi.org/10.1080/15421406.2011.609343.
[247] K. Wu, J. Li, Effects of high-low-frequency electromagnetic radiation on vibrational resonance in FitzHugh–Nagumo neuronal systems, Eur. Phys. J. B 96 (2023) 126, http://dx.doi.org/10.1140/epjb/s10051-023-00594-z.
[248] Z. He, C. Yao, J. Shuai, T. Nakan, Enhanced vibrational resonance in a single neuron with chemical autapse for signal detection, Chinese Phys. B 29 (2020) 128702, http://dx.doi.org/10.1088/1674-1056/abb7f9.
[249] X.X. Wu, C. Yao, J. Shuai, Enhanced multiple vibrational resonances by Na+ and K+ dynamics in a neuron model, Sci. Rep. 5 (2015) 7684, http://dx.doi.org/10.1038/srep07684.
[250] G. Wang, D. Yu, Q. Ding, T. Li, Y. Jia, Effects of electric field on multiple vibrational resonances in Hindmarsh-Rose neuronal systems, Chaos Solitons Fractals 150 (2021) 111210, http://dx.doi.org/10.1016/j.chaos.2021.111210.
[251] R. Jothimurugan, K. Thamilmaran, S. Rajasekar, M.A.F. Sanjuán, Experimental evidence for vibrational resonance and enhanced signal transmission in Chua's circuit, Int. J. Bifurcation Chaos 23 (2013) 1350189, http://dx.doi.org/10.1142/S0218127413501897.
[252] B.I. Usama, S. Morfu, P. Marquie, Vibrational resonance and ghost-vibrational resonance occurrence in Chua's circuit models with specific nonlinearities, Chaos Solitons Fractals 153 (2021) 111515, http://dx.doi.org/10.1016/j.chaos.2021.111515.

[253] L. Fortuna, M. Frasca, M.G. Xibilia, Chua's Circuit Implementations: Yesterday, Today and Tomorrow, World Scientific, Singapore, 2009, http://dx.doi.org/10.1142/7200.
[254] P. Sarkar, S. Paul, D.S. Ray, Subharmonics and superharmonics of the weak field in a driven two-level quantum system: Vibrational resonance enhancement, Phys. Rev. E 104 (2021) 014202, http://dx.doi.org/10.1103/PhysRevE.104.014202.
[255] V.N. Chizhevsky, E. Smeu, G. Giacomelli, Experimental evidence of vibrational resonance in an optical system, Phys. Rev. Lett. 91 (2003) 220602, http://dx.doi.org/10.1103/PhysRevLett.91.220602.
[256] V.N. Chizhevsky, Amplification of an autodyne signal in a bistable vertical-cavity surface-emitting laser with the use of a vibrational resonance, Tech. Phys. Lett. 44 (2018) 17–19, http://dx.doi.org/10.1134/S1063785018010066.
[257] V.N. Chizhevsky, Enhancement of response of a bistable VCSEL to modulated orthogonal optical feedback by vibrational resonance, Opt. Lett. 37 (2012) 4386–4388, http://dx.doi.org/10.1364/OL.37.004386.
[258] V.N. Chizhevsky, Experimental evidence of vibrational resonance in a multistable system, Phys. Rev. E 89 (2014) 062914, http://dx.doi.org/10.1103/PhysRevE.89.062914.
[259] S. Rajasekar, J. Used, A. Wagemakers, M.A.F. Sanjuán, Vibrational resonance in biological nonlinear maps, Commun. Nonlinear Sci. Numer. Simul. 17 (2012) 3435–3445, http://dx.doi.org/10.1016/j.cnsns.2011.12.014.
[260] A. Jeevarekha, M. Santhiah, P. Philominathan, Enriched vibrational resonance in certain discrete systems, Pramana 83 (2014) 493–504, http://dx.doi.org/10.1007/s12043-014-0815-5.
[261] C.A. Monje, Y. Chen, B.M. Vinagre, D. Xue, V. Feliu, Fractional-Order Systems and Controls: Fundamentals and Applications, Springer, London, 2010, http://dx.doi.org/10.1007/978-1-84996-335-0.
[262] K. Zhao, L. Ning, Vibrational resonance in a fractional order system with asymmetric bistable potential and time delay feedback, Chinese J. Phys. 77 (2022) 1796–1809, http://dx.doi.org/10.1016/j.cjph.2021.11.003.
[263] J.H. Yang, M.A.F. Sanjuán, C.J. Wang, H. Zhu, Vibrational resonance in a duffing system with a generalized delayed feedback, J. Appl. Nonlinear Dyn. 2 (2013) 397–408, http://dx.doi.org/10.5890/JAND.2013.11.006.
[264] W. Guo, L. Ning, Vibrational resonance in a fractional order quintic oscillator system with time delay feedback, Int. J. Bifurcation Chaos 30 (2020) 2050025, http://dx.doi.org/10.1142/S021812742050025X.
[265] L. Ning, W. Guo, The influence of two kinds of time delays on the vibrational resonance of a fractional Mathieu-Duffing oscillator, Pramana 94 (2020) 1–10, http://dx.doi.org/10.1007/s12043-019-1905-1.
[266] Z. Yan, X.B. Liu, Fractional-order harmonic resonance in a multi-frequency excited fractional duffing oscillator with distributed time delay, Commun. Nonlinear Sci. Numer. Simul. 97 (2021) 105754, http://dx.doi.org/10.1016/j.cnsns.2021.105754.
[267] I.A. Khovanov, P.V.E. McClintock, Synchronization of stochastic bistable systems by biperiodic signals, Phys. Rev. E 76 (2007) 031122, http://dx.doi.org/10.1103/PhysRevE.76.031122.
[268] Z.Q. Wang, J.H. Yang, Aperiodic resonance of a nonlinear system excited by aperiodic binary signal or M-ary signal, Acta Phys. Sin. 72 (2023) 222501, http://dx.doi.org/10.7498/aps.72.20231154.
[269] S. Sun, B. Lei, On an aperiodic stochastic resonance signal processor and its application in digital watermarking, Signal Process. 88 (2008) 2085–2094, http://dx.doi.org/10.1016/j.sigpro.2008.02.010.
[270] J. Li, L. Zeng, Stochastic resonance in a bistable system subject to multi-time-delayed feedback and aperiodic signal, J. Phys. A 43 (2010) 495002, http://dx.doi.org/10.1088/1751-8113/43/49/495002.
[271] L. Zeng, B. Xu, Effects of asymmetric Lévy noise in parameter-induced aperiodic stochastic resonance, Physica A 389 (2010) 5128–5136, http://dx.doi.org/10.1016/j.physa.2010.07.032.
[272] I. Daubechies, The.wavelet. transform, Time-frequency localization and signal analysis, IEEE T. Inform. Theory 36 (1990) 961–1005, http://dx.doi.org/10.1109/18.57199.
[273] L.B. Almeida, The fractional Fourier transform and time-frequency representations, IEEE T. Signal Proces. 42 (1994) 3084–3091, http://dx.doi.org/10.1109/78.330368.
[274] P. Flandrin, G. Rilling, P. Goncalves, Empirical mode decomposition as a filter bank, IEEE Signal Proc. Let. 11 (2004) 112–114, http://dx.doi.org/10.1109/LSP.2003.821662.
[275] T. Tanaka, D.P. Mandic, Complex empirical mode decomposition, IEEE Signal Proc. Let. 14 (2007) 101–104, http://dx.doi.org/10.1109/LSP.2006.882107.
[276] N.E. Huang, Z. Shen, S.R. Long, M.C. Wu, H.H. Shih, Q. Zheng, N.C. Yen, C.C. Tung, H.H. Liu, The empirical mode decomposition and the Hilbert spectrum for nonlinear and non-stationary time series analysis, P. Roy. Soc. A-Math. Phy. 454 (1998) 903–995, http://dx.doi.org/10.1098/rspa.1998.0193.
[277] R. Storni, H. Ando, K. Aihara, K. Murali, S. Sinha, Manipulating potential wells in logical stochastic resonance to obtain XOR logic, Phys. Lett. A 376 (2012) 930–937, http://dx.doi.org/10.1016/j.physleta.2011.12.036.
[278] C.G. Yao, Z.W. He, M. Zhan, High frequency forcing on nonlinear systems, Chinese Phys. B 22 (2013) 030503, http://dx.doi.org/10.1088/1674-1056/22/3/030503.
[279] H. Yabuno, M. Miura, N. Aoshima, Bifurcation in an inverted pendulum with tilted high-frequency excitation: analytical and experimental investigations on the symmetry-breaking of the bifurcation, J. Sound Vib. 273 (2004) 493–513, http://dx.doi.org/10.1016/S0022-460X(03)00507-8.
[280] M. Belhaq, S.M. Sah, Fast parametrically excited van der pol oscillator with time delay state feedback, Int. J. Nonlin. Mech. 43 (2008) 124–130, http://dx.doi.org/10.1016/j.ijnonlinmec.2007.10.009.
[281] M. Belhaq, S.M. Sah, Horizontal fast excitation in delayed van der Pol oscillator, Commun. Nonlinear Sci. Numer. Simul. 13 (2008) 1706–1713, http://dx.doi.org/10.1016/j.cnsns.2007.02.007.
[282] M. Belhaq, A. Fahsi, Hysteresis suppression for primary and subharmonic 3: 1 resonances using fast excitation, Nonlinear Dynam. 57 (2009) 275–287, http://dx.doi.org/10.1007/s11071-008-9438-z.
[283] A. Fahsi, M. Belhaq, Effect of fast harmonic excitation on frequency-locking in a van der Pol-Mathieu-Duffing oscillator, Commun. Nonlinear Sci. Numer. Simul. 14 (2009) 244–253, http://dx.doi.org/10.1016/j.cnsns.2007.07.010.
[284] J.S. Jensen, D.M. Tcherniak, J.J. Thomsen, Stiffening effects of high-frequency excitation: experiments for an axially loaded beam, J. Appl. Mech. 67 (2000) 397–402, http://dx.doi.org/10.1115/1.1304824.
[285] J.J. Thomsen, Theories and experiments on the stiffening effect of high-frequency excitation for continuous elastic systems, J. Sound Vib. 260 (2003) 117–139, http://dx.doi.org/10.1016/S0022-460X(02)00916-1.
[286] J.J. Thomsen, Slow high-frequency effects in mechanics: problems, solutions, potentials, Int. J. Bifurcation Chaos 15 (2005) 2799–2818, http://dx.doi.org/10.1142/S0218127405013721.
[287] A. Fidlin, J.J. Thomsen, Non-trivial effects of high-frequency excitation for strongly damped mechanical systems, Int. J. Nonlin. Mech. 43 (2008) 569–578, http://dx.doi.org/10.1016/j.ijnonlinmec.2008.02.002.
[288] J.J. Thomsen, Effective properties of mechanical systems under high-frequency excitation at multiple frequencies, J. Sound Vib. 311 (2008) 1249–1270, http://dx.doi.org/10.1016/j.jsv.2007.10.012.

[289] H. Sheheitli, On the dynamics of a spinning top under high-frequency excitation, part I: pivot point under vertical harmonic vibration, Nonlinear Dynam. 90 (2017) 765–779, http://dx.doi.org/10.1007/s11071-017-3609-8.
[290] H. Sheheitli, On the dynamics of a spinning top under high-frequency excitation, part II: pivot point under horizontal harmonic vibration, Nonlinear Dynam. 90 (2017) 2269–2276, http://dx.doi.org/10.1007/s11071-017-3800-y.
[291] Z.Q. Lu, D.H. Gu, H. Ding, W. Lacarbonara, L.Q. Chen, Nonlinear vibration isolation via a circular ring, Mech. Syst. Signal Pr. 136 (2020) 106490, http://dx.doi.org/10.1016/j.ymssp.2019.106490.
[292] A. Ichiki, Y. Tadokoro, M. Takanashi, Linear response analysis of vibrational resonance in over-damped systems, J. Phys. A 45 (2012) 385101, http://dx.doi.org/10.1088/1751-8113/45/38/385101.
[293] J.H. Yang, X.B. Liu, Sequential vibrational resonance in multistable systems, 2011, arXiv preprint https://arxiv.org/abs/1106.3431.
[294] H. Kantz, P. Grassberger, Repellers, semi-attractors, and long-lived chaotic transients, Physica D 17 (1985) 75–86, http://dx.doi.org/10.1016/0167-2789(85)90135-6.
[295] A.S. de Paula, M.A. Savi, F.H.I. Pereira-Pinto, Chaos and transient chaos in an experimental nonlinear pendulum, J. Sound Vib. 294 (2006) 585–595, http://dx.doi.org/10.1016/j.jsv.2005.11.015.
[296] J. Yang, D. Zhou, Re-Scaled Resonance Theory and Applications in Fault Diagnosis, Sci. Press, Beijing, 2020, in Chinese.
[297] D. Huang, J. Yang, J. Zhang, H. Liu, An improved adaptive stochastic resonance with general scale transformation to extract high-frequency characteristics in strong noise, Internat. J. Modern Phys. B 32 (2018) 1850185, http://dx.doi.org/10.1142/S0217979218501850.
[298] N. Hu, M. Chen, X. Wen, The application of stochastic resonance theory for early detecting rub-impact fault of rotor system, Mech. Syst. Signal Pr. 17 (2003) 883–895, http://dx.doi.org/10.1006/mssp.2002.1470.
[299] Q. He, J. Wang, Y. Liu, D. Dai, F. Kong, Multiscale noise tuning of stochastic resonance for enhanced fault diagnosis in rotating machines, Mech. Syst. Signal Pr. 28 (2012) 443–457, http://dx.doi.org/10.1016/j.ymssp.2011.11.021.
[300] T. Gong, J.H. Yang, Z. Shan, Z.L. Wang, H.G. Liu, Optimal resonance response of nonlinear system excited by nonlinear frequency modulation signal, Acta Phys. Sin. 71 (2022) 050503, http://dx.doi.org/10.7498/aps.71.20211959.
[301] T. Gong, J. Yang, M.A.F. Sanjuán, H.G. Liu, Z. Shan, Vibrational resonance by using a real-time scale transformation method, Phys. Scr. 97 (2022) 045207, http://dx.doi.org/10.1088/1402-4896/ac5bc5.
[302] Z. Shan, Z. Wang, J. Yang, D. Zhou, H. Liu, Extracting non-stationary signal under strong noise background: Time-varying system analysis, J. Vib. Control 29 (2023) 4036–4045, http://dx.doi.org/10.1177/10775463221109715.
[303] Y. Leng, T. Wang, Y. Guo, Y.G. Xu, S.B. Fan, Engineering signal processing based on bistable stochastic resonance, Mech. Syst. Signal Pr. 21 (2007) 138–150, http://dx.doi.org/10.1016/j.ymssp.2005.08.002.
[304] H.L. He, T.Y. Wang, Y.G. Leng, Y. Zhang, Q. Li, Study on non-linear filter characteristic and engineering application of cascaded bistable stochastic resonance system, Mech. Syst. Signal Pr. 21 (2007) 2740–2749, http://dx.doi.org/10.1016/j.ymssp.2007.02.004.
[305] Y. Yao, J. Ma, Logical chaotic resonance in a bistable system, Int. J. Bifurcation Chaos 30 (2020) 2050196, http://dx.doi.org/10.1142/S0218127420501965.
[306] Y. Yao, J. Ma, R. Gui, G. Cheng, Enhanced logical chaotic resonance, Chaos 31 (2021) 023103, http://dx.doi.org/10.1063/5.0037032.
[307] Y. Yao, Logical chaotic resonance in the FitzHugh–Nagumo neuron, Nonlinear Dynam. 107 (2022) 3887–3901, http://dx.doi.org/10.1007/s11071-021-07155-y.
[308] L. Gammaitoni, Stochastic resonance and the dithering effect in threshold physical systems, Phys. Rev. E 52 (1995) 4691–4698, http://dx.doi.org/10.1103/PhysRevE.52.4691.
[309] R.A. Wannamaker, S.P. Lipshitz, J. Vanderkooy, Stochastic resonance as dithering, Phys. Rev. E 61 (2000) 233–236, http://dx.doi.org/10.1103/PhysRevE.61.233.
[310] J. Yang, C. Yang, X. Zhuang, H. Liu, Z. Wang, Unknown bearing fault diagnosis under time-varying speed conditions and strong noise background, Nonlinear Dynam. 107 (2022) 2177–2193, http://dx.doi.org/10.1007/s11071-021-07078-8.
[311] Z. Wang, J. Yang, Y. Guo, Unknown fault feature extraction of rolling bearings under variable speed conditions based on statistical complexity measures, Mech. Syst. Signal Pr. 172 (2022) 108964, http://dx.doi.org/10.1016/j.ymssp.2022.108964.